

**DANISH METEOROLOGICAL
INSTITUTE**

— SCIENTIFIC REPORT —

01-08

Sea Level Variations in the North Sea
- from Tide Gauges, Altimetry and Modelling

Vibeke Huess



Copenhagen 2001

ISSN Nr 0905-3263 (printed)
ISSN Nr 1399-1949 (online)
ISBN Nr 87-7478-447-1

Sea Level Variations in the North Sea - from Tide Gauges, Altimetry and Modelling

Vibeke Huess

PhD thesis

Danish Meteorological Institute
Copenhagen, Denmark

Niels Bohr Institute for Astronomy, Physics and Geophysics
University of Copenhagen, Copenhagen, Denmark

October 2000

This PhD thesis has been accepted by the Faculty of Science at University of Copenhagen to fulfill the requirements for a PhD degree.

The PhD project has been carried out as part of the Danish research project *Geoid and Sea Level of the North Atlantic Region* (GEOSONAR) under the Earth Observations programme supported by the Danish Space Board, the Danish Agricultural and Veterinary Research Council, the Danish Natural Science Research Council and the Danish Technical Research Council.

Contents

1	Introduction	1
1.1	The GEOSONAR Project	3
1.2	Structure of This Thesis	5
2	Sea Level Information	6
2.1	Tide Gauges	6
2.1.1	Time Series Analyses	7
2.1.2	Pressure Instrument at Horns Rev	9
2.2	Altimeters	10
2.2.1	Signal Corrections	13
2.3	Hydrodynamical Models	14
2.3.1	The Mike 21 Model	14
3	Tides	16
3.1	The Tidal Potential and the Equilibrium Tide	17
3.2	Harmonic Analysis	19
3.2.1	The Nodal Modulation	20
3.3	Response Analysis Method	21
3.4	Shallow Water Tides	22
3.4.1	Shallow Water	22
3.4.2	Non-linear Interaction	23
3.4.3	Linear Superposition	23
3.4.4	The Nodal Modulations	24
3.5	Choice of Constituent Set	24
3.6	Internal Tides	26
4	Seasonal Variations in the Main Tidal Constituent	27
4.1	Introduction	27
4.2	Annual and Seasonal Variations in the M_2 Constituent	28
4.3	Altimeter Observations	31
4.4	Tide Gauge Observations	33
4.4.1	Validation of the altimeter observations	33
4.4.2	Comparison of the Total Annual Variation and the Modulation Wave	33

4.4.3	The Modulation Wave for north-west European Shelf Stations	36
4.4.4	The Modulation Wave for Stations Outside the North Sea	43
4.5	Numerical Modelling	43
4.5.1	Barotropic Model	44
4.5.2	Atmospheric Interaction	52
4.5.3	Baroclinic Model	58
4.5.4	Bed Friction Test	58
4.6	Summary of Seasonal Variations in M_2	60
5	Atmospheric Effects on Sea Level	63
5.1	The Wind Effect	63
5.1.1	The Ekman Transport	63
5.2	The Pressure Effect	63
5.2.1	The Inverse Barometer Effect	64
5.2.2	Deviations from the Inverse Barometer Effect	64
5.2.3	Estimation of the IB Effect in the Eastern North Sea	66
5.3	Atmospheric Tide	66
5.4	“The Summer Wave 1998”	67
6	Tidal Modelling	71
6.1	Tidal Forcing	71
6.2	Tidal Validation and Model Inter comparison	73
6.3	Atmospheric Forcing	75
6.3.1	The Atmospheric Influence on the Tidal Constituents	75
7	Observed and Modelled Sea Level Variability in the North Sea	78
7.1	Study in the Eastern Part of the North Sea	78
7.1.1	On-shore Tidal Amplification	79
7.1.2	On-shore Sea Level Amplification	80
7.2	Validation of Model and Altimetry data	83
7.2.1	Validation with the Horns Rev off shore observations	83
7.2.2	Altimetry and model inter-validation	83
8	Conclusion	86
	Acknowledgments	88
	References	89
	Appendixes	95
A	Sea Level Calculations at Horns Rev	95
B	The M_2 Modulation Wave	103

C	Vector Root-Sum-Square	105
D	The Modulation Wave from the NEAC 2D-model T runs	106
E	Plots of the NEAC 2D-model Modulation Wave	109
F	Paper submitted to Geophysical Research Letters	122

Chapter 1

Introduction

The topography of the ocean is a result of a variety of geophysical processes on different scales with respect to both time and space. If the ocean was homogeneous and motionless, the surface of the ocean would adjust to an equipotential surface of the earth's gravity field. This specific equipotential surface is named the geoid. Determination of the geoid is important for investigations of the gravity field. The ocean is neither homogeneous nor motionless, so the sea level will not in general coincide with the geoid. Deviations in the actual sea level from the geoid are caused by tidal currents, atmospherically induced currents, and currents caused by changes in the salinity, temperature and pressure. The currents are altered by friction and the Coriolis force.

The tidal energy is described by a discrete line spectrum in the frequency band. The main part of this energy is concentrated at diurnal and semi-diurnal periods, but tidal energy can be detected on a large frequency range with periods from hours to tens of thousands of years. The tides are to a high degree predictable from previous observed sea level variations, even for locations where only a short data record of a few months are available. Tidal elevations along coast lines may be of several metres.

The predictability of the energy input to the ocean from the atmosphere is on the contrary highly limited due to the limited predictability of the weather systems being a few days. The energy in the ocean transferred from the atmosphere is described as a continuous spectrum in the frequency band, with time scales from seconds for small wind waves to much longer waves, and wind set-up with persistencies of hours to days.

The sea level changes caused by the wind depend on the strength of the wind, i.e. the square of the wind speed, the duration of the wind, and the distance over which the wind has been working called the *fetch*. The wind energy input has a much larger impact in shallow waters than in deeper parts of the ocean, as the energy density will increase for decreasing water depth, resulting in larger sea level changes in shallow water areas.

Besides the wind effect, changes in the atmospheric pressure will also cause sea level changes. For a fully developed stationary pressure system, the *inverse barometer effect* will cause an inverse sea level response of approximately 1 cm for an atmospheric pressure anomaly of 1 hPa. An atmospheric system with a pressure anomaly of tens of hPa may therefore set-up a significant

horizontal pressure gradient in the water and generate the propagation of a long ocean wave. For a moving atmospheric pressure system, the magnitude of the sea level response will depend on the relative velocity between the atmospheric pressure system and the ocean wave, and large deviations in the sea level response from the static inverse barometric effect can be expected. This is known as the *dynamical inverse barometric effect* (Proudman, 1953).

Along a coast a quasi-stationary atmospheric system may build a wind set-up - a storm surge - and cause sea level changes of several metres.

Changes in the sea level due to salinity and temperature differences happen on spatial scales from a relatively small spatial area influenced by river run-off and ice melting, to larger scales due to changes in the evaporation and precipitation patterns and advection of water masses. The seasonal solar heat input does also cause density changes with minimum density and thereby maximum sea level in autumn, and maximum density with minimum sea level in spring. This is called the *steric effect*. For the Danish area, the steric effect is of the order of up to 10-20 cm (Højerslev and Andersen, 1990)

For large spatial areas the rotation of the earth becomes important for the currents, and a horizontal pressure gradient that set up a current will be balanced by the Coriolis force and form a geostrophic current system. Rossby's radius of deformation scales the effect of the rotation, and defines at which horizontal scale the earth's rotation becomes important. For the North Sea the Rossby's barotropic radius of deformation is of the order of

$$a = \frac{c_f}{f} = \frac{\sqrt{g h}}{f} \approx 200 km$$

where c_f is the phase velocity for a long non-rotating gravity wave, and f the Coriolis parameter. Geostrophic currents may form quasi-stationary systems and sea level changes. Additionally, external forces may influence the ocean and sea level. This can be a severe and abrupt underwater seismic activity that may cause a significant pressure wave, a *tsunami*. A tsunami may, despite the relatively small scale phenomena both temporal and spatial, cause catastrophic damage on coastal areas even far from the generation of the wave, due to a high degree of conservation of the momentum.

Information of the sea level and sea level changes are important for a variety of processes and research interests on a large range on both temporal and spatial scales. This is from local storm surge forecasting on time scales of hours to days, and to climate research studies of effects on the global mean sea level due to global warming with changes in precipitation, evaporation, steric effect and ice melting on time scales of decades and centuries. Accurate measurements of the sea level are, therefore, of great importance and observations of the sea level have been obtained with accurate coastal tide gauges at many locations for more than one century. Along the Danish coast the first ten tide gauge were established in the period 1888-1893, and have been operating continuously since. International data banks for sea level information as the *Permanent Service for Mean Sea Level* (PSMSL) located at the Proudman Oceanographic Laboratory (POL), Bidston, U.K., and the *Global Level Of the Sea Surface* (GLOSS) programme, coordinated by the Intergovernmental Oceanographic Commission (IOC), were established for

compilation of sea level information world wide. Information about the PSMSL and GLOSS programmes and data bases are available at <http://www.pol.ac.uk/psmsl>. These data banks for tide gauge observations together with information from deployed off-shore stations (e.g. *Smithson* (1992)) form a valuable amount of information of the sea level. However, the location of the tide gauges along coast lines, and the relatively limited number of off-shore stations make a severe limit for a global coverage of the world oceans. Satellite altimetry that in the last decades has become available has, therefore, provided valuable new information about off-shore sea level changes. The first radar altimeter instruments operating from space were launched in 1973 on the Skylab satellite, in 1975 on the GEOS-3 satellite, and the SEASAT satellite in 1978. These missions resulted in significant improvements of the technology, and the determination of the mean sea surface (*Wunsch and Stammer*, 1998), and have been followed up by the GEOSAT satellite in 1985, the ERS-1 in 1991, the TOPEX/POSEIDON (T/P) in 1992, and the ERS-2 in 1995. The data banks with the in-situ sea level observations have provided a valuable tool for validation and error estimations of the satellite provided sea level observations. From the satellite observations global tidal models have been developed with impressive results with root-mean-square errors to the in-situ data of a few cm in the main tidal constituents (*Andersen et al.*, 1995; *Shum et al.*, 1997). Additionally, estimates of the global mean sea level and global mean sea level rise have been produced (e.g. *Mitchum* (1994); *Cazenave et al.* (1998)). One example of the variety of future applications of altimetry data is shown by *Cazenave et al.* (1999), who have demonstrated that it is possible to observe local mean sea level changes due to vertical land motions caused by volcanic eruptions. The satellites carrying the altimeters were mainly put into operation for research studies of the geoid, the global tidal signal and the global ocean circulation. However, the good accuracy of measuring the sea level has resulted in a growing interest for using altimetry data in a more operational sense by using altimetry data to correct and validate operational ocean models for the off-shore area with respect to information about the mean sea level, the variability, and the tides.

1.1 The GEOSONAR Project

The very impressive results obtained from satellite altimetry with respect to the understanding and determination of the processes that cause deviations in the sea level from the geoid is of interest to different disciplines as oceanography, geodesy and gravity field studies. This has resulted in the Danish interdisciplinary research project *Geoid and Sea Level of the North Atlantic Region* (GEOSONAR), and this PhD project has been carried out as part of the GEOSONAR project. The GEOSONAR consortium includes the following Danish research institutes:

- National Survey and Cadastre (KMS), Geodetic Division (project coordinator)
- University of Copenhagen, Geophysical Department
- Technical University of Denmark, Department of Mathematical Modelling
- Royal Danish Administration of Navigation and Hydrography, Oceanography Division
- Danish Meteorological Institute (DMI), Department for Operational Oceanography

The objective of the GEOSONAR project is to investigate the geoid, and the sea level variations on a regional scale in the northern Atlantic and North Sea by using multiple data sources, and integration of multi sensor and multi channel satellite data.

DMI's interest in this research study is in the oceanographic part and is primarily focused on the North Sea which is the main area of interest with respect to the Danish storm surge warning system. The interests are to investigate to what degree altimetry observations can provide new information, and improve the storm surge system in both a pre-operational mode, including model calibration and validations, and in a more operational mode for future applications.

The North Sea is a shallow water area where non-linear interaction is not negligible and complicates the understanding of the processes, and the sea level variations, compared to the deep ocean dominated by linear dynamic. For propagation of long ocean waves onto shelves the wave velocity decreases with depth because of the dependency in the phase velocity on the square root of the depth. The decrease in the wave speed reduces the wave lengths and by that the horizontal scales of the waves. Quasi-conservation of the momentum will enhance the vertical elevations of the waves for propagation from the deep ocean to a shelf area. The shelves do therefore make up an area for testing the ability of the altimetry observations to resolve the strong tidal signal on relatively small horizontal scales. Previous work have investigated tidal signals derived from altimetry observations in the North Sea and adjacent seas. *Woodworth and Thomas* (1990) found promising results of the northwest European continental shelf for the two major semi-diurnal tidal constituents, M_2 and S_2 , with altimetry data from the early GEOSAT satellite mission. Also observations from the ERS-1 and T/P missions have provided impressive results for the major tidal constituents in the North Sea (*Andersen*, 1994, 1995). Recently *Andersen* (1999) has shown that shallow water tidal constituents can be resolved in the North Sea from T/P observations, despite the small horizontal scale and large spatial variability in those constituents.

The objectives for this PhD project have been to obtain new knowledge about sea level changes in the North Sea area by combining the different available sources of sea level information provided by altimetry, tide gauges and numerical models. The sea level changes that have been investigated are variations with time scales on hours to years. Specifically, the different contributions to the sea level changes from the tidal elevations, the atmospherically induced surges, and the interaction between these processes have been highlighted. To investigate the performance of the altimetry observations in a near-coastal area a bottom pressure instrument was deployed by the GEOSONAR project. The instrument was deployed approximately 50 km off the Danish North Sea coast for validation of the altimetry observations in a highly shallow water area, but away from the coast where the radar signal may be falsely influenced by the sea-land border. New and improved estimations of the oceanic "noise" signal in the altimetry derived sea level height in the North Sea area will contribute to the GEOSONAR project by improving the determination of the mean sea surface in the North Sea.

1.2 Structure of This Thesis

This thesis contains first a short introduction in Chapter 2 about the available sources of sea level information from coastal in-situ tide gauge data, satellite altimetry, and numerical model simulations. In Chapter 3 is given an introduction to tidal theory and tidal analyses with focus on shallow water tides. Changes in the main tidal constituents on an annual time scale have been known for a long time from tide gauge observations. The altimetry observations provide new knowledge about the spatial behaviour of this formerly coastal-observed phenomena. This new knowledge has resulted in new investigations with numerical models within this PhD project, and have resulted in an improved overall understanding of the main part of the signal. These investigations and results are described in Chapter 4. In Chapter 5 an introduction is given to the atmospherically induced sea level changes caused by atmospheric pressure systems (both quasi-stationary and non-stationary), and the wind effect. As a special illustration of how the atmospheric influence may cause severe and abrupt sea level changes - for the Danish area - the situation in the North Sea at July 21. 1998 is described in Section 5.4. In Chapters 6 and 7 are described the obtained results from validation of the altimetry and the numerical simulations with the coastal tide gauges and the deployed off-shore instrument. Validation of the tidal constituents, and the atmospheric influence on the tides are described in Chapter 6, and the results about the sea level variability are described in Chapter 7 with focus on the near-coastal performance of the altimetry observations. A discussion of the obtained results and future applications for use of altimetry data in an operational ocean model is described in Chapter 8. Derivations of equations, and additionally plots and tables supporting the text are attached in Appendix A – E, and the paper *Seasonal variations in the tidal constituents from altimetry data* submitted to Geophysical Research Letters in June 2000 is attached in Appendix F.

Chapter 2

Sea Level Information

The sea level and sea level variations are measured by coastal tide gauges mainly located in harbour basins. Additionally, off-shore instruments are deployed for shorter time periods to provide information for the off-shore area, but the off-shore area is still extremely poorly covered. The altimetry observations with a nearly global coverage have therefore provided valuable new information for the off-shore area, despite the sparse time sampling of several days up to a month. In addition to the observations, information about the sea level can be obtained from numerical simulations. The main objectives for doing model simulations are the feasibility to make predictions for the sea level and to investigate the effect from different causes, by including or excluding the processes of interest. The model results have previously been validated with the coastal tide gauges, but the altimetry observations that have become available for the last decade have made additional and improved validations of the models possible.

For absolute validation of the different sources of sea level information care must be taken due to the different sea level reference systems. The tide gauges measure the sea level relative to land and includes land movements, whereas the altimetry observations measure relative to the center of the earth. The sea level measured by tide gauges are often leveled with respect to a national reference system.

In this Chapter tide gauges and the information that can be obtained by time series analyses will be shortly described followed by a short introduction to altimetry and the correction terms applied to the signal before the sea level height can be obtained. Last in this Chapter the models applied in this study are shortly described.

2.1 Tide Gauges

Different systems are in operation for measuring the sea level. The Danish tide gauge network operated by DMI consists currently of different systems. Most frequently used is an instrument with a float in a well located in the harbour basin. The well with a diameter of 1.25 m is connected to the water in the harbour basin by a pipe with a diameter of 0.1 m to prevent the effects from high frequency wind waves to propagate into the well. For the well gauges the float measures the instantaneous sea level in the well with an accuracy of 1 cm at a sampling interval of

15 min. The absolute measure of the sea level is referenced to the common reference level Dansk Normal Nul (DNN) for all the stations by leveling. DNN is defined as the level of the weighted means of the mean sea level for ten sea level stations (Esbjerg, Hirtshals, Frederikshavn, Århus, Fredericia, Slipshavn, Korsør, Hornbæk, København and Gedser). The fix point in the DNN system is a point in Århus cathedral. Accurate measurements of the land movements at the tide gauge locations are crucial, and especially for climate studies of long sea level records. One disadvantage to the well/float tide gauge system is the possibility of fresh water to be trapped inside the well. This may cause errors in the sea level measurements of up to several cm for stations at locations with large density variabilities. A replacement of the float instruments at the Danish stations to new CTD instruments is currently taking place.

Sea level information around the North Sea coast have been obtained for this study by tide gauge data provided by the different national authorities. The locations of these tide gauges are shown in Figure 2.1.

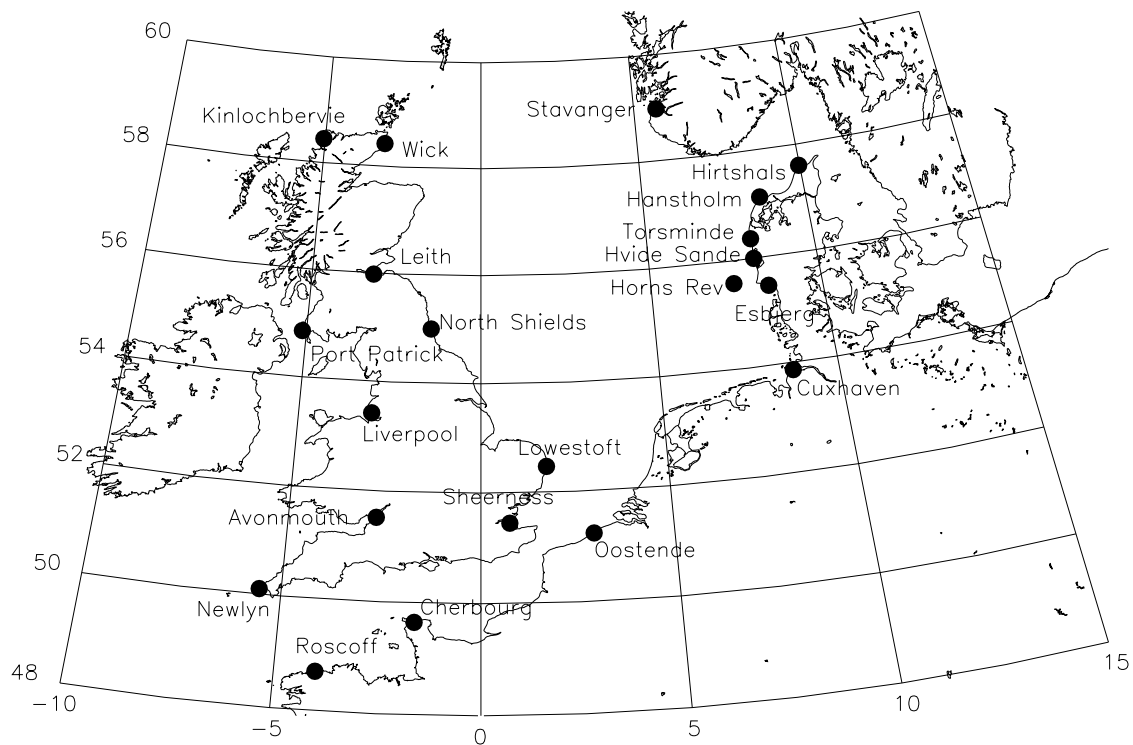


Figure 2.1: Location of tide gauges around the North Sea used for this study.

2.1.1 Time Series Analyses

The long records and the high time resolution cause tide gauge observations to contain high quality sea level information on a broad range of time scales. As tide gauges sample the sea level

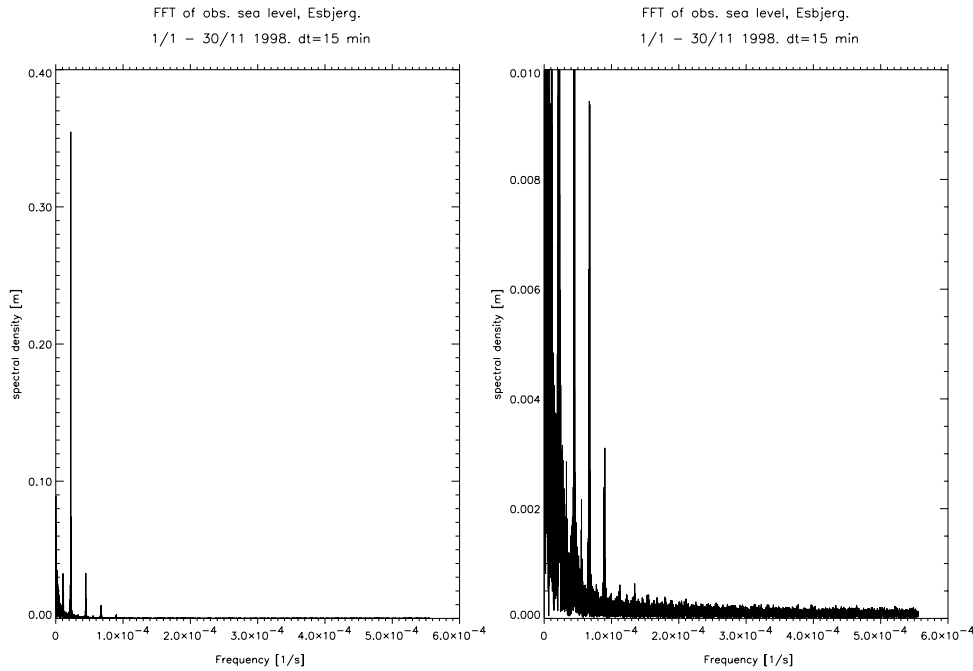


Figure 2.2: *FFT analysis of 15 min sampled sea level data from Esbjerg, Denmark.*

variations in the time domain, information in the frequency domain can be obtained by making Fourier transformations of the sea level time series. The lowest frequency that can be resolved is determined by the length of the time series T , and is named the fundamental frequency $f_{min} = \frac{1}{T}$. The highest frequency that can be resolved, the Nyquist or critical frequency, is given by $f_c = \frac{1}{2\Delta t}$, where Δt is the sampling interval. The number of sampled data points in the time domain defines the maximum number of independent frequencies that can be resolved. For a complete bandwidth time series within the Nyquist frequency limit, i.e. that no spectral energy occurs at frequencies higher than f_c , the discrete samples will completely describe the function. However, the energy in the sea level time series are not in general completely bandwidth within the Nyquist frequency limit, and all the spectral energy that lies outside this frequency limit will be falsely translated - aliased - into the frequency domain $f < f_c$. To estimate the effect of aliasing in tide gauge data an example with data from Esbjerg is shown in Figure 2.2. The Nyquist frequency is for this analysis $f_c = 1/(2 \times 15 \text{ min}) = 5.56 \cdot 10^{-4} \text{ Hz}$. To the left in Figure 2.2 is shown the spectral energy [m] for the positive frequency spectrum, and to the right a close up of the lower frequency part. A significant dominance with a peak of 0.355 m occurs at the frequency $f = 2.236 \cdot 10^{-5} \text{ Hz}$, corresponding to an amplitude of 71 cm at the semi-diurnal M_2 tidal period ($T = 12.42 \text{ hours}$) in the time domain. The sea level signal in Esbjerg is seen to be dominated by tidal variations at semi-diurnal, diurnal, and fourth-diurnal periods, but also with a relative large amount of energy in the low frequency range. Less than 0.1% of the total energy is located at frequencies $|f| > 1.0 \cdot 10^{-4} \text{ Hz}$. As a tide gauge instrument is working as a low pass filter and not measuring sea level variations in the high frequency range, such

as wind induced small scale waves, there is no reason to believe that tide gauge measured sea level data should contain significant energy at frequencies higher than the Nyquist frequency at $f_c = 5.56 \cdot 10^{-4}$ Hz, and therefore aliasing in sea level analyses is seen to be of minor significance. Furthermore it is seen that sea level data with a sampling time of 1 hour ($f_c = 1.4 \cdot 10^{-4}$ Hz) may not introduce a significant aliasing problem either.

The autocorrelation of the sea level data is another way to estimate the dominating time periods and persistencies in the signal. In Figure 2.3 is shown the autocorrelation for 3 years of tide gauge data (1993-1995) from Esbjerg for the total sea level signal to the left and for the residual signal (the sea level minus the estimated tidal signal) to the right. The correlation in the signal is shown for time lags up to 30 days (720 hours). The semi-diurnal tidal signal is clearly seen to dominate the sea level signal, and also the tidal fortnightly and monthly periods are seen. Other processes than the tidal variations are only possible to detect in the residual signal, where a large correlation is seen up to a time lag of several days mainly caused by the persistence of the meteorological systems. After approximately 4 days the correlation coefficient is less than $r=0.2$. For a time lag of nearly 10 days, which is the sampling time of the T/P altimeters the correlation of the residual signal is small.

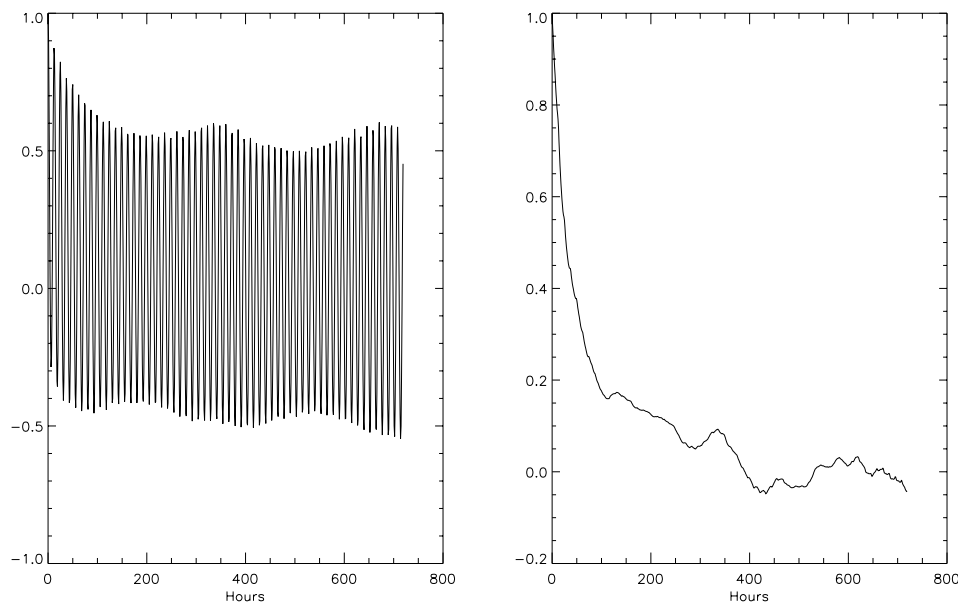


Figure 2.3: *Autocorrelation of the sea level signal (left) and residual signal (right) for 3 years of tide gauge data from Esbjerg.*

2.1.2 Pressure Instrument at Horns Rev

An off-shore tide gauge station has been deployed in the eastern North Sea by the GEOSONAR project. The off-shore instrument was established with the objectives to identify and investigate

any local effects on the sea level variations obtained from the existing on-shore tide gauges, and to validate the T/P altimetry observations in a near coastal area in the North Sea. The deployed off-shore instrument is a pressure instrument and measures at the sea bed the total pressure above the instrument, the temperature and the conductivity. The optimal location for the off-shore station would have been at a satellite cross-over between two paths for the T/P radar altimeters. However, to facilitate data collection and to minimize the risk for the instrument to disappear due to trawling, it was decided to establish the new off-shore station close to an existing buoy, and the buoy at Horns Rev, operated by The Royal Danish Administration of Navigation and Hydrography was chosen. The Horns Rev buoy at (55° 34.519' N; 07° 26.140' E) is located approximately 34 km NE of the nearest T/P satellite cross-over point. The instrument was placed at the bottom at approximately 22 m depth, and pressure data are sampled every 15 minutes. The station was established August 26, 1997. Inspection and data collection of the station was performed by The Royal Danish Administration of Navigation and Hydrography. At data collection the instrument was picked up and a new instrument is re-mounted. It is not possible to place the instrument at the exact same position and these slightly different positions of the instruments may affect the results when data from more than one period are analysed. The station was inspected each fourth month for data collection. The third inspection in August 1998 turned out un-successfully, as it was not possible to find the instrument. The data from the off-shore station at Horns Rev do, therefore, only cover the two periods:

1. period: August 26. 1997 - December 4. 1997
2. period: December 4. 1997 - April 29. 1998

Data is missing for the period 24/9 - 2/10 1997. An off-set in the calculated sea level from the 1. period to the 2. period shows that the new re-mounted instrument was placed at a slightly different position at 15-20 cm less water depth than during the 1. data period. A description of the sea level calculations from the pressure observations is found in Appendix A, and the obtained results from Horns Rev are described in Chapter 7.

2.2 Altimeters

A satellite altimeter measures the nadir round-trip travel time from the emission to the receiving of a radar pulse. Knowing the travel time and the radar signal velocity the sea surface height η relative to the geoid can, as seen in Figure 2.4, be deduced from

$$\eta = H - h - N - E, \quad (2.1)$$

where H is the total height of the satellite relative to the earth's center of mass, h the measured distance from the satellite to the surface, E the distance from the earth's center to the reference ellipsoid, and N the height of the geoid above the reference ellipsoid.

The altimetry data used in this study are from the T/P mission. The T/P satellite was launched in August 1992 as a joint American-French research project. The T/P satellite circles the earth at an altitude of about 1300 km above the surface and covers the surface of the earth from 66° S - 66° N with a repeat period of 9.9 days, and a ground track spacing at equator of 316 km \pm 1km. A detailed overview of the T/P mission can be found in *Fu et al.* (1994). The ground

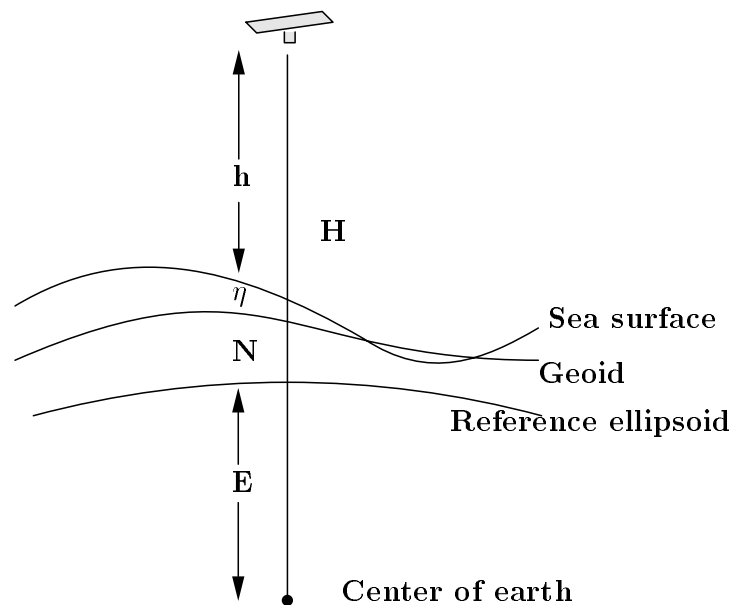


Figure 2.4: *The measurement principle in altimetry.*

track for the T/P satellite in the North Sea is shown in Figure 2.5. The data sampling interval of nearly 10 days gives that ocean signals of periods less than approximately 20 days are aliased into longer periods.

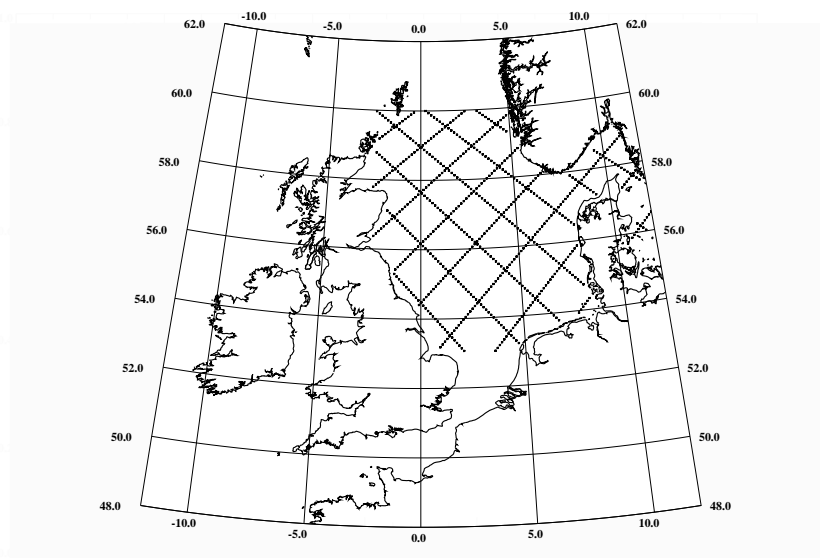


Figure 2.5: *Ground track for the T/P satellite in the North Sea.*

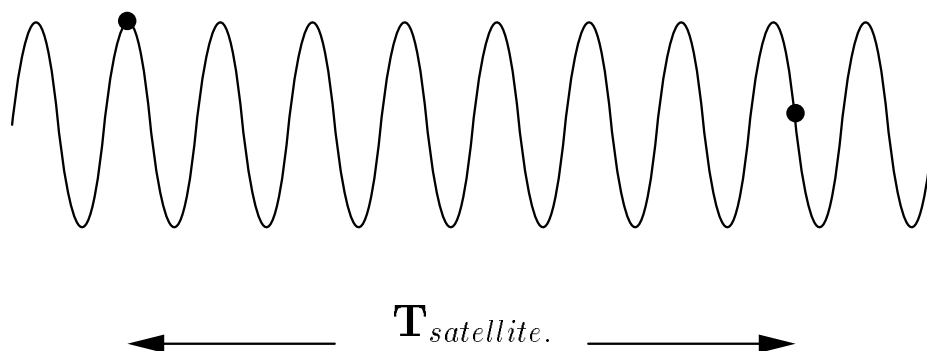


Figure 2.6: *The principle in observing tidal information from an altimeter. The black dots indicate altimeter observations. From these altimeter observations with a much larger repeat period than the tidal period of interest, the tidal signal can be resolved by the information from the alias period.*

The alias period i.e. the minimum time period needed for sampling a tidal constituents by an altimeter is intuitively seen from Figure 2.6 and is obtained by estimating the shift in the phase lag Δg from two subsequent samplings by the altimeter at the repeat period $T_{altimeter}$

$$T_{alias} = \frac{2\pi}{\omega_{alias}} = \frac{2\pi}{\Delta g/T_{altimeter}}$$

The T/P altimeter will for the M_2 constituent with a period of 12 h 25 min observe a phase lag of 58° between two subsequent samplings with the repeat period of 9.91 days, resulting in a minimum of 62 days needed for the T/P altimeter to resolve the M_2 signal. In Table 2.1 is shown the alias periods for some of the other important tidal constituents for the North Sea (Andersen, 1995, 1999).

Constituent	Alias periods [days]
K_1	173
O_1	46
P_1	89
Q_1	69
M_2	62
S_2	59
N_2	50
M_4	31
MS_4	1089
M_6	21

Table 2.1: *Alias periods for some diurnal, semi-diurnal and shallow water tidal constituents from the T/P observations (after Andersen (1995, 1999)).*

2.2.1 Signal Corrections

It requires knowledge and measurements of a variety of different processes to obtain accurate measurements of the sea surface height observed from space. References are here mainly given to *Fu et al.* (1994); *Wunsch and Stammer* (1998), where reviews can be found of the different corrections and further references. First of all an accurate measure of the sea surface elevation requires accurate measures of the satellite orbit and the geoid. At the T/P mission a precise orbit determination is obtained by using three different systems such as a laser system, a ground-beacon Doppler system, and the GPS. The orbit error is currently estimated to be of approximately 2 cm (*Wunsch and Stammer*, 1998). The geoid is removed from the observations by applying a gravity field model.

Besides the orbit and geoid determinations, corrections have to be applied to the radar signal due to the propagation through the ionosphere and atmosphere. The speed of electromagnetic radiation is weakened by the index of refraction of the medium, and the speed of the radar signal will be modified by the content of free electrons in the ionosphere, and the water vapour in the troposphere. The content of the free electrons is corrected for by application of a dual frequency altimeter, and the water vapour is directly measured by a three frequency microwave radiometer. The radar signal is also delayed by the dry air mass in the troposphere, and sea level atmospheric pressure fields obtained from the European Centre for Medium-Range Weather Forecast (ECMWF) are used to correct for this signal modification. The corrections of each of these signal modifications are of the order of 1 cm (*Wunsch and Stammer*, 1998; *Fu et al.*, 1994).

The interference of the radar signal with the sea surface introduces further modifications of the obtained signal. The footprint of the radar signal is of 6-7 km at the surface and the backscattered signal depends on the curvature of the surface. Waves in the ocean do not in general have a symmetric form, but more a cnoidal form with longer wave troughs than crests, and the troughs will therefore dominate in the backscattered signal. This is named the electromagnetic bias or sea-state bias. Furthermore the roughness of the surface due to the wind will reduce the backscattered signal. More work still need to be done to obtain an accurate estimate of these surface effects (*Wunsch and Stammer*, 1998).

For studies of the general non-tidal ocean current systems the tidal signal has to be removed from the observations. Tidal signals are introduced into the observations from the ocean tide, the solid earth tide, the atmospheric tide and tidal loading, with the ocean tide as the dominating contribution. The ocean tidal contribution is removed by information from high accurate global tidal models that have been developed and highly improved by the use of altimetry observations. Also a correction to removal of the atmospheric load or the inverse barometer effect is an option for the altimetry users. This correction is made from global sea level pressure fields obtained from the numerical weather simulations provided by ECMWF.

The overall data accuracy of an absolute observation of the sea surface height from the T/P altimeters is estimated by *Fu et al.* (1994) to be of 4.7 cm. Further information about the altimeter signal corrections can be found on the URL:

<http://neptune.gsfc.nasa.gov/~krachlin/opf/algorithms.html>.

2.3 Hydrodynamical Models

The numerical simulations performed within this study have been made with the hydrodynamical model Mike 21 developed at the Danish Hydraulic Institute (DHI) and used at DMI in the operational storm surge warning system.

During a half year visit at the Proudman Oceanographic Laboratory (POL), U.K., model simulated sea level results were available for several years of integration. In addition to the Mike 21 runs, results from a 2D and a 3D model, both developed at POL, have been used for the investigations of the seasonal signal in the tidal constituents described in Chapter 4.

2.3.1 The Mike 21 Model

Mike 21 is a 2D model solving the depth integrated shallow water equations for momentum and mass. The equations are solved as finite differences on an Arakawa C grid (DHI, 1998). The model enables a nesting facility and all the Mike 21 simulations have been run with the set-up shown in Figure 2.7. The large domain has a resolution of 9 nautical miles (n.m.) i.e. 16.668 km. A subdomain with a finer resolution of 3 n.m. (5.556 km) has been included for the transition zone between the North Sea and the Baltic, and a subdomain of 1 n.m. (1.852 km) for the internal Danish waters. Additionally, a subdomain with a resolution of 1 n.m. has been included for the Wadden Sea.

The eddy viscosity in the model has been resolved using a Smagorinsky eddy formulation with a constant value of 0.3 (non-dimensional). For the bed friction the Manning number formulation has been used as it provides a depth dependent bed friction F_b given as

$$\mathbf{F}_b = \frac{g}{M^2 h^{1/3}} |\mathbf{V}| \mathbf{V}, \quad (2.2)$$

where \mathbf{V} is the horizontal velocity vector, h the water depth, and M [$\text{m}^{1/3}/\text{s}$] the Manning number. A typical value of the Manning number for the North Sea area is in the interval M 30-50 $\text{m}^{1/3}/\text{s}$.

The tides and meteorological forcing used in the simulations are described in detail in Chapter 6 in relation to the model results.

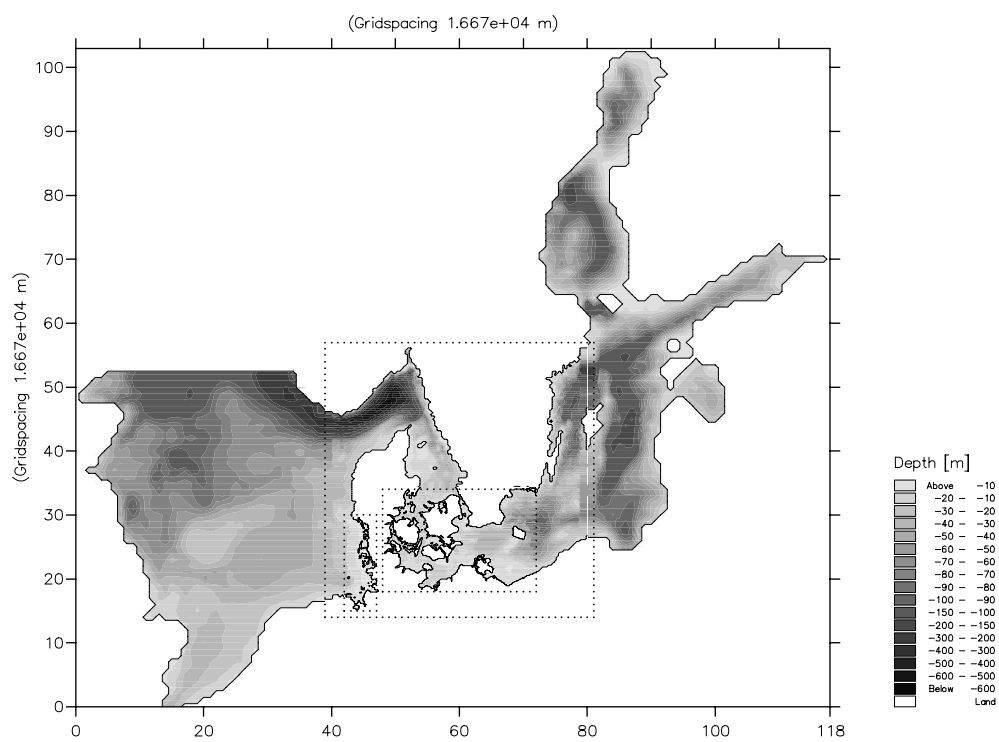


Figure 2.7: *Mike 21* set-up used for the model simulations described in Chapter 6.

Chapter 3

Tides

The tides on the earth are caused by the gravity from the moon and the sun. Effects from other planets and stars are negligible. Despite the much larger mass of the sun the contribution from the moon makes up about twice the contribution from the sun. This is due to the inverse square dependence on the distance in the gravity force, and the much shorter distance to the moon from the earth. The tidal force on the earth originates from the small force difference between the gravity force and the centrifugal force. The centrifugal force caused by the rotation of the system, i.e either the earth-moon or the earth-sun system, is a fictitious and homogeneous force with a uniform distribution over the earth, whereas the gravity force is non-homogeneous depending on the distance to the causing object. This force difference results in a small tidal force everywhere on the earth, except at the center of mass where the two forces are balanced. The tidal force is illustrated in Figure 3.1 for the earth-moon system. The vertical component of the tidal force is small compared with the earth's gravity, and it is therefore mainly the horizontal component that forces the water masses to move, and generate the long tidal waves that causes the sea level to rise and fall. The dominance of the semi diurnal tide is due to

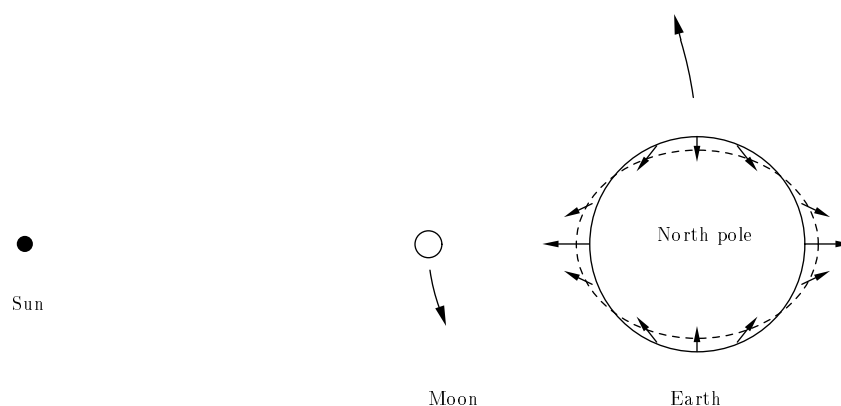


Figure 3.1: *Illustration of the tidal force on the earth. The equilibrium tide is indicated as the dotted line.*

the rotation of the earth. The theoretical elevation of the sea surface that would result if the earth was totally covered by water, and the water had negligible inertia, and therefore respond instantaneously to the tidal force, is defined as the *equilibrium tide*. The observed tide in the ocean differs from the equilibrium tide, but the equilibrium tide serves as an important reference for calculating the real tide. The equilibrium tide is indicated in Figure 3.1 by the dotted line (the magnitude is exaggerated). The real tide is complicated by the waters non-instantaneous response to the tidal force, and the existence of the continents that prevent the propagation of the tidal waves around the earth. The calculations of the real tide on the earth are further complicated by the positions of the sun, the moon and the earth in different geometric planes, the mutual movements of these planes, and the altering of the mutual distances.

The tides in the North Sea are dominated by two tidal waves propagating into the region from the northern Atlantic through the Channel, and through the northern entrance between Scotland and Norway. These two waves propagate cyclonically around in the North Sea as Kelvin waves. The local tidal force acting on the water masses inside the North Sea also generates a contribution to the tide in the North Sea. However, simulations have shown that the tides in the North Sea can be sufficiently simulated without inclusion of the tidal potential, as the uncertainty in the tidal waves on the open boundaries are of the same order of magnitude as the local generated contribution (*Verboom et al.*, 1992). It is therefore common practice to neglect this local contribution in hydrodynamical simulations of the North Sea.

The regular rise and fall of the sea level has been studied for several centuries. A major contribution to the tidal studies was made in the 17. century by I. Newton with his understanding of the gravity forces. The nomenclature used today was mainly introduced by A. Doodson, who provided a complete algebraic formulation of the tidal potential (*Doodson*, 1921). Important extensions and recalculations of the tidal potential by using Fourier analyses was carried out by *Cartwright and Taylor* (1971); *Cartwright and Edden* (1973).

In this chapter a short introduction to tidal analysis will be given with the focus on the treatment and solution of the shallow water constituents in tidal analysis programmes.

3.1 The Tidal Potential and the Equilibrium Tide

The tidal potential at a point on the surface of the earth is fully given by

$$\begin{aligned} \Omega_{tidal} = \Omega_{moon} + \Omega_{sun} = & \frac{GMa^2}{R_m^3} \sum_{j=2}^{\infty} \left(\frac{a}{R_m}\right)^{j-2} P_j(\cos \zeta_m) \\ & + \frac{GSa^2}{R_s^3} \sum_{j=2}^{\infty} \left(\frac{a}{R_s}\right)^{j-2} P_j(\cos \zeta_s) \end{aligned} \quad (3.1)$$

where G is the gravity constant, a the radius of the earth, M and S is the mass of the moon and the sun, respectively, R_m and R_s the distance to the moon and the sun, respectively, and ζ_m and ζ_s the “latitude” angle for the observation point to the plane for the moon and the sun, respectively. The P_j ’s are Legendre polynomials. The tidal potential caused by the moon can

Variable	Description	Period of variable	Corresponding frequency
τ	The lunar day	$T=1.04$ days	ω_1
s	The sidereal month	$T=27.3$ days	ω_2
h	The tropical year	$T=365.24$ days	ω_3
p	The moon's perigee	$T=8.85$ years	ω_4
N'	The regression of the moon's nodes	$T=18.6$ years	ω_5
p'	The perihelion	$T=20\ 942$ years	ω_6

Table 3.1: *Doodson's astronomical variables (given as phases) and the corresponding periods and frequencies for the astronomical motions.*

be calculated to be 2.1 times the tidal potential from the sun (see for instance *Godin (1972)*). Instead of the dependence on the actual position of the observation point with respect to the moon and the sun (i.e. ζ_m and ζ_s), *Doodson (1921)* transformed the dependent variables into six variables describing the astronomical motions. These six fundamental astronomical variables are listed in Table 3.1. All six variables are given as phases relative to the Greenwich meridian. The motions of the moon around the earth and the earth around the sun can be described by two ellipses. Ellipses are described by their periods and their axes, or the eccentricity. The six variables listed in Table 3.1 are the periods of the two ellipses s and h for the moon's orbit around the earth and the earth's orbit around the sun, respectively. The distances in the ellipses are represented by the perigee p and the perihelion p' , where the moon is closest to the earth and the earth is closest to the sun, respectively. Further the rotation of the earth is included as the lunar day τ , and the intersection of the two ellipses N' .

The tidal potential can be expressed in terms of the latitude of the observation point θ , and these six basic astronomical variables, as (truncated at $j = 4$) (*Godin, 1972*)

$$\Omega_{tidal} = \sum_{i_0=0}^3 \left[G_{i_0}(\theta) \sum_{j_0 k_0 l_0 m_0 n_0}^{-6,6} A(j_0, k_0, l_0, m_0, n_0) \times \cos(V(t)) \right. \\ \left. + G'_{i_0}(\theta) \sum_{j_0 k_0 l_0 m_0 n_0}^{-6,6} B(j_0, k_0, l_0, m_0, n_0) \times \sin(V(t)) \right] \quad (3.2)$$

where

$$V(t) = i_0\tau + j_0s + k_0h + l_0p + m_0N' + n_0p'$$

is the astronomical argument (phase), and the integers $i_0, j_0, k_0, l_0, m_0, n_0$ are named the Doodson numbers. The $G(\theta)$ and $G'(\theta)$ are the geodetic coefficients. The A 's and B 's are the amplitudes in the tidal potential. The tidal potential in Eqn. 3.2 has been truncated at $j = 4$ compared with Eqn. 3.1.

The Doodson numbers have values in the range $[-6,6]$. The astronomical argument can to a

first order approximation with respect to time be written as

$$V_n(t) = V_n(t_0) + \frac{\partial V_n(t)}{\partial t} \Delta t = V_n(t_0) + \omega_n \Delta t. \quad (3.3)$$

where t_0 is a reference time for calculations of the astronomical argument, and Δt is given relative to t_0 . Each set of the Doodson numbers $(i_0, j_0, k_0, l_0, m_0, n_0)$ defines a constituent and corresponds to a frequency in the tidal potential given by

$$\omega = i_0\omega_1 + j_0\omega_2 + k_0\omega_3 + l_0\omega_4 + m_0\omega_5 + n_0\omega_6. \quad (3.4)$$

The tidal potential defines a line spectrum with an infinite number of constituents, and for all data analyses only a small part of the constituents will be resolved. Constituents with equal i_0 are named *species*, and are separated in the frequency band by 1 cycle/day. Constituents having equal i_0 and j_0 are named a *group*, and neighbouring groups are separated in the frequency band by 1 cycle/month. Constituents with equal i_0 , j_0 and k_0 are named a *cluster*. The constituent with the largest amplitude calculated from the tidal potential gives the name to the cluster. The other constituent members in the cluster are named *satellites*. Clusters are separated in the frequency band by 1 cycle/year.

The elevation of the sea surface in equilibrium with the tidal forces - the equilibrium tide - is a level surface $\bar{\eta}$ for the resulting force from the gravity and the tidal force. The equilibrium tide can be directly expressed in terms of the tidal potential from the definition of the equilibrium tide, as $g\bar{\eta} + V_{tidal} = 0$. The equilibrium tide serves as a very important reference system in tidal analysis, as it enables the calculations of the relative importance among the huge amount of constituents, and is used as basic knowledge in the tidal analyses. The continents, the finite water depth and the inertia in the water masses prohibit the existence of the equilibrium tide with long waves propagating unimpeded around the world. For the deep and open oceans the equilibrium tide does however indicate the range of the tidal constituents. For the largest two constituents, the semi-diurnal constituent caused by the moon M_2 and the sun S_2 , the amplitudes calculated from the equilibrium tide are 26 cm and 12 cm, respectively, and the combined effect of these two constituents that account for a large part of tidal range gives a maximum amplitude of 39 cm at new and full moon, and a minimum amplitude of 14 cm at the moon's quarter. The real tide will for many locations, and especially for on-shore locations, differ significantly from the equilibrium tide, and for accurate tidal predictions analyses of sea level data recorded at the considered location are necessary.

3.2 Harmonic Analysis

The harmonic analysis technique is the most common used analysis package for studying the tides. The tidal analyses performed within this study have been carried out by using the harmonic analysis package *Tidal Analysis Software Kit* developed at POL, U.K. (*Bell et al.*, 1999) and the *Tidal Heights Analysis and Prediction* package developed at Institute of Ocean Sciences, Victoria, B.C. Canada (*Foreman*, 1977).

In the harmonic analysis it is assumed that the tidal variations in the ocean $T(t)$ can be represented by a finite sum N of harmonic terms with frequencies determined from the equilibrium

tide

$$\begin{aligned}
 T(t) &= \sum_{n=1}^N A_n(t) \cos(\sigma_n t - \phi) \\
 &= \sum_{n=1}^N H_n f_n(t) \cos(\omega_n t - g_n + V_n(t_0) + u_n(t))
 \end{aligned} \tag{3.5}$$

where H_n is the unknown amplitude of the n 'th constituent and g_n the unknown phase lag at the actual location. The phase lag g_n is measured relative to the phase lag of the equilibrium tide $V_n(t_0)$ that is defined relative to the Greenwich meridian. The choice of the reference time t_0 varies from different analyses packages. The frequency ω_n for each constituent is given from the equilibrium tide (Eqn. 3.4). The f_n and u_n are named nodal modulations, and are small adjustment in the amplitude and phase, respectively. They are introduced due to the presence of satellites with frequencies ω_4 and ω_5 , which are not included in the analysis due to the limited time range of the data record. The modulation of the included constituents caused by these two frequencies (with the corresponding periods $T=8.85$ years and $T=18.6$ years) are corrected for by the inclusion of f_n and u_n calculated from the equilibrium tide. Effects from the frequency ω_6 are always neglected in a sea level analysis, as the changes in the perihelion has a period of about 21 000 years. The derivations of the f_n and u_n will be shortly described in Section 3.2.1. Assuming that the number of observations is larger than the number of unknowns (i.e the amplitudes and phases for the constituents to be included in the analysis) the system to be solved is seen to be over-determined. The most common optimization criterion is the least squares method, and the unknown amplitude and phases for the wanted constituents are computed by solving $\sum \text{residual}^2 = \text{minimum}$, where the residual is given by the computed tidal contribution subtracted from the observed sea level. The numbers and choice of constituent to include in the analysis will be shortly described in Section 3.5.

3.2.1 The Nodal Modulation

The amplitudes and phases calculated from the harmonic analysis are the accumulated amplitudes and phases from all the constituents in each cluster; both the main constituent and the satellites due to the unresolved frequencies ω_4 and ω_5 . To get the wanted numbers for only the main constituent the f and u factors were introduced in Eqn. 3.5. The amplitude of the total cluster can be approximated by (following *Godin* (1972))

$$a_n \approx a_{n0} + \sum_{j=1}^m a_{jn} \tag{3.6}$$

where m is the number of unresolved satellites in the cluster. The definition of the main constituent is $|a_{n0}| \gg |a_{jn}|$, and the amplitude of the total cluster can be approximated to

$$a_n \approx f_n a_{n0} \tag{3.7}$$

The amplification f_n of the main constituent is calculated from the assumption that there exists the same relationship between the different constituents in the equilibrium tide as in the actual

tidal response in the ocean (*Godin, 1972*)

$$a_{jn} = c A_{jn} \quad (3.8)$$

where the a_{jn} 's and the A_{jn} 's are the amplitudes in the real tide and the equilibrium tide, respectively. The nodal modulations in the amplitude are then given by

$$f_n = 1 + \sum_{j=1}^m \frac{a_{jn}}{A_{n0}} \quad (3.9)$$

The nodal modulation of the phase, u_n in Eqn. 3.5 is the angle between the vectors for the main constituent and the total cluster.

For low frequency constituents, with periods larger than diurnal, the low frequency noise may be up to an order of magnitude larger than the nodal modulations, and in some harmonic analysis packages the low frequency constituents are therefore not corrected with the nodal modulations (*Foreman, 1977*).

3.3 Response Analysis Method

The harmonic analysis method is not using the smoothness in the system, displayed by the fact that the ocean tends to make a smooth respond to adjacent tidal frequencies. In the harmonic analysis all the constituents are treated independently even for constituents close in the frequency band. The smoothness is only used in the nodal modulations. *Munk and Cartwright (1966)* pointed out this disadvantage, and introduced the Response Analysis Method that includes this inherent smoothness of the tidal system.

In the Response Analysis Method an admittance function calculates the ocean tide at every location directly from the tidal potential as input. *Munk and Cartwright (1966)* transformed the tidal potential into spherical harmonics, and the tidal variations in the ocean is calculated as a weighted sum of these spherical harmonics (*Munk and Cartwright, 1966*)

$$T(t) = \sum_{m,n} \sum_{s=-S}^{s=S} \left[u_n^m(s) a_n^m(t - s\Delta t) + v_n^m(s) b_n^m(t - s\Delta t) \right]$$

where the input to the response function is the time dependent part of the tidal potential expressed in terms of spherical harmonics (*Munk and Cartwright, 1966*)

$$\Omega_{tidal} = g \sum_{m,n} \left[a_n^m(t) U_n^m(\theta, \lambda) + b_n^m(t) V_n^m(\theta, \lambda) \right]$$

and the response in the ocean, i.e the weights, are given by (*Munk and Cartwright, 1966*)

$$w(s) = u_n^m(s) + i v_n^m(s)$$

θ and λ are spherical coordinates, and $S\Delta t$ the maximum time lag to be included. The weights are calculated, as the amplitudes and phases in the harmonic analysis method, from the least

square method by minimizing the \sum residual², where the residual is the observations minus the tidal computations. The weights have in principle to be calculated at each locality. One of the advantages of the Response Analysis Method is that the tides can be predicted with less tidal constituents as input than in the harmonic analysis method (*Pugh, 1987*). The Response Analysis Method has been demonstrated to have an advantage in analyzing short tidal records (*Groves and Reynolds, 1975*). *Amin (1976)* found that the Response Analysis Method was able to separate small perturbations from the primary constituent, but on the other hand, not able to further separate the perturbation into eventually different contributions. One disadvantage of the Response Analysis Method is the non-unique determination of the weights in the admittance function, and the Response Analysis Method has not been used for tidal analyses of the tide gauge data within this study.

3.4 Shallow Water Tides

In the deep ocean the equations of motions are dominated by the linear terms, and the tides are in general linear with a direct correspondence between the generating tidal potential and the real tides. In shallow water areas the non-linearity in the system becomes not neglectable, and results in non-linear interaction between the frequencies. These new frequencies are named shallow water tides.

3.4.1 Shallow Water

In shallow water the governing equation of motion is

$$\frac{\partial \mathbf{V}}{\partial t} + \mathbf{V} \cdot \nabla \mathbf{V} = -\mathbf{g} \nabla \eta - \mathbf{gk} - \mathbf{fk} \times \mathbf{V} - \tau |\mathbf{V}| \mathbf{V}, \quad (3.10)$$

where $\mathbf{V} = (u\mathbf{i}, v\mathbf{j}, w\mathbf{k})$ is the velocity vector, $h(t, x, y) = H(x, y) + \eta(t, x, y)$ the total water depth, f the Coriolis parameter, g the earth gravity and τ the friction parameter. The non-linearity in the system is introduced into the equations by the advective term $\mathbf{V} \cdot \nabla \mathbf{V}$ and the friction term $-\tau |\mathbf{V}| \mathbf{V}$.

The phase velocity for a long wave is in the linear case given by

$$c_f = \frac{uh}{\eta} = \sqrt{gh} \quad (3.11)$$

For the shallow water case, when the wave amplitude may not be ignored compared to the water depth, a Taylor series of the long wave velocity from the linear case (Eqn. 3.11) gives

$$c_f = \sqrt{gh} = \sqrt{g(H + \eta)} = \sqrt{gH} \left(\sqrt{1 + \frac{\eta}{H}} \right) \approx \sqrt{gH} \left(1 + \frac{1}{2} \frac{\eta}{H} - \frac{1}{8} \left(\frac{\eta}{H} \right)^2 \right), \quad (3.12)$$

where H is the undisturbed water depth, and η the surface elevation due to the wave amplitude. The dependence of the wave velocity on the total water depth results in the wave trough being retarded relative to the wave crest and distorts the original wave. This non-symmetrical wave can be approximated by a harmonic wave composed of the original harmonic wave superposed by harmonic waves having twice, triple, fourth etc. frequency of the original introduced frequency (see for instance *Aas (1986)*).

3.4.2 Non-linear Interaction

The non-linear terms in the governing equations will likewise cause shallow water tides to be generated from the frequencies prescribed in the tidal potential. The advection term $\mathbf{V} \cdot \nabla \mathbf{V}$ will for the very simple case with a tidal wave consisting of one harmonic with the frequency ω_1 produce an additional harmonic with the frequency $2\omega_1$. For the still very simple case where the tidal wave consists of two harmonics with the frequencies ω_1 and ω_2 the advection term gives a response made up of the frequencies $2\omega_1$, $2\omega_2$, $\omega_1 + \omega_2$ and $\omega_1 - \omega_2$. The friction term will for a tidal wave consisting of the two frequencies ω_1 and ω_2 generate a response made up of the frequencies ω_1 , ω_2 , $3\omega_1$, $3\omega_2$, $2\omega_1 - \omega_2$, $2\omega_2 - \omega_1$, $2\omega_1 + \omega_2$ and $2\omega_2 + \omega_1$ (see for instance *Godin* (1972)). As an example, the following additional shallow water terms will be produced for the case of a tidal wave consisting of the two major constituents M_2 and S_2 :

from the advection term : M_4, S_4, MS_4 and MS_f

from the friction term : $M_6, S_6, 2MS_2, 2SM_2, 2MS_6$ and $2SM_6$

For a more realistic case where the tidal wave consists of harmonics of several different frequencies a large amount of new shallow water frequencies may be generated. These new shallow water frequencies can be divided into two principal different groups (*Amin*, 1976):

- shallow water constituents having a different astronomical argument compared to all other constituents, and therefore in theory can be separated.
- shallow water constituents which astronomical argument coincide with other existing constituents.

If the first type of shallow water constituents can be separated within the length of the data record, the separation will always improve the tidal analysis and prediction. For the second type of shallow water constituents this will not always be true, as the improvement will depend on the number of perturbing constituents, their magnitude and their nodal variation (*Amin*, 1976). The shallow water generated constituent may have frequencies both in the low and high end in the frequency band, as seen above. In the low frequency range the astronomical constituents may be highly contaminated by shallow water constituents occurring at the same frequencies. The monthly and fortnightly constituent may be contaminated by frequency differences between different diurnal and semi-diurnal constituent. Likewise the annual constituent S_a that also contains the inter annual atmospherically induced sea level variations may interact with the major semi diurnal constituent M_2 . This will be described in Chapter 4.

Also interaction between tides and storm surges are caused by the non-linearity. *Keers* (1968); *Prandle and Wolf* (1978) found that interaction causes a phase shift for the maximum sea level for storm surge cases along the Great Britain. The maximum residual tended to appear on increasing tide, and the magnitude of the interaction was found to have a nearly linear dependence to the storm surge height (*Keers*, 1968).

3.4.3 Linear Superposition

The higher harmonics are in general generated by the non-linear effects, but once the higher harmonics are generated, linear interaction between the tidal wave constituents can complicate

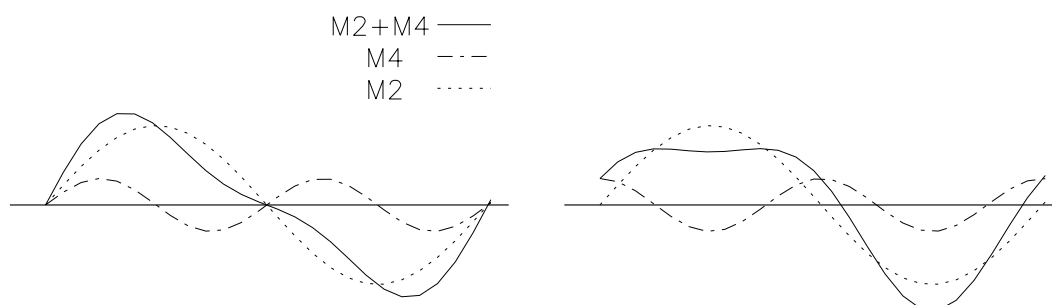


Figure 3.2: A linear superposition of M_2 and M_4 shown for two different phase lag situations (after Pugh (1987)).

the tidal pattern further. A linear superposition of a harmonic and one or more of its higher harmonics can cause disturbances of the harmonic itself. These disturbances may change the symmetrical appearance of the harmonic as for instance double high or low waters depending on the phase difference, but it can never generate new frequencies (Pugh, 1987). This situation is sketched in Figure 3.2 for M_2 and its higher harmonic M_4 . The amplitude of the M_4 constituent has to be at least 25% of the M_2 amplitude for the double highs or lows to occur. The double highs or lows that are observed may therefore often be caused by the combined effect from several shallow water constituents (Pugh, 1987).

3.4.4 The Nodal Modulations

The presence of shallow water constituents may cause distortions in the harmonic analysis method due to the nodal modulations. For calculation of the nodal modulations for the primary tidal constituents, information is used from the equilibrium tide (Eqn. 3.8), but for the shallow water constituents no information are available. The nodal modulations of the shallow water constituents are instead computed as sums of the modulations from the principal constituents the shallow water constituent is derived from. Amin (1976) analyzed tide gauge data from Southend, at the mouth of the River Thames, from a data record exceeding the lunar nodal period of 18.61 years. With this data record Amin was able to calculate the nodal modulations f and u , and found that those values differed from the values calculated from the equilibrium tide, which is the standard values used in harmonic analysis. The reason for the differences is the contamination of the principal constituents by a large amount of shallow water constituents. For instance, for a case where a shallow water constituent is very close in frequency to a main constituent (i.e within the cluster bandwidth) the resultant nodal modulation for the main constituent will be influenced by the energy contribution from the shallow water constituent.

3.5 Choice of Constituent Set

The choice of the constituent set included in a harmonic analysis will affect the result of the tidal analysis, and the ability to find an optimal constituent set is of fundamental importance

for the quality of an analysis. The number of frequencies included in the analysis determines the degree of freedom in the programme during the analysis. The number of constituents in the different frequency bands determines the capacity of the analysis to resolve the energy of the sea level variations in the frequency bands. For the astronomical constituents mainly the length of the time series determines the set of constituents, whereas more information about the specific location of the tide gauge station is needed for an optimal set of the shallow water constituents, with respect to the influence and physics from the non-linearity in the area. The tidal potential is used as basic knowledge when a constituent set is constructed. For a constituent to be included a common used criteria is the Rayleigh criterion that requires a constituent has to be separated by a complete period from its neighbouring constituent over the length of the data before it can be included in the analysis:

$$\Delta T = \frac{1}{|f_1 - f_2|} , \quad (3.13)$$

where f_1 and f_2 are the frequencies of two neighbouring constituents and ΔT has to be less than the length of the data record. The Rayleigh criterion may be too restrictive on locations with only little atmospheric noise in the sea level data. On the other hand constituents located in the frequency band where the noise level is high, for instance in the low frequency range, long time series are required to separate these frequencies from the noise. Constituents not fulfilling the Rayleigh criterion may be included by use of the Related Constituent method, where knowledge from the equilibrium tide is used to determine the amplitude factor and phase lag to a neighbouring constituent, already included in the analysis. The constituents to be included are chosen from the amplitudes in the tidal potential. Each new constituent to be included should be compared to its already included neighbouring constituents, and for constituents of approximately the same magnitude in the tidal potential care should be taken to represent the whole frequency spectra. A shallow water constituent should not be included in the analysis before all its main constituents, from which it is derived, are included in the analysis (*Godin, 1972; Foreman, 1977*).

An optimal constituent set may be constructed from different approaches. One approach is to minimize the residual. An objection to this method is that part of the removed signal may be caused by other phenomena than tides, as for instance quasi periodic atmospheric noise, which may be a problem if the data record is too short to identify this as non periodic. Another often used approach is to look at the stability of different constituents for many years (*Nielsen and Nielsen, 1998; Hvidberg-Knudsen et al., 1994*). The stability criteria can be applied on both the phase and the amplitude of the constituents. An objection to this method is that constituents contaminated by atmospheric noise are excluded from the analysis. For prediction purposes this approach may therefore be of interest, but not for investigations of for instance the non-linear tide-surge interaction, where the minimization of the residual may be preferred. Once a constituent set has been calculated for a specific location it is in principle time invariant. However, in shallow water areas changes in the bathymetry and coastline will highly influence the tidal behaviour, and a constituent set has in that case to be recalculated.

3.6 Internal Tides

In addition to the first mode barotropic tidal waves, higher mode tidal waves named internal tides may exist. The generation of internal tidal waves may happen when a first mode barotropic tidal wave propagates across an abrupt change in the topography in stratified water (see for instance *Foreman et al. (1995)*). The change in the topography may cause a vertical displacement in the thermocline or halocline, and by that results in the generation of an internal tidal wave. The internal tidal waves have much shorter wave lengths than the original first mode tidal wave, as the frequency is a conserved parameter, and the phase velocity of the internal wave depends on the gravity, i.e $\lambda = c_f/f$, where $c_f = \sqrt{g'h}$ is the phase velocity for the tidal wave at a baroclinic mode. The g' is the reduced gravity given by $g' = g \frac{\Delta\rho}{\rho}$, where ρ is the density and $\delta\rho$ the density difference.

Recently, it has been shown that is it possible to detect internal tides with altimetry observations, which may give new knowledge about sources of generation of internal tides, and conversion and dissipation rates (*Ray and Mitchum, 1996*).

Chapter 4

Seasonal Variations in the Main Tidal Constituent

4.1 Introduction

Seasonal variations in the main tidal constituents have been known for a long time. In 1934 R. H. Corkan reported about this phenomenon. Corkan investigated tide gauge data from the station in Liverpool, United Kingdom and observed a smaller amplitude for the tide in the winter period than averaged through the year and larger amplitude in the summer (*Corkan, 1934*). The tide in this area is dominated by the M_2 constituent and to account for this observed annual perturbation of the tides, Corkan suggested to include two small semi-diurnal constituents in the analysis that respectively loses and gains approximately 1° in the phase per day on M_2 . These two constituents appear on each side of the M_2 constituent in the semi diurnal frequency band with the same frequency difference to M_2 , and are named MA_2 and MB_2 (sometimes H_1 and H_2).

By using the response analysis method, *Cartwright (1968)* identified two contributions to the observed annual perturbation of the M_2 constituent. One purely gravitational effect is caused by the influence from the solar parallax on the moons orbit, i.e. the anomalistic year with the period $T=365.2596$ days, and a non-gravitational effect due to the solar declination, i.e. the tropical year with the period $T=365.2422$ days. These two contributions to the annual perturbations in the M_2 constituent will in all practical data analyses be non-separable, but Cartwright made a clear distinction between these two sources and defined the variation due to the anomalistic year as an *annual modulation* and the variation due to the tropical year as a *seasonal modulation*. From the gravity potential *Cartwright and Taylor (1971)* calculated the potential for the constituents MA_2 and MB_2 to be 0.345% and 0.305% of the M_2 potential, respectively. Deviations from these values of the MA_2 and MB_2 constituents are, therefore, caused by other contributions than the astronomical tidal contribution. Variations with observed size of up to several percent of the M_2 amplitude - together with its possible causes - have previously been investigated from coastal tide gauge data mainly located around the United Kingdom. *Baker and Alcock (1983)* investigated the seasonal variations in the main tidal groups from tide gauge data around

the United Kingdom and found variations in the M_2 amplitude of up to 6%, with the largest variations in shallow water areas, and concluded that non-linear dynamics might be the causing factor. They also found variations in the S_2 constituent on an annual time scale and suggested the atmospheric tide to be the causing factor, whereas they suggested variations in the largest diurnal constituent, K_1 to be caused by both on-shore winds and atmospheric tides. *Pugh and Vassie* (1976, 1994) also investigated the seasonal effect in tide gauge data from around the United Kingdom. They found a very systematic variation of the MA_2 and MB_2 phase lags along the east coast, but a non-systematic spatial variation in the amplitudes, and suggested that the seasonal variations were influenced by local effects.

Pugh and Vassie's work on seasonal variations clearly identified the existence of a seasonal signal in M_2 around the British Isles, with a signal varying in strength from zero to more than 6% of the M_2 amplitude, and suggested that the signal was a shallow water effect and might be caused locally. They observed pronounced inter-annual variations and investigated an interaction of sea level with the atmospheric forcing, but no significant correlations were found (*Pugh and Vassie*, 1976, 1994). These investigations of the causing effect were limited by the locations of the observations being mainly from tide gauges placed along the coast or in very shallow water. Observations can be extended beyond this relatively small number of coastal tide gauges to include the large amount of off-shore information that have become available from altimetry. The accuracy of altimetry data has increased in the recent years, and the several years of altimetry data available now is potentially enough to observe these modulations in the M_2 constituent of a few centimeters, providing a large amount of new information. This information would, of course, add a valuable amount of new observations to the relatively limited number of observations from the existing coastal tide gauges, but, more importantly, it would contribute to new knowledge about the spatial behavior of the modulations for the off-shore region. With the objective of investigating if the accuracy of the altimetry data is high enough to provide this valuable additional information about the seasonal modulations, results from analyses of T/P data will be described in this Chapter. The altimetry data are validated by the in-situ data from the coastal tide gauges, and the new knowledge about the spatial distribution of the modulations in the M_2 constituent, obtained from the altimetry data, are then used as information for the off-shore area for validation of a numerical model. The tests with the numerical model are subsequently used to investigate the cause of these seasonal variations. Results from both a barotropic and a baroclinic model will be presented.

As described, modulations on an annual time scale have been reported for the other main constituents as well as in the M_2 constituent (*Baker and Alcock*, 1983; *Thomsen*, 1973), but due to the dominance of the M_2 wave in the North Sea, focus will here be on the modulation in the M_2 constituent alone.

4.2 Annual and Seasonal Variations in the M_2 Constituent

Cartwright (1968) identified two annual periods as the causing factors to the MA_2 and MB_2 frequencies. The Doodson's numbers for the two MA_2 constituents are (2 0 -1 0 0 0) and (2 0 -1 0 0 1) for the non-gravitational and the gravitational contribution respectively, and for

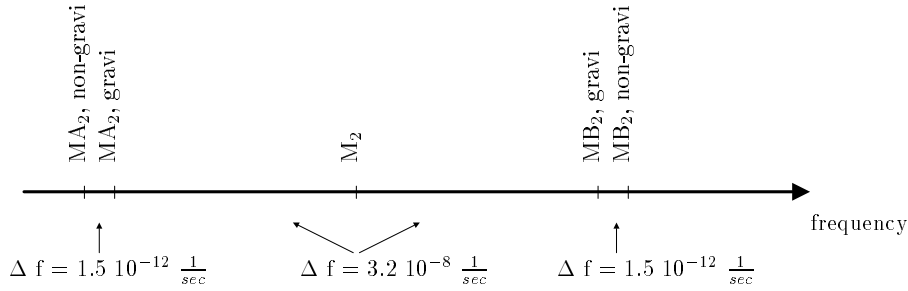


Figure 4.1: The location of the MA_2 , MB_2 and M_2 constituents in the frequency band.

the two MB_2 constituents $(2\ 0\ 1\ 0\ 0\ 0)$ and $(2\ 0\ 1\ 0\ 0\ -1)$, for the non-gravitational and the gravitational contribution, respectively. The difference between the two contributions to each of the two constituents is given by the basic astronomical frequency $\omega_6 = 2\pi \cdot 1.3 \cdot 10^{-7}$ cycles/day corresponding to a period of $T=20\ 942$ years (see Table 3.1 in Chapter 3).

The gravitational contribution to MA_2 and MB_2 is caused by the anomalistic year with the period

$$T_{gravi.} = \left\{ \begin{array}{l} \frac{2\pi}{\omega_{M_2} - \omega_{MA_2}} = \frac{2\pi}{2\omega_1 - (2\omega_1 - \omega_3 + \omega_6)} \\ \frac{2\pi}{\omega_{MB_2} - \omega_{M_2}} = \frac{2\pi}{(2\omega_1 + \omega_3 - \omega_6) - 2\omega_1} \end{array} \right\} = 365.2596 \text{ days.}$$

The anomalistic year defines the time for the Earth to rotate around the sun from the perihelion point and back to the perihelion point again, and includes the movement of the perihelion and aphelion with the angular speed ω_6 .

The non-gravitational contribution to MA_2 and MB_2 is caused by the tropical year defined as the time between two successive vernal equinoxes, and does not include the movement of the perihelion and aphelion. The period for the tropical year is given by

$$T_{non-gravi.} = \left\{ \begin{array}{l} \frac{2\pi}{\omega_{M_2} - \omega_{MA_2}} = \frac{2\pi}{2\omega_1 - (2\omega_1 - \omega_3)} \\ \frac{2\pi}{\omega_{MB_2} - \omega_{M_2}} = \frac{2\pi}{(2\omega_1 + \omega_3) - 2\omega_1} \end{array} \right\} = 365.2422 \text{ days.}$$

The location of the tidal constituents in the frequency band is shown schematically in Figure 4.1. The two different contributions to each of the constituents will for all harmonic analyses be non-separable, but due to the difference in origin a separation of the two factors is important for the investigation of the overall signal.

A linear combination of the three harmonics for the M_2 , MA_2 and MB_2 constituents gives (originally suggested by *Corkan* (1934); here following the notation in *Woodworth et al.* (1991))

$$\begin{aligned} h(t) = & A_{M_2} e^{i(\omega_{M_2}t - g_{M_2} + V_{M_2})} \\ & + A_{MA_2} e^{i(\omega_{MA_2}t - g_{MA_2} + V_{MA_2})} \\ & + A_{MB_2} e^{i(\omega_{MB_2}t - g_{MB_2} + V_{MB_2})} , \end{aligned} \quad (4.1)$$

where A is the amplitude, ω the frequency, g the phase lag and V the astronomical argument for each of the three constituents. This linear combination can be shown to give a main contribution that can be interpreted as a M_2 carrier wave with a modulation in the amplitude at a period of $T = \frac{2\pi}{\Delta\omega} \approx 1$ year (see Appendix B for derivation)

$$[A_{M_2} + S(t)] \cos(\omega_{M_2}t - g_{M_2} + V_{M_2}), \quad (4.2)$$

where the modulation wave $S(t)$ is given by

$$\begin{aligned} S(t) = & A_{MA_2} \cos(-\Delta\omega t - g_{MA_2} + g_{M_2} + (V_{MA_2} - V_{M_2})) \\ & + A_{MB_2} \cos(\Delta\omega t - g_{MB_2} + g_{M_2} + (V_{MB_2} - V_{M_2})). \end{aligned} \quad (4.3)$$

The astronomical arguments for the gravitational and non-gravitational MA_2 and MB_2 constituents are

$$\begin{aligned} V_{MA_{2\text{gravi.}}} &= 2\tau - h + p' = V_{M_2} - 280.19^\circ + 281.22^\circ = V_{M_2} + 1.03^\circ \\ V_{MB_{2\text{gravi.}}} &= 2\tau + h - p' = V_{M_2} + 280.19^\circ - 281.22^\circ = V_{M_2} - 1.03^\circ \\ \\ V_{MA_{2\text{non-gravi.}}} &= 2\tau - h = V_{M_2} - 280.19^\circ \\ V_{MB_{2\text{non-gravi.}}} &= 2\tau + h = V_{M_2} + 280.19^\circ \end{aligned}$$

The gravity potential for the M_2 , $MA_{2\text{gravi.}}$ and the $MB_{2\text{gravi.}}$ constituents are 0.90809, -0.00313 and 0.00277 , respectively, corresponding to amplitudes for $MA_{2\text{gravi.}}$ and $MB_{2\text{gravi.}}$ on 0.345% and 0.305% of the M_2 amplitude (*Cartwright and Taylor, 1971; Cartwright and Edden, 1973*). As the gravitational and non-gravitational contributions to the MA_2 and MB_2 constituents for all practical data analyses are non-separable, the amplitudes and phase lags calculated from a tidal harmonic analysis will contain both the gravitational and non-gravitational part. The annual (gravitational) variation can only explain at most 0.649% of the variation in the M_2 amplitude, and the observed much larger MA_2 and MB_2 amplitudes makes investigations of the non-gravitational part - the seasonal contribution - interesting with the objective to understand the causing factors. Note, that the name seasonal will be used throughout this Chapter to designate the total annual modulation signal in the M_2 constituent caused by the MA_2 and MB_2 constituents, i.e. the seasonal signal will here include both the *annual* and the *seasonal* contributions according to Cartwrights definitions. This is due to the practical problem that it is not possible to distinguish and subtract the annual contribution from the total signal.

According to the Rayleigh criterium (Eqn. 3.13) a time series of a minimum length of 1 year is needed for the MA_2 and MB_2 constituents to be included in a harmonic analysis, and be properly separated from M_2 .

The modulation wave $S(t)$ used for calculation of the seasonal signal in M_2 is given by

$$S(t) = A_{MA_2} \cos(-\Delta\omega t - g_{MA_2} + g_{M_2} - 280.19^\circ) + A_{MB_2} \cos(\Delta\omega t - g_{MB_2} + g_{M_2} + 280.19^\circ). \quad (4.4)$$

where the amplitudes and phase lags are calculated from harmonic analyses, but the modulation wave will for the remaining of this Chapter be referred to as having the form:

$$S(t) = A \cos(\omega t - g), \quad (4.5)$$

where $\omega = 2\pi \cdot 1 \frac{\text{cycles}}{\text{year}}$, A the amplitude of the modulation wave, and g the phase lag corresponding to the time in the year for the maximum of the modulation wave.

4.3 Altimeter Observations

To obtain observations for the off-shore area, altimeter data have been investigated. Analyses of the annual variations in the tidal constituents calculated from altimetry have been carried out by Ole B. Andersen, Kort & Matrikelstyrelsen (National Survey and Cadastre, Denmark), as part of the GEOSONAR project (*Leeuwenburgh et al.*, 1999). Four years of data from the T/P altimeters (cycle 1 to 134) were analyzed in the north-west European shelf region. The sea level data set used for this investigation were corrected by all the standard corrections (see Section 2.2.1), but for the tidal correction. Instead of the standard tidal correction model that already has been corrected with altimetry data, a pure hydrodynamical global tide model, the FES94.1 model (*Provost et al.*, 1994), was used. The four years of corrected sea level data were merged into one year to enhance the temporal coverage. Tidal analyses using the Response Analysis Method were then carried out for a 3 months data window shifted by 10 days (1 repeat cycle) on the sea level differences between subsequent measurements (*Leeuwenburgh et al.*, 1999). At each measurement point a time series of amplitudes for the M_2 constituent was then found. The maximum deviation from the mean M_2 amplitude in each measurement point is shown in Figure 4.2 (top) and the corresponding phase lag (bottom), indicating when this maximum in the amplitude occurs in the year, with 0° corresponding to January 1. and 360° to December 31. The T/P data are seen to identify an annual signal in the M_2 amplitude in the eastern part of the North Sea. The largest deviations with more than 5.0 cm are found in July in the south eastern part of the North Sea. This corresponds to deviations of up to 8% of the M_2 amplitude in this region and indicates the existence of a strong seasonal signal for this area. The results from the altimeter data will in the next section be validated in the coastal areas by means of tide gauge data. Note that due to the sparse time sampling of the altimeter data, separation of the MA_2 and MB_2 frequencies from the M_2 frequency was not possible. The variations in the M_2 constituent observed from the altimeter data may, therefore, contain contributions from other processes at a slightly larger frequency range, than the MA_2 and MB_2 frequencies used for the analyses of the tide gauge data.

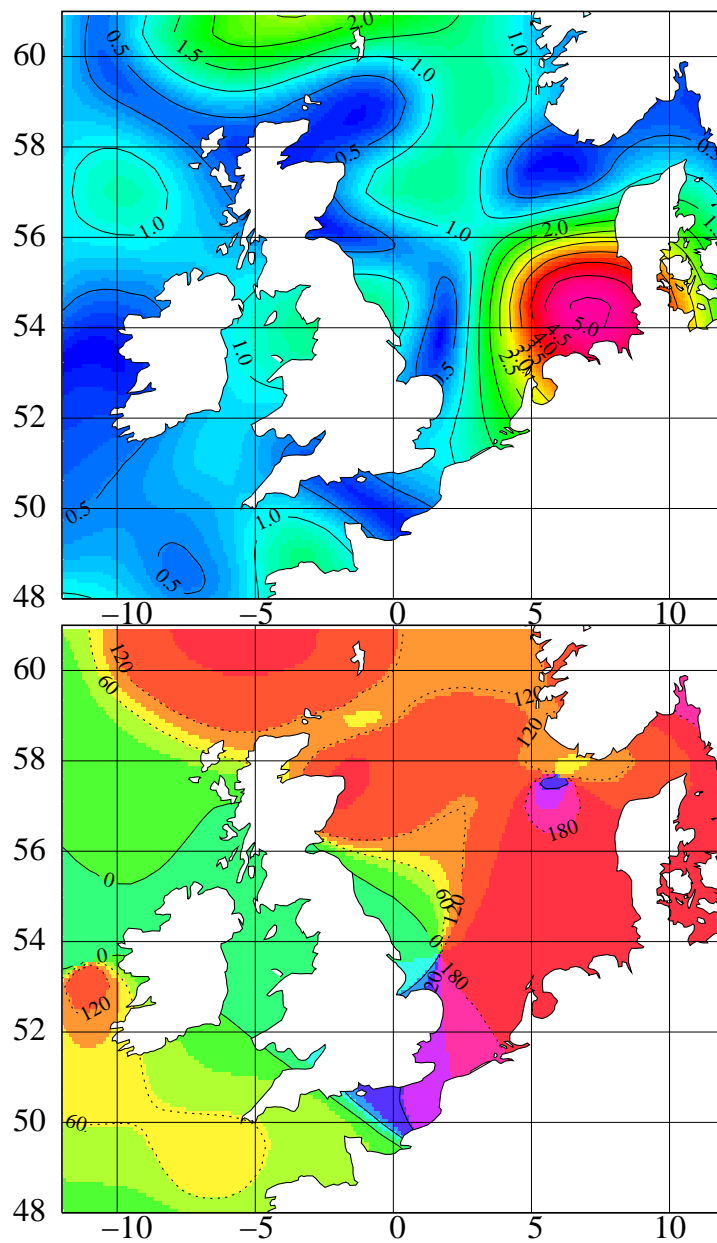


Figure 4.2: Annual variations in the M_2 constituent from T/P data found from a running analysis on a 3 month data window shifted by 10-days. The maximum deviation in cm from the mean amplitude at each grid point is shown at top and the corresponding phase lag for this maximum to occur is shown at bottom with $0^\circ = 1/1$ and $360^\circ = 31/12$ (Leeuwenburgh et al., 1999).

4.4 Tide Gauge Observations

Tide gauge data from countries located around the North Sea, have been collected and analyzed to get a coastal in-situ data set for validation of the altimetry observations of the modulation in the M_2 constituent. Efforts have been taken to obtain a data set with a large spatial coverage, in order to be able to demonstrate any local or geographical effect on the size of the modulation. Data have been analyzed from 10 tide gauge stations around the British Isles. The 10 stations are located on both the east and west coast and from both north to south. Along the European continental coastline, data from four tide gauges have been analyzed together with four Danish stations on the eastern coast of the North Sea. For coverage of the northern part of the North Sea, one tide gauge record from Norway has been analyzed. The locations and time spans of all the data records are shown in Tables 4.1, 4.2 and 4.3 and in Figure 2.1. All the data records have a time step of maximum 1 hour, and hourly values have been used in the tidal analyses.

4.4.1 Validation of the altimeter observations

To validate the total annual variation in the M_2 constituent observed from the altimetry, estimates of the corresponding total variation from the in-situ tide gauge data set have been calculated. A harmonic analysis with a 3 months data window shifted by 10 days through the length of the data record has been carried out. Results are presented in Figure 4.3 for nine of the tide gauge stations located around the North Sea.

Variations in the M_2 constituent on an annual time scale are observed at all locations but with large variability in magnitude. The largest M_2 amplitudes are in general seen in spring to summer. The largest variations in the tide gauge data are, as observed in the altimetry data, found in the south eastern part of the North Sea. The tide gauge station at Cuxhaven shows a maximum in the M_2 amplitude of 5-10 cm in June, in good agreement with the altimeter observations. Variations in the M_2 amplitude of 3-5 cm and 2-3 cm are observed for Esbjerg and Hanstholm at the Danish coast, respectively, also in good agreement with the altimetry. For the two stations in the British Isles and the two French stations, variations in the amplitudes of 2-3 cm are seen in the tide gauge data, but not captured in the altimeter observations. The poor spatial data resolution in the altimetry data, which is particularly important for shelf-sea areas such as the Irish Sea and the Channel may provide a partial explanation.

4.4.2 Comparison of the Total Annual Variation and the Modulation Wave

The variation in the M_2 constituent from the altimeter observations was estimated from a moving analysis through the data record. To estimate any differences between the two different analysis methods used here

- the total annual variation in M_2 calculated from a moving harmonic analysis through the data record
- the seasonal signal calculated from the modulation wave, $S(t)$ (Eqn.4.4)

a comparison of the results from the two analysis methods has been carried out. The reason for the use of the moving analysis through the data record is the fact that it is not possible to

Station	Latitude	Longitude	Time span	Data Missing
Newlyn	50° 06' N	5° 33' W	01 1994 - 12 1998	2%
Avonmouth	51° 31' N	2° 43' W	01 1994 - 12 1998	10%
Liverpool	53° 25' N	3° 00' W	01 1994 - 12 1998	1%
Port Patrick	54° 51' N	5° 07' W	01 1994 - 12 1998	2%
Kinlochbervie	58° 27' N	5° 03' W	01 1994 - 12 1998	5%
Wick	58° 26' N	3° 05' W	01 1992 - 12 1998	4%
Leith	55° 59' N	3° 11' W	01 1992 - 12 1998	3%
North Shields	55° 00' N	1° 26' W	01 1992 - 12 1992	0%
North Shields	-	-	01 1994 - 12 1998	4%
Lowestoft	52° 28' N	1° 45' E	01 1992 - 12 1998	4%
Sheerness	51° 27' N	0° 45' E	01 1992 - 12 1998	0%

Table 4.1: *Tide gauge data from the British stations, provided by the British Oceanographic Data Centre.*

Station	Latitude	Longitude	Time span	Data Missing
Roscoff ¹	48°42' N	4°00' W	01 1991 - 12 1996	6%
Cherbourg ¹	49°39' N	1°39' W	01 1991 - 12 1996	3%
Oostende ²	51°14' N	2°55' E	01 1991 - 12 1996	0%
Cuxhaven ³	53°52' N	8°43' E	01 1991 - 12 1996	0%
Stavanger ⁴	58°59' N	5°44' N	01 1991 - 12 1996	0%

Table 4.2: *Tide gauge data from the European continental coast. Provided by 1: Service Hydrographique et Oceanographique de la Marine, France, 2: Coastal Hydrographic Office, Belgium, 3: Bundesamt für Seeschifffahrt und Hydrographie, Germany and 4: Norges Sjøkartverk, Norway.*

Station	Latitude	Longitude	Time span	Data Missing
Esbjerg ¹	55°28' N	8°26' E	01 1992 - 12 1997	6%
Hvide Sande ²	56°00' N	8°07' E	01 1992 - 12 1994	5%
Hvide Sande ²	-	-	01 1997 - 12 1998	0%
Torsminde ²	56°22' N	8°07' E	01 1992 - 12 1998	3%
Hanstholm ¹	57°07' N	8°36' E	01 1992 - 12 1998	2%
Hirtshals ¹	57°36' N	9°58' E	01 1992 - 12 1998	2%

Table 4.3: *Tide gauge data from the Danish stations. 1: operated by the Danish Meteorological Institute; 2: operated by the Danish Coastal Authority.*

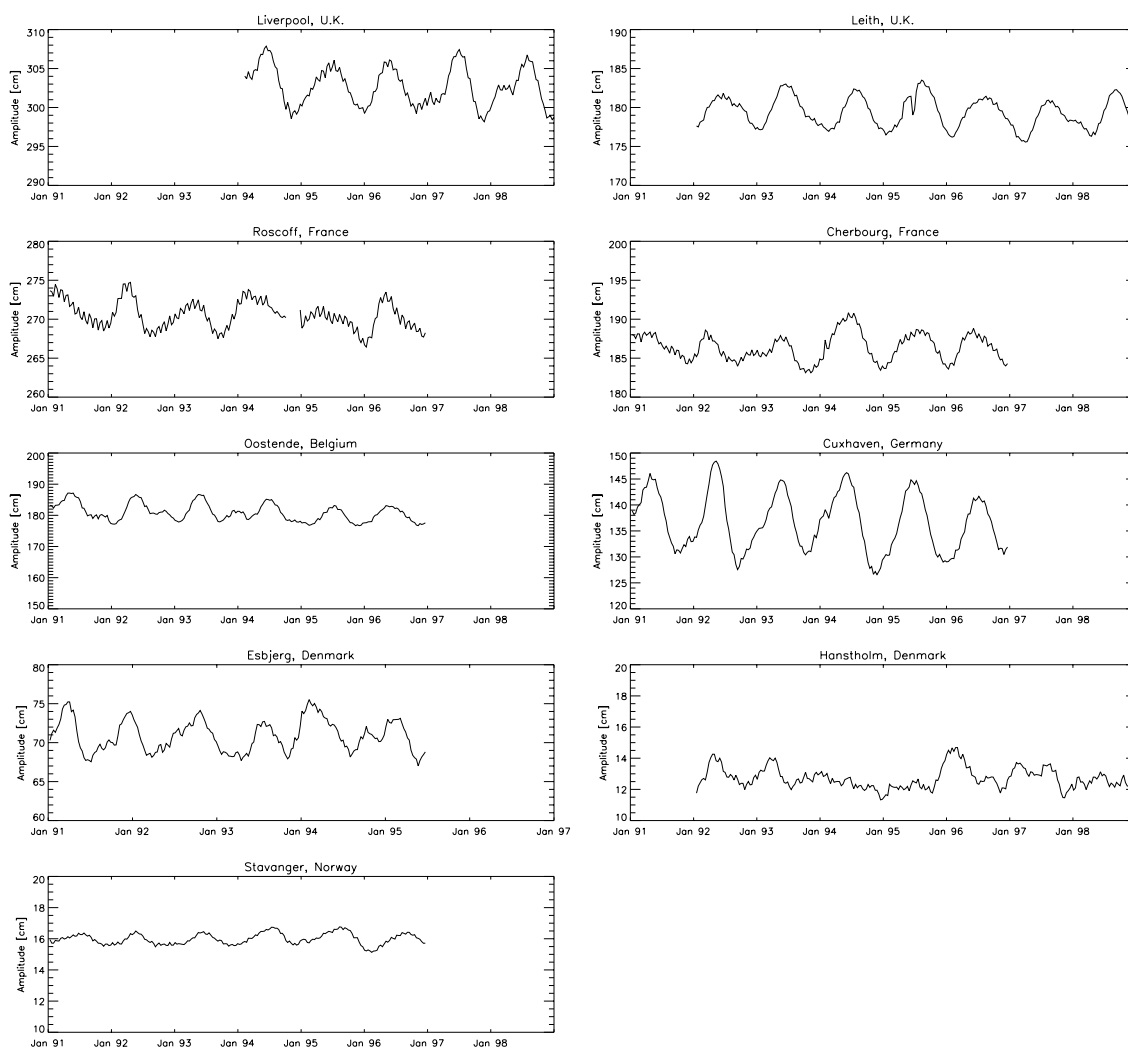


Figure 4.3: M_2 amplitudes for nine tide gauge stations around the North Sea. Calculated with a running 3 months harmonic analysis window, shifted by 10 days. Note the different scales on the y-axis.

estimate the MA_2 and MB_2 constituent from the T/P observations and by that calculate the modulation wave, $S(t)$.

The comparison of the two analysis methods has been carried out for the tide gauge station at Esbjerg on the Danish North Sea coast for the years 1992 - 1997 and are shown in Figure 4.4. The overall deviations in the M_2 amplitude from the mean is shown for each 3 months analysis shifted 10 days throughout the years, and the maximum deviation in the M_2 amplitude calculated from the modulation wave fit is shown as stars. The largest deviations between the two different analysis methods are seen to be of 1 month in the phase lag (for 1992 and 1996) and of about 1.5 cm for the size (1992 and 1996). For these two years the seasonal wave fit is seen to capture about 2/3 of the total annual variation. For the other four years investigated a high agreement between the two analysis methods is seen. This makes it sensible to compare the altimeter observations of the total variations in the M_2 constituent with the calculations of the seasonal modulation wave $S(t)$ from the tide gauge data.

Figure 4.4 clearly displays that the winter 1995-1996 shows a very different pattern for the seasonal behaviour of the M_2 constituent compared to the other years.

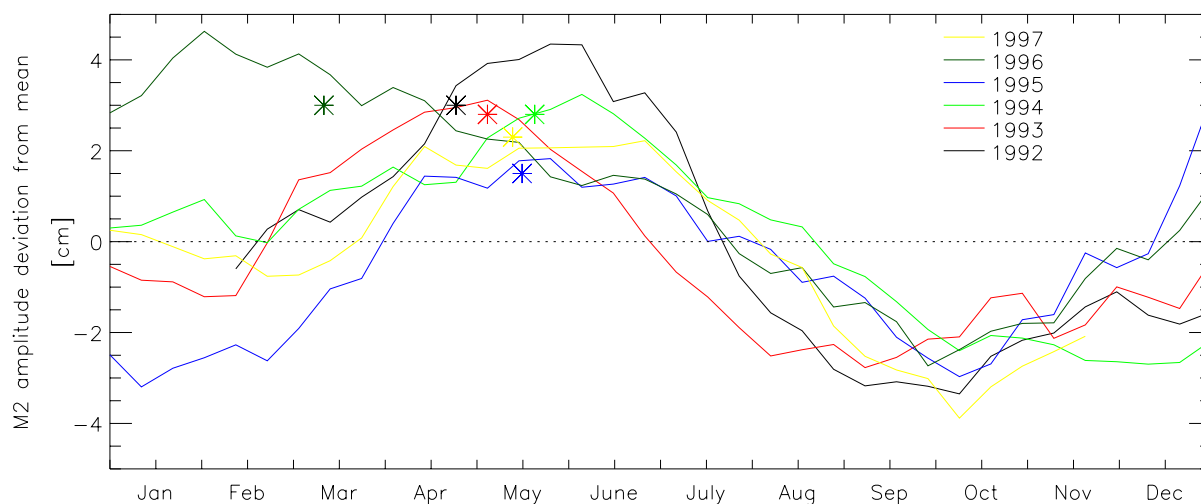


Figure 4.4: Comparison of the two analysis methods for calculating the seasonal change in the M_2 constituent calculated for Esbjerg for the years 1992-1997. The total variation found from the moving harmonic analysis is shown with the six different color lines for each 3-month analysis shifted by 10 days throughout the year. The results from the seasonal wave fit analysis are shown as stars with the corresponding color for each year.

4.4.3 The Modulation Wave for north-west European Shelf Stations

The focus in the investigations of the annual M_2 deviations will be on the modulation wave fits because they provide a more robust measurement than the 3 months moving harmonic analysis

window. The behaviour of the MA_2 and MB_2 constituents in the North Sea and adjacent seas has, therefore, been investigated.

Influence on MA_2 and MB_2 amplitudes of shallow water tidal propagation

The influence on the MA_2 and MB_2 amplitudes of the tidal propagation in shallow waters is shown in Figure 4.5. The relative amplitudes, in per cent of the M_2 amplitude, are plotted for the five stations on the British west coast from south to north in the direction of propagation for the tidal wave in the Irish Sea. For the North Sea area, the amplitudes are similarly plotted as a function of the distance for the propagation of the tidal wave; from north to south along the British east coast, from west to east along the European continent, and from south to north along the Danish coast. The yearly analyses are shown for five years of data. The gravitational contribution to the MA_2 and MB_2 amplitudes are indicated as horizontal lines at 0.345% and 0.305% for MA_2 and MB_2 , respectively. Large variations in the amplitudes are seen both with respect to the location of the stations and from year to year. For the five stations on the British west coast, the largest amplitudes are seen at Avonmouth, located in the inner part of the Bristol Channel. Along the east coast of Britain, the amplitudes are in general a little larger than for the stations on the west coast. Along the European continent and the Danish coast a slight dependency can be seen to the tidal wave propagation in shallow waters. The area west of Jutland is dominated by friction (described in Chapter 7). The two constituents are in general seen to have the same dominance for all the stations, but Lowestoft and Sheerness. At Lowestoft a large MB_2 constituent is observed together with a relatively small MA_2 constituent, and the opposite situation is seen at Sheerness with a small MB_2 constituent together with a large MA_2 constituent. Both Lowestoft and Sheerness differs from the other stations, by being influenced from two tidal waves, one propagating in the North Sea coming from north and one propagating through the Channel. This tidal wave interaction may eventually explain a part of the significant different pattern at those two stations. They are also both located in very shallow water areas and Sheerness is located close to the Thames. The observed large inter-annual variations in the seasonal modulation wave will be investigated further in Section 4.5.

Influence of local effects on MA_2 and MB_2

The effect of any local influence in the generation of the MA_2 and MB_2 constituents can be estimated from the phase lag differences between the M_2 constituent and the MA_2 and MB_2 constituents. The differences between the phase lag for M_2 and the phase lags for MA_2 and MB_2 are shown in Figure 4.6 (left and right, respectively) for the British, the European continental and Danish stations. If no local effects were present in the generation of the seasonal variations, the phase lag differences $g_{M_2} - g_{MA_2}$ and $g_{MB_2} - g_{M_2}$ would give two horizontal lines. Figure 4.6 shows this is not the case, and large variations in the dominance of the local effects are seen. Along the west coast of the Britain, the M_2 - MA_2 phase lag difference is somewhat different at Port Patrick compared to the four other stations. For the MB_2 - M_2 phase lag difference, a very different value is seen for all five stations, except for Liverpool and Port Patrick. Along the British east coast, no M_2 - MA_2 phase lag difference is seen between the three northern stations, i.e. Wick, Leith and North Shields, whereas a decrease in the MB_2 - M_2 phase lag difference is

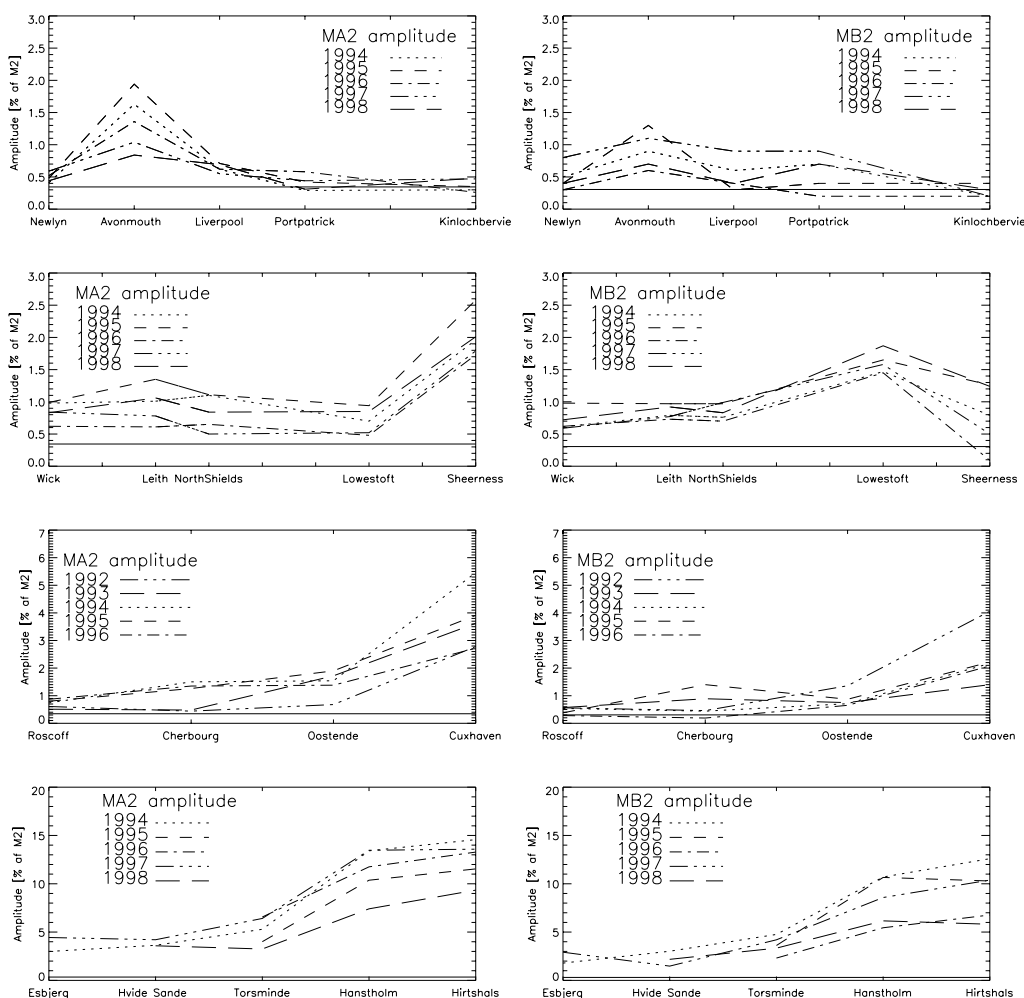


Figure 4.5: MA_2 (left) and MB_2 (right) amplitudes (in % of the M_2 amplitude) plotted for 5 years of data from tide gauge stations along the British west and east coast, the European continent, and the Danish North Sea coast. Note the different scale at the y-axes.

seen for those three stations. For the European continental stations a local influence is seen for the MB_2 - M_2 phase lag, but not for the M_2 - MA_2 phase lag difference. Along the Danish coast, only limited local effects are seen for both terms. Figure 4.6 allows us to conclude that local generation plays a role in the production of MA_2 and MB_2 at the tide gauge stations. Also noticed is that the influence of the local effect is significantly varying in strength.

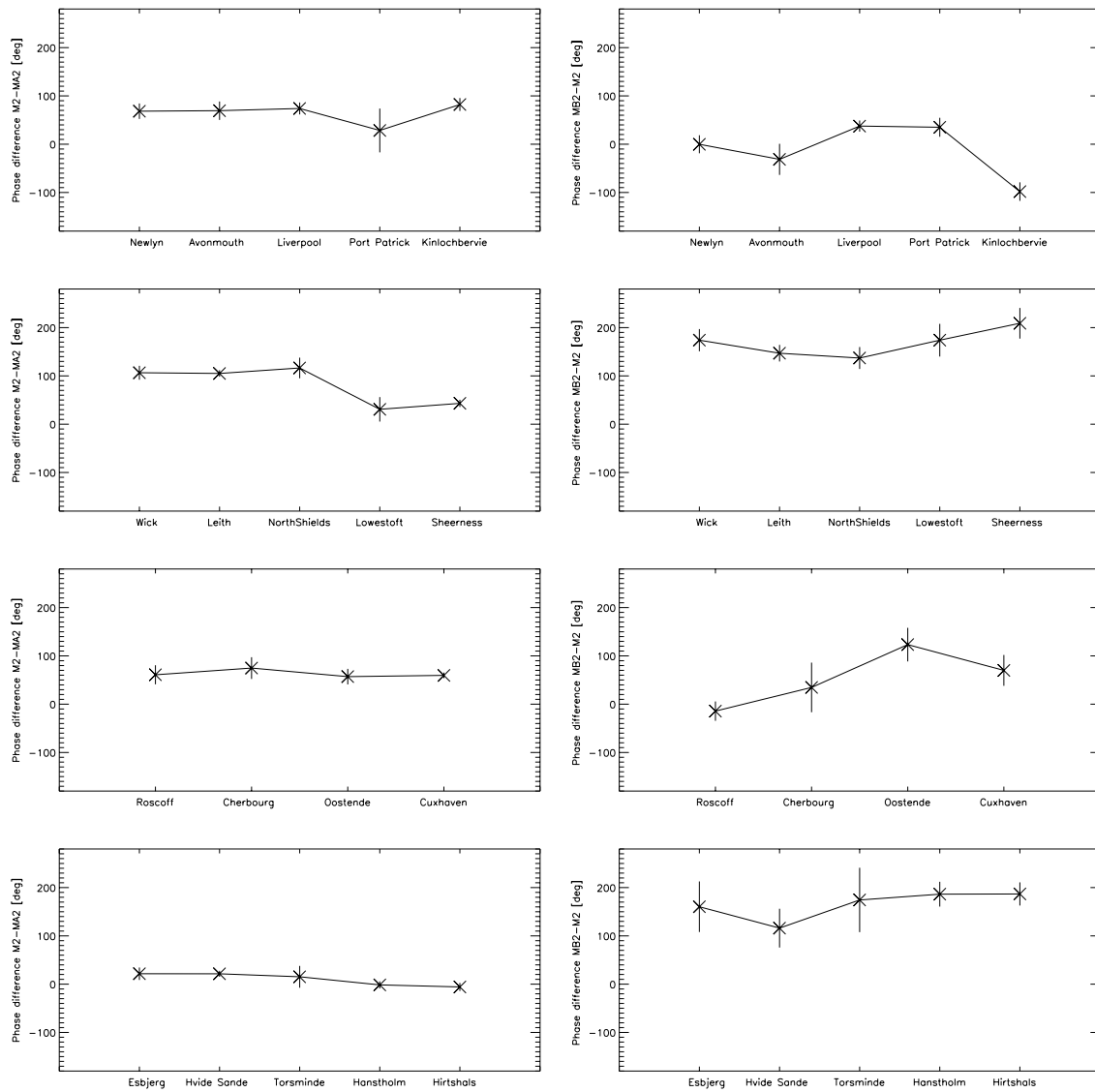


Figure 4.6: *Phase lags for the differences $M_2 - MA_2$ (left) and $MB_2 - M_2$ (right) for the British, European continental and Danish tide gauge stations. The mean values from five yearly analysis are plotted together with the standard deviations.*

Calculations of the Modulation Wave fit

The seasonal signal calculated from Eqn. 4.4 for the tide gauge stations in the Irish Sea and along the North Sea coasts are shown in Table ???. Also shown are the amplitudes of the M_2 , MA_2 and MB_2 constituents. The size of the seasonal signal is shown both in absolute values and relative to the M_2 amplitude. The phase lag for the maximum in the seasonal signal to occur is shown in degrees with 0° corresponding to January 1. and 360° to December 31. The

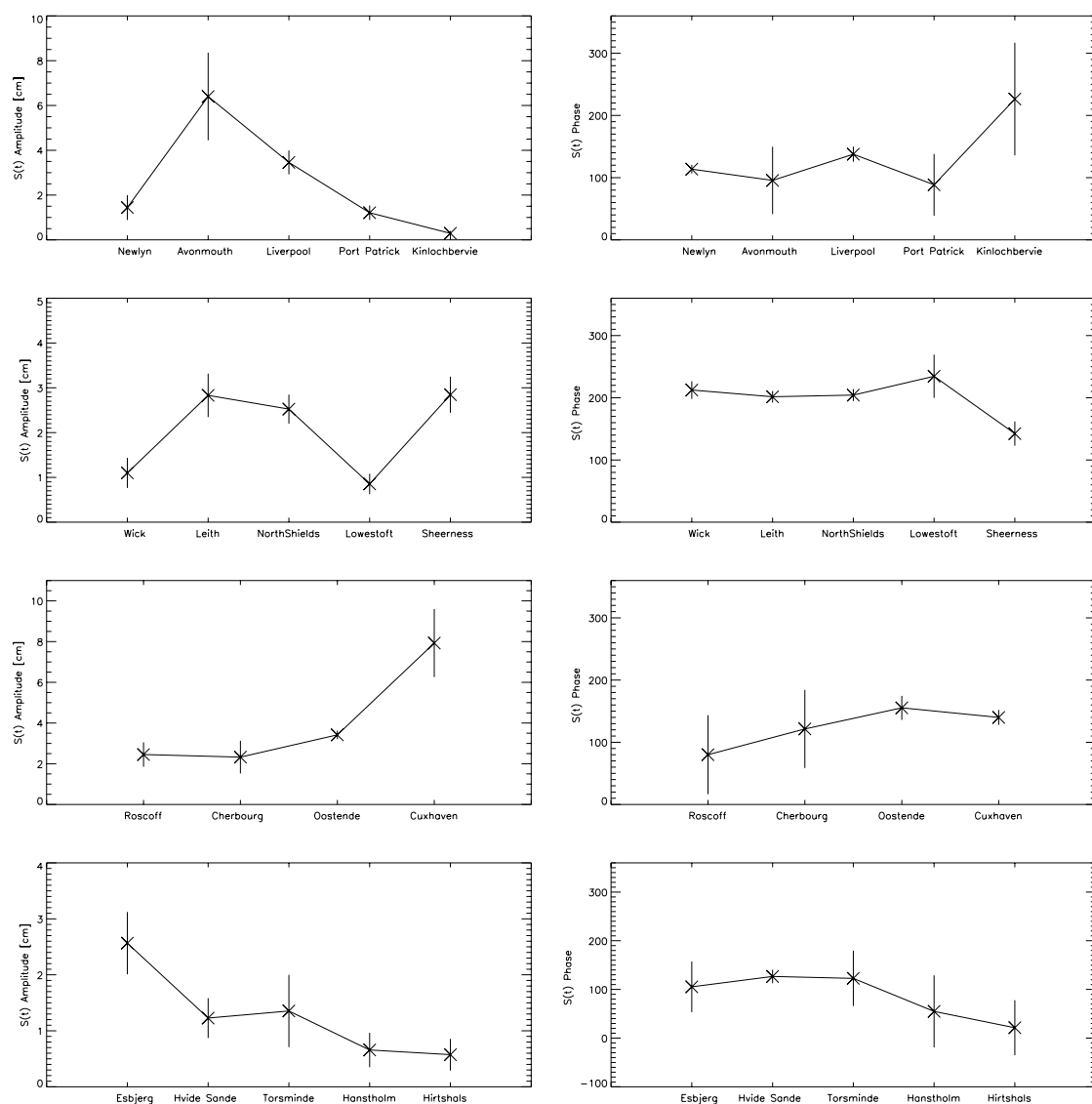


Figure 4.7: The seasonal wave fit calculated for the for the British, European continental and Danish tide gauge stations. The mean values from five yearly analysis are plotted together with the standard deviations for the seasonal wave amplitude (left) and the corresponding time in the year for the maximum M_2 amplitude to occur (in 360 degrees; right).

corresponding number for the month in the year are shown in brackets. The mean values with the standard deviation error bars for the amplitude and phase lag for the seasonal wave are also shown in Figure 4.7. Along the British west coast all the stations, except for Kinlochbervie in the north, show seasonal variations in the M_2 constituent. On the west coast the largest signal is observed at Avonmouth and Liverpool both located in narrow and shallow water areas. At the

British North Sea coast an increase in the seasonal signal is seen from Wick in the north with 1.1% of the M_2 amplitude to Leith and North Shields with a signal of order 1.6%. A decrease in the signal is seen for the two stations Lowestoft and Sheerness, but they do still show a seasonal signal of 1.2% and 1.4%, respectively. For the tide gauge stations at the European coast, large variations in the dominance of the seasonal modulations in the M_2 constituents are seen. From almost no seasonal effect at Roscoff located at the outermost part of the Channel, an increase is seen as the tidal wave propagates through the Channel and into the southern part of the North Sea. The maximum variation of nearly 8 cm, corresponding to nearly 6% of the M_2 amplitude, is seen at Cuxhaven in the German Bight. Additionally, results from a one year (1975) harmonic analysis of data from the Helgoland island located in the German Bight provided by D. L. Blackman, POL, UK, give a modulation wave of 5 cm, and a M_2 amplitude of 108 cm, corresponding to a relative signal of 5% with maximum at the end of May. At all five Danish stations, relative variations of 4% - 5% are observed. At Stavanger in the northern part of the North Sea a relative amplitude of nearly 3% is observed. The maximum in the M_2 amplitude occurs at all the stations in the period from spring to late summer. For the stations around Britain, the maxima on the western coast are seen to occur in May, which is 1-2 months earlier than for the stations located on the British North Sea coast with maxima, where maximum occur in August. The most southern station on the east coast, Sheerness, shows a maximum in June. As mentioned earlier, the tidal behaviour at Sheerness might differ from the other stations because of the location close to the Channel. For Cherbourg and Oostende in the Channel and Cuxhaven in the German Bight, maxima occur around May - June. Along the Danish North Sea coast, maximum occurs for the 3 southern most stations in late April to mid May, as for Cuxhaven, whereas for the two northern Danish stations maximum takes place earlier, in the beginning of March and April.

The largest seasonal signal in the M_2 constituent for the North Sea with adjacent seas is found in the south eastern part of the North Sea with an amplitude of more than 7 cm. This is in good agreement with the observations from the T/P data (Figure 4.2), where the largest deviation from the mean M_2 amplitude is more than 5 cm. The T/P data show a maximum in the M_2 constituent for the German Bight and the eastern North Sea at around June, in agreement with the seasonal signal in the tide gauge data set. As described above, the tide gauges show seasonal effects for most of the coastal areas located around the North Sea. The T/P data do not capture all those signals. For instance the signal of more than 6 cm at Avonmouth in the Bristol Channel is not captured in the altimeter observations, and along the British east coast a wrong phase lag is seen. This might be due to the complicated shapes of the shallow shelf areas, as is the case for both Avonmouth and Liverpool. However, in addition, the poor spatial resolution for the altimeter data, even along a straight coastline, may be a reason for the failure of the altimetry to capture the M_2 variations observed from the tide gauges that, as shown above, do reveal relatively strong local variations, and therefore short spatial scale effects.

The large inter-annual variations observed in the MA_2 and MB_2 constituents from the tide gauge data imply large inter-annual variations in the fits in terms of the seasonal modulation wave. This will be described further in Section 4.5, where results from numerical models are investigated to test the ability of the models to describe the observed variations.

Station	M_2 amp. [cm]	MA_2 amp. [cm]	MB_2 amp. [cm]	$S(t)$ amp. [cm]	$S(t)$ phase lag [°]	$S(t)$ amp. [%]
Newlyn	171 ± 0.6	0.8 ± 0.1	0.9 ± 0.3	1.4 ± 0.6	114 (5) \pm 7	0.8
Avonmouth	425 ± 4.4	5.9 ± 2.0	4.0 ± 1.3	6.4 ± 2.0	114 (5) \pm 14	1.5
Liverpool	303 ± 0.5	1.9 ± 0.2	1.7 ± 0.7	3.4 ± 0.5	138 (5/6) \pm 12	1.1
Portpatrick	133 ± 0.3	0.5 ± 0.2	0.8 ± 0.4	1.2 ± 0.3	108 (4/5) \pm 7	0.9
Kinlochbervie	144 ± 0.2	0.5 ± 0.1	0.4 ± 0.1	0.3 ± 0.1	172 (7) \pm 69	0.2
Wick	101 ± 0.3	0.9 ± 0.2	0.7 ± 0.1	1.1 ± 0.3	212 (8) \pm 14	1.1
Leith	179 ± 0.5	1.7 ± 0.4	1.5 ± 0.2	2.8 ± 0.5	202 (7) \pm 9	1.6
North Shields	160 ± 0.5	1.4 ± 0.4	1.4 ± 0.2	2.5 ± 0.3	204 (8) \pm 10	1.6
Lowestoft	69 ± 0.7	0.5 ± 0.2	1.1 ± 0.2	0.9 ± 0.2	235 (9) \pm 35	1.2
Sheerness	200 ± 1.8	3.8 ± 0.7	1.8 ± 0.9	2.8 ± 0.4	142 (6) \pm 19	1.4

Station	M_2 amp. [cm]	MA_2 amp. [cm]	MB_2 amp. [cm]	$S(t)$ amp. [cm]	$S(t)$ phase lag [°]	$S(t)$ amp. [%]
Roscoff	270 ± 0.7	1.8 ± 0.4	1.3 ± 0.4	2.5 ± 0.6	112 (5) \pm 18	0.9
Cherbourg	186 ± 0.7	1.7 ± 0.9	1.0 ± 0.6	2.3 ± 0.8	137 (5/6) \pm 29	1.2
Oostende	181 ± 1.4	2.9 ± 1.0	1.5 ± 0.5	3.4 ± 0.2	155 (6) \pm 19	1.9
Cuxhaven	137 ± 1.0	4.8 ± 1.5	3.2 ± 1.2	7.9 ± 1.7	140 (5/6) \pm 12	5.8

Station	M_2 amp. [cm]	MA_2 amp. [cm]	MB_2 amp. [cm]	$S(t)$ amp. [cm]	$S(t)$ phase lag [°]	$S(t)$ amp. [%]
Esbjerg	71 ± 0.5	2.9 ± 1.5	1.5 ± 1.1	2.6 ± 0.6	117 (5) \pm 25	3.6
Hvide Sande	33 ± 1.1	1.1 ± 0.3	0.7 ± 0.2	1.2 ± 0.4	127 (5) \pm 14	3.7
Torsminde	26 ± 0.4	1.3 ± 0.3	0.9 ± 0.3	1.4 ± 0.6	130 (5) \pm 39	5.2
Hanstholm	13 ± 0.3	1.4 ± 0.3	1.1 ± 0.3	0.7 ± 0.3	87 (4) \pm 55	5.2
Hirtshals	12 ± 0.3	1.4 ± 0.2	1.1 ± 0.3	0.6 ± 0.3	71 (3) \pm 44	4.7
Stavanger	16 ± 0.1	0.5 ± 0.0	0.3 ± 0.1	0.5 ± 0.1	184 (7) \pm 20	2.9

Table 4.4: The mean and standard deviations of the amplitudes for the M_2 , MA_2 and MB_2 constituents, and for the amplitude and phase lag for the seasonal wave fit $S(t)$. The statistics are for each station calculated over the available data record shown in Table 4.1 - Table 4.3. Also shown is the relative seasonal wave amplitude to the M_2 amplitude (mean values). The time in the year for the maximum in the seasonal wave to occur is shown as a phase lag (\mathcal{O} corresponds to 1/1) and the corresponding month in the year is shown in the brackets.

4.4.4 The Modulation Wave for Stations Outside the North Sea

To estimate the size of a seasonal signal outside the North Sea, data from one bottom pressure recorder located at the Scottish Shelf slope, and several tide gauges located outside the north-west European shelf have been analyzed. The locations of the stations are shown in Table 4.5. The stations are located in both hemispheres and in both the Atlantic and the Pacific oceans.

Station	Latitude	Longitude	Time span	Data Missing
Station 1.1.75, Scottish Shelf	57°19' N	009°53' W	04 1982 - 02 1983	0%
Reykjavik, Iceland	64°09' N	021°56' W	01 1985 - 12 1995	6%
Ponta Delgada, Azores	37°44' N	025°40' W	01 1985 - 06 1991	25%
Johnston Is., N. Pacific	16°44' N	169°32' W	01 1990 - 12 1992	2%
Ascension Is., S. Atlantic	07°55' S	014°25' W	06 1993 - 06 1998	2%
St. Helena, S. Atlantic	15°55' S	005°43' W	11 1993 - 10 1995	0%
Rarotonga, S. Pacific	21°12' S	159°47' W	01 1990 - 12 1993	0%
Juan Fernandez, S. Pacific	33°37' S	078°50' W	08 1990 - 12 1992	0%

Table 4.5: *Tide gauge stations from outside the European shelf. Data provided by the WOCE (World Ocean Circulation Experiment) and the PSMSL programmes.*

The seasonal signal calculated from fits to the modulation wave $S(t)$ (Eqn. 4.4) are shown in Table ?? for the tide gauges. Statistics have been performed for stations with a data record of minimum three years. A significant seasonal signal is seen at at least two of the stations; St. Helena in the southern Atlantic and at Johnston Island in the northern Pacific. A clear latitude dependence is not seen, and 7 stations are clearly too few observations to form firm conclusions. A modest conclusion on the analyses of the tide gauge data from outside the North Sea region is that seasonal modulations in the M_2 constituent do indeed occur outside the North Sea.

For the station along the Scottish shelf-slope (Station 1.1.75) observations were only available from April 1982 to mid February 1983. A variation in the M_2 amplitude for the half year of data of 0.7% was found, and by that no evidence of a significant seasonal signal along the shelf slope has been observed.

4.5 Numerical Modelling

To investigate the cause of the large seasonal contributions to the MA_2 and MB_2 constituents observed for the North Sea, data from numerical models have been investigated. The clear advantage of using numerical models in studying the cause of the seasonal signal is the capability to switch on and off the atmospheric and tidal forcings. Results from model runs forced with tides only, and runs forced with both tides and atmospheric fields, were analyzed to estimate the effect from the interaction between the tidal wave and the atmospherically induced surges. With the objective to investigate if the physics of the seasonal signal is mainly barotropic or baroclinic, data from both a 2D barotropic and a 3D baroclinic model were analyzed. Results

Station	M_2 amp. [cm]	MA_2 amp. [cm]	MB_2 amp. [cm]	$S(t)$ amp. [cm]	$S(t)$ phase lag [°]	$S(t)$ amp. [%]
Reykjavik	132 ± 0.5	2.1 ± 1.1	2.0 ± 0.9	0.9 ± 0.3	$120 (5) \pm 36$	0.7
Ponta Delgada	49	0.2	0.3	0.4	347 (12)	0.7
Johnston Is.	27 ± 0.2	0.5 ± 0.2	0.6 ± 0.4	1.0 ± 0.6	$32 (1-2) \pm 34$	3.8
Ascension Is.	34 ± 0.2	0.1 ± 0.1	0.2 ± 0.0	0.2 ± 0.0	$52 (2) \pm 129$	0.7
St. Helena	32	0.1	0.5	0.5	348 (12)	1.7
Rarotonga	27 ± 0.3	0.3 ± 0.1	0.2 ± 0.2	0.4 ± 0.1	$340 (12) \pm 68$	1.4
Juan Fernandez	32	0.3	0.2	0.3	263 (10)	1.0

Table 4.6: *The mean and standard deviations of the amplitudes for the M_2 , MA_2 and MB_2 constituents, and for the amplitude and phase lag for the seasonal wave fit $S(t)$ for the tide gauge stations located outside the north-west European shelf area. The statistics are for each station calculated over the available data record shown in Table 4.5. Also shown is the relative seasonal wave amplitude to the M_2 amplitude (mean values). The time in the year for the maximum in the seasonal wave to occur is shown as a phase lag (0° corresponds to 1/1) and the corresponding month in the year is shown in the brackets.*

from the barotropic model are described in Sections 4.5.1 and 4.5.2, and from the baroclinic model in Section 4.5.3. Good results are obtained from the barotropic model and the main focus in this Chapter will, therefore, be on this model.

4.5.1 Barotropic Model

Results from a 2D hydrodynamical model developed by Roger Flather, POL, U.K., have been investigated. Sea level data from the model simulations were kindly provided by Roger Flather and Jane Williams at POL. The model solves the shallow water equations on a finite difference grid with a grid resolution of approximately 35 km. (20' Lat. and 30' Long.). For more technical details about the model, see *Flather (1976)*. The model setup covers the north eastern Atlantic and is referred to as the NEAC model (North East Atlantic Cut off). The NEAC model is forced by tidal elevations at the open boundaries with tidal waves generated by the following 26 tidal harmonic constituents:

Diurnal: Q_1, O_1, P_1, K_1
Semi-diurnal: $MNS_2, 2N_2, \mu_2, N_2, \nu_2, M_2, \lambda_2, L_2, T_2, S_2, K_2, MSN_2, 2SM_2$
Third-diurnal: MO_3, MK_3
Fourth-diurnal: MN_4, M_4, MS_4
Sixth-diurnal: $M_6, 2MS_6, 2MK_6, 3M_2S_2$

The MA_2 and MB_2 constituents are not included in the forcing of the model. The atmospheric forcing of the model consists of reanalyzed fields from the Norwegian Meteorological Institute (*Reistad and Iden, 1998*).

Sea level data for the years 1992-1997 have been analyzed from model simulations forced with tides only, and simulations forced with both tides and atmospheric fields. Harmonic analyses

were performed at each grid point for each 1-year data set, and the seasonal modulation wave $S(t)$ calculated from the MA_2 and MB_2 amplitudes and phase lags.

Results are shown in Figure 4.8 for year 1992. The amplitude of the seasonal signal is plotted in absolute values [cm] together with the phase lag for the maximum, with 0° at January 1. Results are shown from the model simulation forced with tides only - called a T model run - and from the model simulation forced with both tidal and atmospheric fields - called a T+S (i.e. tides and surges) model run. Plots of the modulation wave for all the model runs for the years 1992 - 1997 are shown in Appendix E. The model simulations confirm the existence of the MA_2 and MB_2 constituents in the shelf area, even though they were not introduced in the model forcing. The energy at the MA_2 and MB_2 frequencies is generated from interaction between M_2 and an annual frequency made up from combinations of the 26 constituents. The model clearly reveals the seasonal signal as a shallow water phenomenon caused by non-linear interaction. An increase in the size of the modulation wave is seen for the T+S model runs compared to the T model runs. This reflects that a strong interaction between the tidal wave and the atmospherically induced surges takes place. Large inter-annual variations are seen for the T+S model run, indicating a dependence on the strength of the atmospheric forcing. For the T model runs, the non-linear interaction can occur only between the tidal components.

Validation with Altimetry

The strong signal in a large area of the south eastern North Sea having a maximum M_2 amplitude in the summer period observed from the altimetry data (Figure 4.2) is seen to be relatively well captured in the T+S model runs, and also partly in the T model runs. However, the T+S model runs do in general not reproduce the same strength in the signal as observed from both the altimeters and tide gauge data (see Table 4.7), but shows the same pattern with a strong increase in the signal in the south eastern part of the North Sea. The different distribution of the signal seen between the altimetry data and the model data may be caused by the poor spatial data coverage in the T/P data. The model reveals a seasonal signal along the British east coast, as observed in the tide gauge data but not in the T/P data. The poor spatial data coverage in the altimetry data may again be the most likely explanation. Amphidromical points are observed for the modulation wave. The T/P data (Figure 4.2) reveals two amphidromical points: one located in the south western part of the North Sea off the British coast and one south of Norway. These two amphidromical points are also found in both the T and T+S model simulations. The point south of Norway is simulated to be at the same location as found from the T/P data, whereas the southern point is simulated in the model to be located a bit more to the south, closer to the Channel. The model results reveal one more amphidromical point in the south eastern North Sea for some of the model runs (for instance 94 T+S, 95 T and T+S and 96 T+S). The model runs show slightly different locations of the amphidromical points from year to year, but they do in general coincide with the location of the amphidromical points in the semi-diurnal M_2 constituent in the North Sea described in Chapter 6.

Validation with Tide Gauges

The in-situ tide gauge data set makes a more direct validation of the model-simulated seasonal signal for the coastal areas. Data from the closest grid point in the model to the tide gauge stations have been extracted for nine British and Danish tide gauges. In Table 4.7 are shown the values for the seasonal signal from the T+S model simulations and the tide gauges. The corresponding table for the T model runs is shown in Appendix D. The inter-annual variations observed from the tide gauges are seen to be relatively well captured in the model. The model-simulated seasonal signal is less than or equal to the amplitude found from the tide gauges, except for two cases (Wick, 1992 and 1993). This indicates that the coarse model grid of app. 35 km might explain only parts of the signals, and that a model with a finer grid resolution might capture more of the near-coastal amplification of the signal.

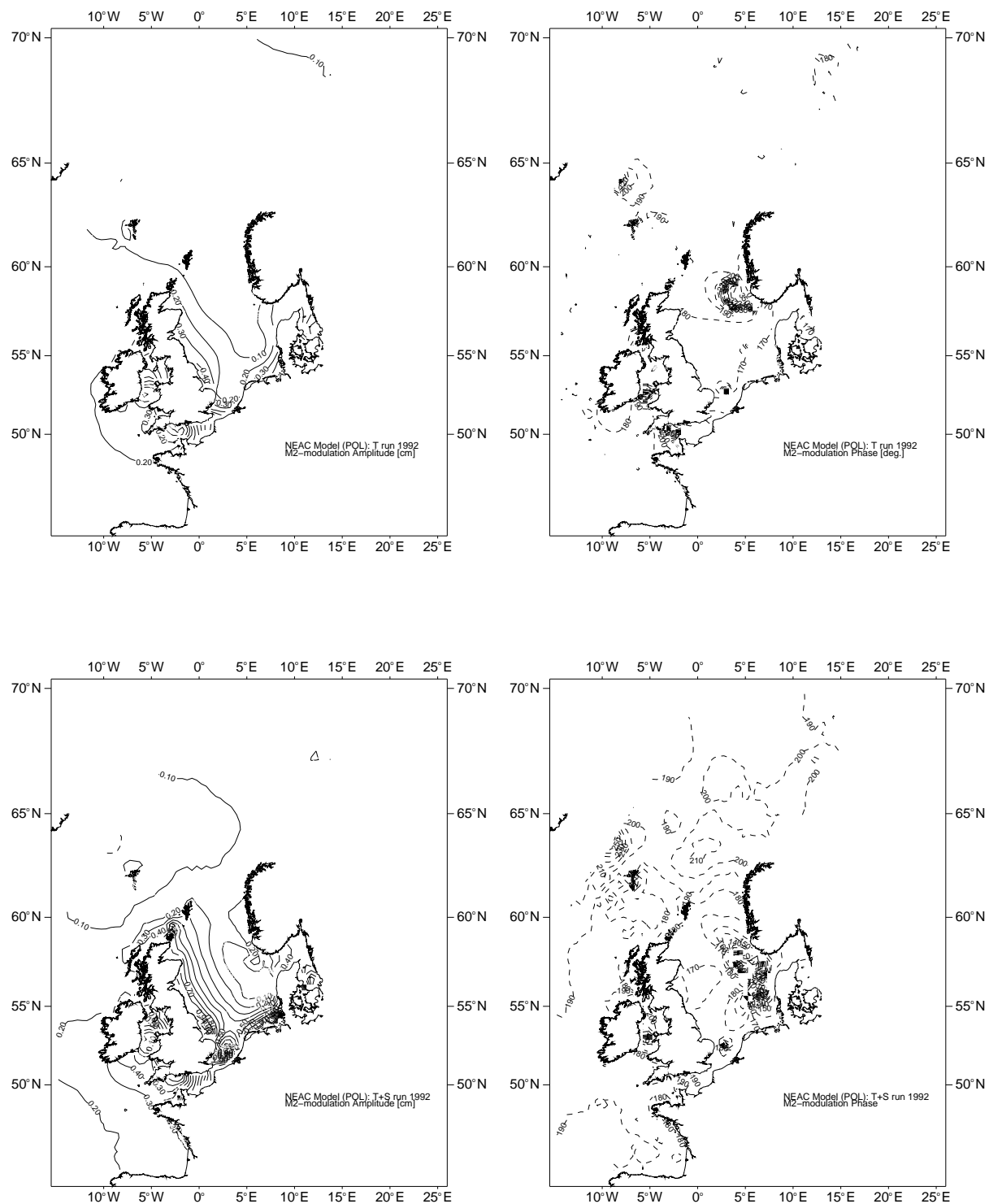


Figure 4.8: The modulation wave $S(t)$ calculated from the NEAC model simulations forced with tides only (top) and tides+atmospheric fields (bottom), for 1992. Contour lines are shown for the amplitude of the modulation [cm] (left) and the phase lag for maximum M_2 (right), with 0° corresponding to January 1. and 360° to December 31.

1992	TG [cm]	TG [%]	TG [°]	2D [cm]	2D [%]	2D [°]
Wick	0.4	0.4	225	0.7	0.9	174
Leith	2.0	1.1	204	1.0	0.5	173
North Shields	1.7	1.0	200	0.9	0.6	170
Lowestoft	1.0	1.4	214	0.5	0.7	176
Sheerness	3.4	1.7	178	1.3	0.7	178
Esbjerg	3.0	4.2	117	0.4	0.6	160
Hvide Sande	1.0	3.0	121	0.0	0.0	162
Hanstholm	1.0	8.1	161	0.4	3.8	170
Hirtshals	0.5	4.3	149	0.5	4.1	165

1993	TG [cm]	TG [%]	TG [°]	2D [cm]	2D [%]	2D [°]
Wick	1.1	1.1	184	1.3	1.1	181
Leith	3.3	1.8	187	2.1	1.1	180
North Shields	-	-	-	1.8	1.1	179
Lowestoft	1.2	1.7	226	1.0	1.5	181
Sheerness	2.7	1.3	150	2.7	1.4	175
Esbjerg	2.8	3.9	120	1.1	1.7	144
Hvide Sande	0.8	2.4	119	0.3	1.1	84
Hanstholm	0.8	5.7	87	0.3	2.9	154
Hirtshals	0.6	4.9	57	0.3	2.5	145

1994	TG [cm]	TG [%]	TG [°]	2D [cm]	2D [%]	2D [°]
Wick	1.4	1.4	216	1.1	0.9	190
Leith	3.0	1.7	207	1.7	0.9	187
North Shields	2.8	1.8	204	1.5	0.9	189
Lowestoft	0.6	0.9	252	0.5	0.7	202
Sheerness	2.4	1.2	138	2.0	1.1	203
Esbjerg	2.8	4.0	135	0.9	1.4	184
Hvide Sande	1.3	4.0	149	0.1	0.4	96
Hanstholm	0.4	3.3	105	0.1	1.0	240
Hirtshals	0.2	2.0	61	0.1	0.8	301

Table 4.7: *The modulation wave $S(t)$ calculated for the British and Danish tide gauge data (TG) along the North Sea coast and the corresponding closest grid point from the NEAC T+S model runs (2D). The absolute [cm] and relative [%] maximum amplitude and time in the year for this maximum are shown for the years 1992 - 1997. (Continues on the next page).*

1995	TG [cm]	TG [%]	TG [°]	2D [cm]	2D [%]	2D [°]
Wick	1.3	1.2	224	0.5	0.4	312
Leith	3.4	1.9	212	0.8	0.4	314
North Shields	2.8	1.8	214	0.7	0.4	309
Lowestoft	0.5	0.7	284	0.3	0.4	321
Sheerness	2.6	1.3	127	0.6	0.3	279
Esbjerg	1.5	2.2	131	0.6	0.9	246
Hvide Sande	-	-	-	0.4	1.5	359
Hanstholm	0.5	3.7	350	0.3	2.9	319
Hirtshals	0.6	5.6	4	0.4	3.3	322

1996	TG [cm]	TG [%]	TG [°]	2D [cm]	2D [%]	2D [°]
Wick	1.2	1.2	206	0.6	0.5	173
Leith	2.4	1.3	193	1.3	0.7	180
North Shields	2.1	1.3	194	1.0	0.6	180
Lowestoft	0.9	1.3	181	0.6	0.9	162
Sheerness	3.3	1.7	120	1.1	0.6	169
Esbjerg	3.0	4.2	68	1.1	1.8	183
Hvide Sande	-	-	-	0.6	2.3	193
Hanstholm	1.1	8.6	52	0.9	9.4	196
Hirtshals	1.2	9.5	45	1.0	9.0	199

1997	TG [cm]	TG [%]	TG [°]	2D [cm]	2D [%]	2D [°]
Wick	1.3	1.3	224	1.0	0.8	192
Leith	2.5	1.4	211	1.7	0.9	194
North Shields	2.3	1.5	213	1.4	0.9	162
Lowestoft	0.9	1.4	249	0.5	0.7	200
Sheerness	2.9	1.5	133	1.9	1.0	187
Esbjerg	2.3	3.3	128	1.1	1.8	182
Hvide Sande	1.3	3.7	126	0.3	1.1	142
Hanstholm	0.6	5.0	83	0.3	3.0	187
Hirtshals	0.4	3.5	69	0.3	2.5	186

Validation Measures

The in-situ tide gauge data set have been used to make statistical measures for the models ability to simulate the observed seasonal signal. The 13 stations Wick, Leith, North Shields, Lowestoft, Sheerness, Roscoff, Cherbourg, Oostende, Cuxhaven, Esbjerg, Hvide Sande, Hanstholm and Hirtshals have been used for a validation of the model in the North Sea. Data from the years 1992-1996 have been used, forming a validation set of 62 data points (values from North Shields, 1993 and Hvide Sande, 1995 and 1996 are missing).

The mean value and the standard deviation calculated for the amplitudes of the seasonal modulation wave fit $S(t)$ for all the 62 validation points are shown in Table 4.8 for the tide gauges, the T model runs, and the T+S model runs. The mean values of the model signal express how good the model runs capture the strength of the observed seasonal signal. About 40% of the variability of the observed signal from the tide gauges are captured by the T+S model runs, whereas only about 20% of the variability is captured by the T model runs. The model simulations have a problem in simulating the strong seasonal signal in the German Bight, as observed in the tide gauge data at Cuxhaven. By exclude Cuxhaven from the validation data set an increase in the models ability to simulate variability in the observed seasonal wave amplitude. The values are shown in the last two columns in Table 4.8. The model simulations with both tidal and meteorological forcing is then able to capture about 60% of the observed variability in the seasonal wave amplitude. The model results identify a strong dependence of the seasonal signal on both the tidal interaction and the tidal-atmosphere interaction.

	N=62		N=57	
	Mean [cm]	St. dev. [cm]	Mean [cm]	St. dev. [cm]
Tide gauges	2.49	2.04	1.99	1.08
T model	0.58	0.45	0.57	0.48
T+S model	1.05	0.76	0.93	0.62

Table 4.8: *The mean and standard deviation calculated for data points around the North Sea for the tide gauges, the T model runs, and the T+S model runs. The first two data columns are calculated for 62 data points, and the last two columns for 57 data points (the same data set, but with Cuxhaven excluded).*

Root-sum-square (RSS) errors have been calculated to estimate the error in the model simulated seasonal signal. Root-sum-square (RSS) errors have been calculated for the amplitude differences and the phase lag differences as well as the total vector difference between the model derived and tide gauge observed signals. The two scalar RSS measures are included to add information on the ability of the model to simulate the modulation wave, as they may reveal if the model has difficulties in reproducing either mainly the amplitude or the phase lag. Large amplitude errors in the model may express problems due to the coarse grid size in the model, whereas phase lag errors may show problems with the propagation of the tidal waves, for instance due to friction.

The scalar RSS measures for the amplitude difference and the phase difference are calculated as

$$RSS_{amp.} = \sqrt{\frac{1}{N} \sum_{i=1}^N (A_{TG} - A_{2D})^2} \quad (4.6)$$

$$RSS_{phase\ lag} = \sqrt{\frac{1}{N} \sum_{i=1}^N (g_{TG} - g_{2D})^2} \quad (4.7)$$

where A_{TG} , g_{TG} , A_{2D} and g_{2D} are the amplitudes and phase lags for the seasonal signal from the tide gauge data and the 2D-model, respectively. The total error between the two modulation waves calculated from the the model and the tide gauges is measured by the vector difference (see Appendix C for derivation)

$$\begin{aligned} RSS_{vector} &= \left[\frac{1}{N} \sum_{i=1}^N \frac{1}{T} \int_0^T \left\| (A_{TG} e^{i(\omega t - g_{TG})} - A_{2D} e^{i(\omega t - g_{2D})}) \right\|^2 dt \right]^{1/2} \\ &= \left[\frac{1}{N} \sum_{i=1}^N \frac{1}{2} [(A_{TG} \cos(g_{TG}) - A_{2D} \cos(g_{2D}))^2 + (A_{TG} \sin(g_{TG}) - A_{2D} \sin(g_{2D}))^2] \right]^{1/2} \end{aligned} \quad (4.8)$$

The sum is made over the total set of data, N . The RSS error calculations for the the T model runs and the T+S model runs validated with the thirteen tide gauges for the years 1992-1996 are shown in Table 4.9. As expected, larger RSS differences to the in-situ tide gauge data set are found for the model runs forced with tides only than for the model runs forced with both tidal and atmospheric fields, proving that the interaction with the atmospheric field is important for the generation of the signal. However, the T model runs show that non-linear interaction between the tidal wave components is responsible for a relatively large part of the seasonal signal. The RSS phase lag errors show that the model does capture the phase lag relatively well with an error of about 2 months for the T+S model runs. As mentioned earlier, the relative large RSS error of 1.1 cm in the amplitude may partly be explained by the coarse model grid size.

	T+S model	T model
$RSS_{amp.}$	2.7 cm	2.1 cm
$RSS_{phase\ lag}$	83°	70°
RSS_{vector}	2.2 cm	1.9 cm

Table 4.9: *RSS measures for amplitudes and phase lags of the seasonal modulation wave fit, $S(t)$. The RSS values for the T model runs and the T+S model runs are calculated on $N=62$ validation points (13 tide gauges for 5 years).*

4.5.2 Atmospheric Interaction

The large inter-annual variations seen in Figure 4.5 and Table 4.7 for the MA_2 and MB_2 constituents indicate a correlation with the inter-annual variability in the atmospheric fields. This was investigated in previous work by *Pugh and Vassie* (1994) and *Baker and Alcock* (1983). Further attempts to identify this correlation with the atmospheric field are carried out here, by using the additional information available from the numerical model runs.

Information about the annual mean wind fields for the North Sea area are shown in Table 4.10 for the years 1992 - 1997 (*Reistad and Iden*, 1998). The mean wind speed and standard deviation from 6 hourly sampled observations are shown for two off-shore oil rigs. The data from the Frigg field (59.9°N; 2.1°E) represents the northernmost part of the North Sea, and the data from the Ekofisk field (56.5°N; 3.2°E) the mid North Sea area. In the brackets in Table 4.10 are shown the corresponding model values from the atmospheric hindcast fields used as the forcing fields for the NEAC model runs (*Reistad and Iden*, 1998). Information of the mean wind, the standard deviation and the most frequent wind direction from the Danish meteorological station at Blåvands Huk (55.6°N; 8.1°E) are included in the Table to represent the eastern part of the North Sea area. The on-shore station at Blåvands Huk is located 23 km NW of the tide gauge station at Esbjerg. Spatial variations in the wind fields are observed with the strongest winds

	Frigg		Ekofisk		Blåvands Huk		
	Mean [m/s]	St.dev. [m/s]	Mean [m/s]	St.dev. [m/s]	Mean [m/s]	St.dev. [m/s]	Most frequent wind dir.
1992	8.4 (8.7)	4.0 (4.2)	8.3 (8.6)	3.9 (3.8)	7.2	3.5	W
1993	8.3 (8.7)	4.6 (4.7)	8.4 (8.7)	4.4 (4.4)	7.2	3.6	W
1994	8.8 (8.8)	4.8 (4.5)	8.1 (8.7)	4.2 (4.1)	7.2	3.5	W
1995	8.9 (8.6)	4.8 (4.6)	8.3 (8.4)	4.2 (4.2)	7.0	3.8	W
1996	8.4 (9.0)	4.6 (4.3)	8.3 (8.8)	4.1 (4.0)	6.6	3.5	E
1997	8.2 (8.8)	4.4 (4.6)	7.5 (8.4)	3.9 (4.2)	6.6	3.7	W

Table 4.10: *Meteorological information for the North Sea area.*

at Frigg in the north and a decrease to the south at Ekofisk and Blåvands Huk. The observed wind field for 1996 differs significant from the other years by being dominated by easterly winds - at least along the Danish coast, where wind directions are available. Differences between the model simulated wind field and the observations are seen in Table 4.10 for the two validation points. It is worth noticing that the atmospheric model simulates the strongest mean wind in 1996, whereas the observations show that 1996 had a relative weak wind field. These differences between the model and the observed wind fields clearly explain part of the differences found between the validation data and those of the NEAC model runs.

To investigate the existence of any dependencies to the atmospheric fields, the amplitude of the seasonal signal has been plotted against the available wind information. The amplitude of the modulation wave as a function of the annual mean wind field for the 6 years of data is plotted in Figure 4.9. The calculations from the tide gauge observations are plotted to the left and from

the T+S model simulations to the right. For the tide gauges, the seasonal amplitude is plotted as a function of the observed wind field (i.e. either Frigg, Ekofisk or Blåvands Huk), and for the model simulated amplitude as function of the atmospheric model wind field at Ekofisk. In Figure 4.10 the seasonal amplitude is plotted against the variability in the annual wind field to investigate the influence from the variability in the wind instead of only the strength. In Figure 4.11 the seasonal amplitude is plotted against the local annual variability in the sea level. This figure is plotted to try to eliminate the effects due to the spatial changes in the wind field caused by the location of the meteorological observations being far away from these coastal validation points. For the tide gauges, the standard deviation in the observed sea level data is used as a measure of the sea level variability. For the model data the standard deviations in the sea level were not directly available, and the amplitude of the annual constituent Sa is used instead, as the Sa constituent can be considered as representing the annual variability in the sea level caused by the atmospheric field (*Amin*, 1982). Information about Sa was available only for five years of model data, as Sa values were not saved from the harmonic analyses for 1995.

Figure 4.9 displays a weak correlation between the amplitude and the annual mean wind particularly for the model data. From Figure 4.10 is seen a modest correlation with an increase in the amplitude for an increase in the wind variability for the three northernmost stations along the British east coast. This pattern is seen for both the tide gauge data and the model simulations. For the model data, the amplitudes for 1995 (with $\text{st.dev.} = 4.2 \text{ m/s}$) fall outside the correlations, but that might be caused by the relatively weak mean wind field in the model data for this year, as seen in Table 4.10.

One pattern that might be important is observed in Figure 4.11. For the model-simulated signal, the four northernmost stations along the British east coast, i.e. Wick, Leith, North Shields and Lowestoft show a larger dependence on the local annual sea level variability than seen for Sheerness and the four Danish stations. Additionally, a comparison of Figures 4.9 and 4.11 reveals for the model-simulated signal at the Danish stations a slightly stronger correlation to the wind fields than the local sea level variability. This may indicate that the seasonal signal in the North Sea has different causes. It seems possible that the signal in the northern part of the North Sea could be more influenced by the local changes in the sea level, than seen for the southern part of the North Sea and especially along the Danish coast. In the southern part of the North Sea, where the tidal wave has propagated longer in shallow waters, the seasonal signal seems to be more influenced by an externally generated signal, as for instance the wind field over the North Sea, and less by the local sea level. Of course, this conclusion is based on a very limited set of data, but at least there seems to be an indication that the signal in the North Sea is caused by different generation mechanisms. More data are needed to investigate this further. Furthermore, this suggestion of different generation mechanisms is mainly obtained from the model-simulated seasonal signal. For the seasonal signal calculated from the tide gauge observations, a more blurred pattern is observed. This might indicate that the mechanisms causing the seasonal signal are more complicated than what is captured in the model. Local effects such as wind set-up inside harbours, where most of the tide gauges are located, may be possible reasons for the differences observed between the tide gauge and model data. Effects of baroclinic processes may also contribute to the observed disagreements between the tide gauges

and the barotropic model results.

The dependence of MA_2 and MB_2 amplitudes on the wind field have been investigated to see if the separation of the seasonal effect into MA_2 and MB_2 constituents show a different dependence on the wind field and the local sea level variability, and consequently complicate the dependence of the combined modulation wave on the wind and sea level variability. These analyses gave no further information for either the tide gauge observations or the model data. To make a more robust statistical investigation, 89 years (1901-1992, except 1980, 1982 and 1990) of analyzed data from the tide gauge station in Esbjerg were obtained via *Hvidberg-Knudsen et al.* (1994). The MA_2 and MB_2 amplitudes are plotted in Figure 4.12 as a function of the Sa amplitudes. A linear fit is shown together with the linear correlation coefficient. A trend with an increase in the MA_2 and MB_2 amplitudes for an increase in the Sa amplitude is seen, but correlation coefficients of less than 0.4 indicate that the local atmospheric influence - here represented by the Sa amplitude - does not play a clearly dominant role for the seasonal tidal signal at Esbjerg. This is in agreement with the findings from *Pugh and Vassie* (1994) who analyzed the correlation of the variation in the M_2 constituent to the residual surges for 30 and 70 years of tide gauge data from Newlyn and Southend, located at the western and eastern side of the southern part of the Britain, respectively, and found little significant correlation.

The findings in Section 4.4.3 concerning the local influence on the MA_2 and MB_2 phase lags are in relatively good agreement with the indications above of different generation mechanisms. In Figure 4.6 only little local influence was found on the MA_2 and MB_2 phase lags in agreement with the indications of a larger dependence on the remote wind field, than on the local sea level variability. For the British coast a change in the behaviour of the phase lag differences was observed between the three northernmost stations and Lowestoft and Sheerness to the south. This does agree with the indications of a more local influence in the northern part of the North Sea and a more external influence in the southern part.

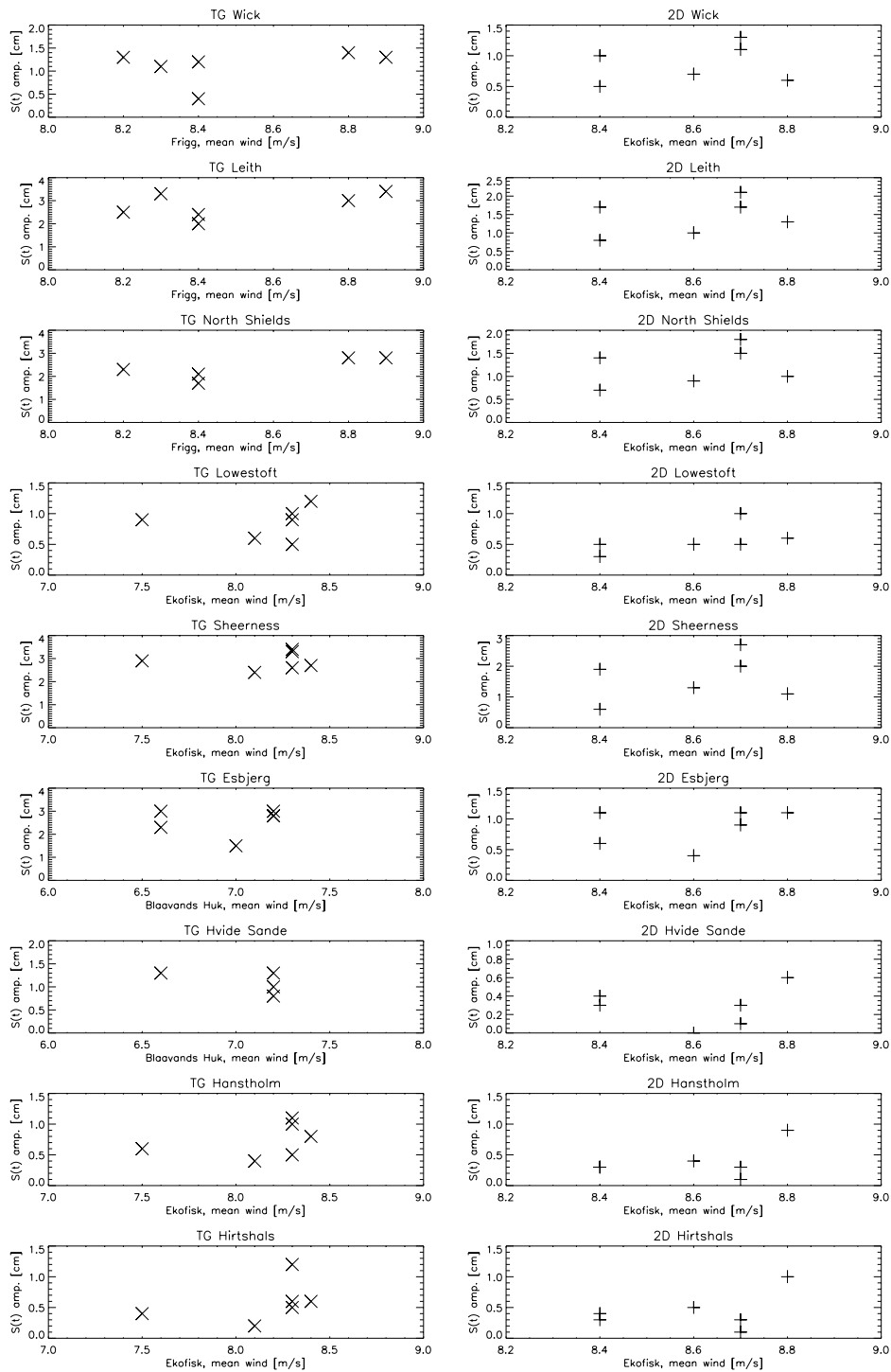


Figure 4.9: Amplitude of the modulation wave plotted as a function of the annual mean wind. Tide gauge data to the left and model simulations to the right.

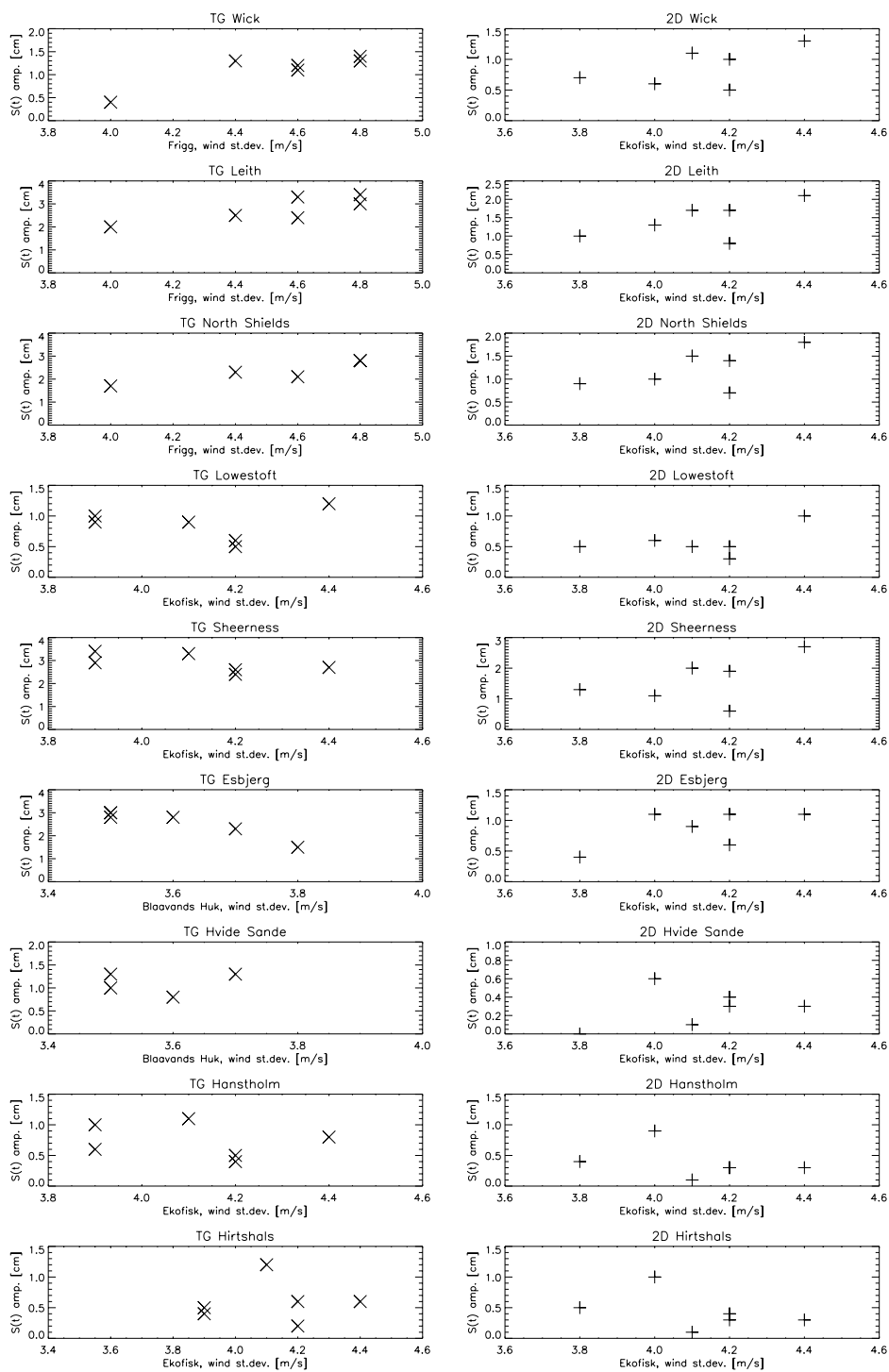


Figure 4.10: Amplitude of the modulation wave plotted as a function of the standard deviation in the annual wind field. Tide gauge data to the left and model simulations to the right.

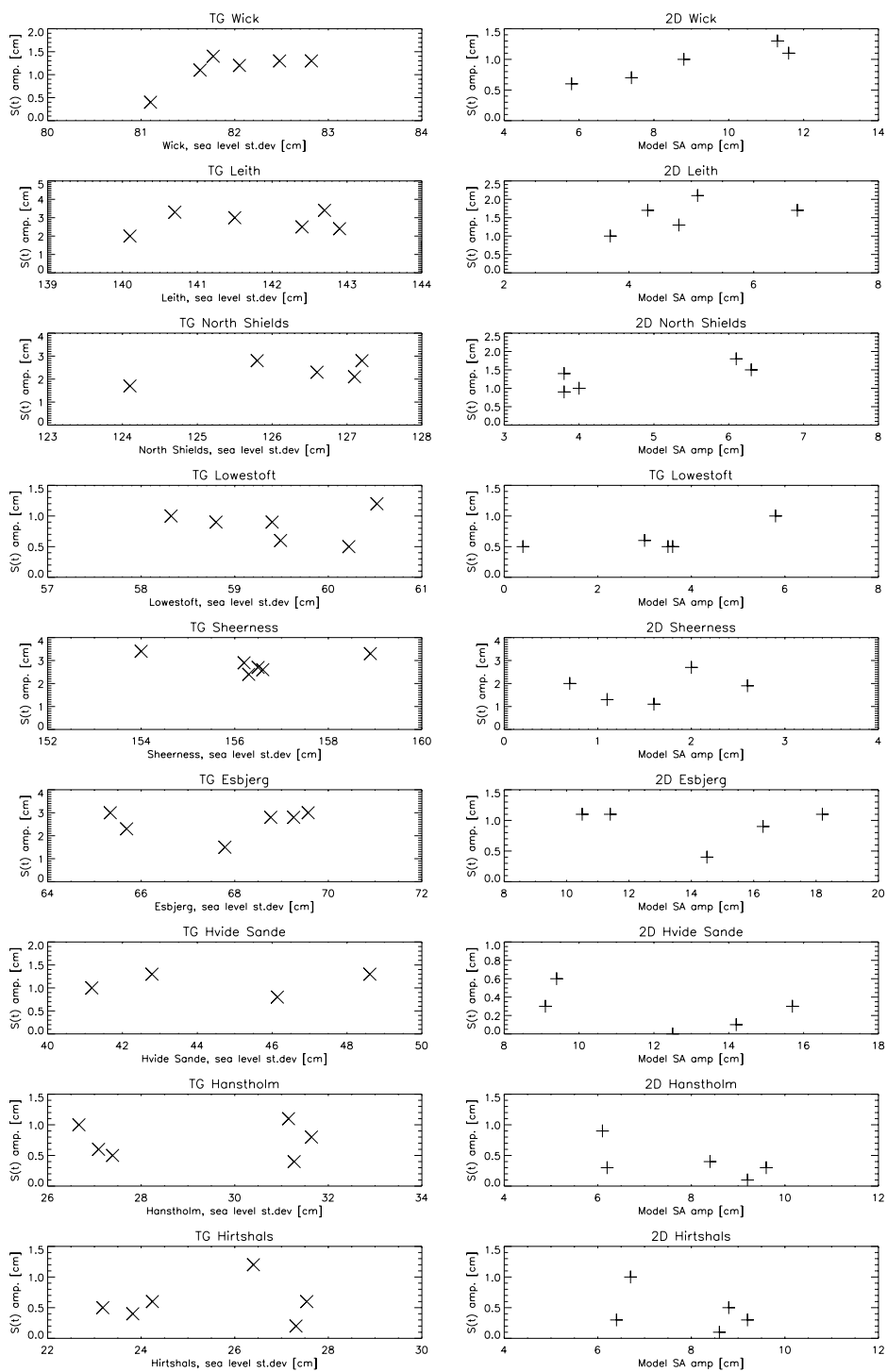


Figure 4.11: Amplitude of the modulation wave plotted as a function of the annual sea level variability. Tide gauge data to the left and model simulations to the right.

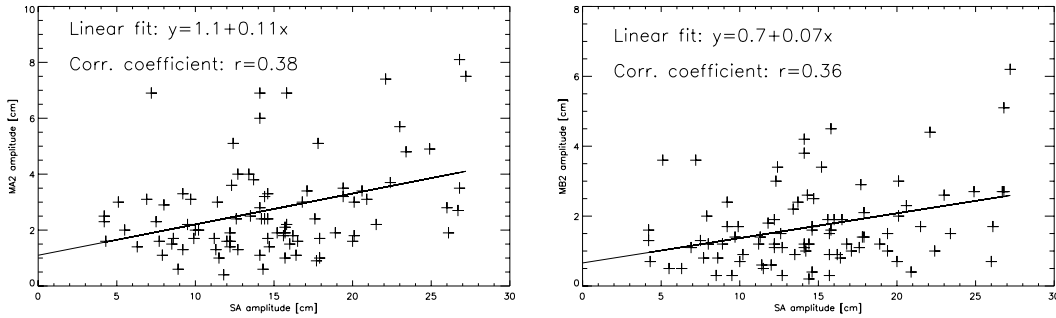


Figure 4.12: Amplitude of the MA_2 and MB_2 constituent plotted as a function of the Sa amplitude for 89 years of data from the tide gauge at Esbjerg.

4.5.3 Baroclinic Model

With the purpose to investigate the effect of baroclinic processes on the seasonal signal, data from a 3D baroclinic model have been analyzed. Results from the baroclinic model developed by Roger Proctor, POL, U.K, with a set-up covering the north western European shelf area have been investigated. The model solves the full 3D equations on a Arakawa B grid using σ -coordinates. The spatial resolution of the model is ($\frac{1}{9}^\circ$) in latitude and ($\frac{1}{6}^\circ$) in longitude (see *Proctor and James (1996)* for more information about the model). Data used for this study were from a model run forced with nine tidal constituent at the open boundaries (Q_1 , O_1 , K_1 , μ_2 , N_2 , M_2 , L_2 , S_2 , and M_4) and forced with atmospheric winds, pressure and solar radiation input. Data from one year of simulation (Nov. 1988 - Oct. 1989) were kindly provided by Jason Holt, POL. Harmonic analyses of the sea level data were carried out for each month. The 3D model clearly captured an annual variation in the M_2 constituent, with maximum amplitudes in mid summer (June) and minimum amplitudes in winter (December). The simulated annual variation in the M_2 amplitude, i.e. the M_2 amplitude in December subtracted from the June amplitude, is plotted in Figure 4.13. In general, the same coastal effect pattern is observed as found from the 2D model simulations, but the model revealed far too large annual variations in the M_2 constituent. For the German Bight area, where the highest variations are found, variations of more than 40 cm are seen, which are unrealistic values. In defence of these poor results from the 3D-model, the model was constructed with the purpose to simulate other parameters, such as temperature and salinity, and the main focus in the calibration of the model is, therefore, not on calibration and validation with respect to sea level. The model is still improved and it is the intention to investigate later versions of the model.

4.5.4 Bed Friction Test

The seasonal effects in the MA_2 and MB_2 constituents are clearly identified as shallow water phenomena. To estimate the influence from non-linear friction, numerical tests with the 2D barotropic model Mike 21 have been carried out. These tests are simple ones, with the objective to estimate the dependence of the bed friction. Two Mike 21 model runs, forced with tides only,

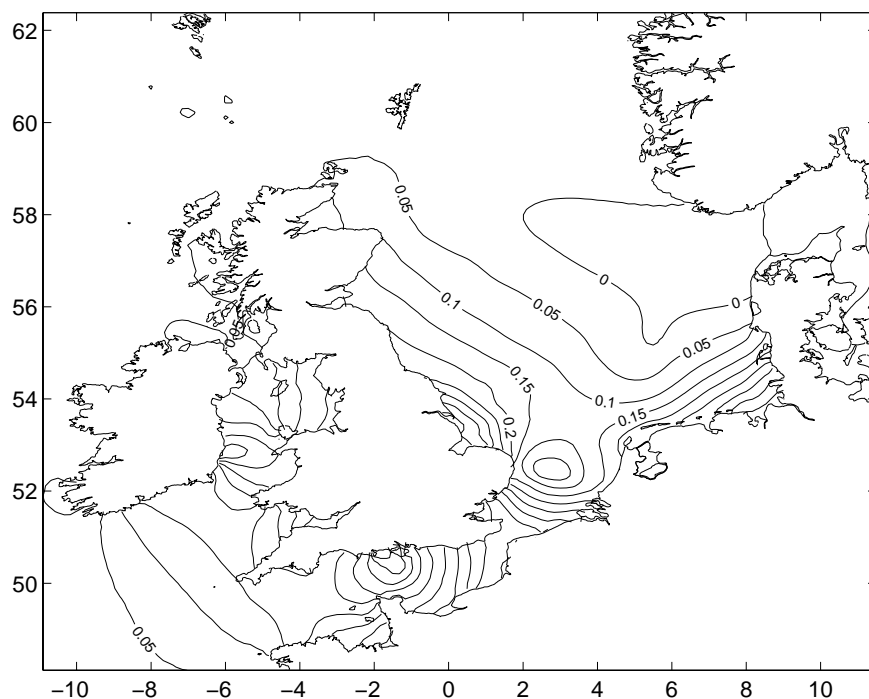


Figure 4.13: Annual variation of the M_2 amplitude from the 3D model. Units are in metres.

were carried out for one year of simulation (1/1 1998 - 1/1 1999), with one model run with a low bed friction coefficient (Manning number, $M=36$ [$\text{m}^{1/3}/\text{s}$] in Eqn. 2.2), and one with a high bed friction coefficient ($M=32$ [$\text{m}^{1/3}/\text{s}$]). The difference in the bed friction corresponds to an increase in the total water column by 43% at all grid points from the high friction model run to the low friction model run, but they are both realistic friction values and within the range used in the current operational model set-up at DMI. These two model runs were carried out to estimate the non-linear interaction between the tidal wave components caused by the bed friction. Two additional Mike 21 model runs were carried out forced with both tidal and atmospheric forcing. These two model runs were carried out with the same two bed friction coefficients, with the objective to estimate the non-linear interaction between the tidal wave and the atmospherically induced sea level changes. In Tables 4.11 and 4.12 are shown the modulation wave $S(t)$ calculated from the four model runs. Results are shown for six data points along a line crossing the southern part of the North Sea from the coast of mid England in the west to the German Bight area in east, and for a grid point near to Esbjerg at the Danish Wadden Sea coast. The locations of the data points are shown in Figure 4.14. In the two tables are shown the amplitude of the modulation wave in absolute values [cm], relative to the M_2 amplitude and the phase lag for the maximum M_2 . For the two model runs forced with tides only (T model runs), the larger bed friction extracts more energy from the water column at the three most westerly points on the line across the North Sea, resulting in smaller tides. However, at points 5, 6 and at the Esbjerg point the higher bed friction results in a larger seasonal signal. This demonstrates

that the non-linear bed friction is at least a significant factor in determining the seasonal signal. A dependence is seen on the propagation time of the tidal wave in shallow water areas, as a clear seasonal signal (i.e. above the annual signal of M_2 by 0.65%) is only found in the eastern part of the North Sea. For the two model runs forced with both tidal and atmospheric fields (T+S model runs), a pronounced increase in the signal is seen at points 4, 5, 6 and Esbjerg for both an increase in the bed friction and compared to the T model runs.

These Mike 21 model runs display that the seasonal signal is caused by non-linear interaction, and partly due to the bed friction, between both the tidal wave components and the tidal-surge interaction, with a significant contribution from the latter. This is in agreement with the NEAC model results in Section 4.5.1. The Mike 21 model runs were carried out with nested areas, which enables a grid resolution of 1 n.m. (1.9 km) in the Wadden Sea, and at Esbjerg the model simulated seasonal signal of 3% agrees well with the tide gauge observations. This supports that the main part of the missing strength in the NEAC model derived seasonal signal compared to the tide gauge observations might be caused by the coarse grid resolution of 35 km in the NEAC model.

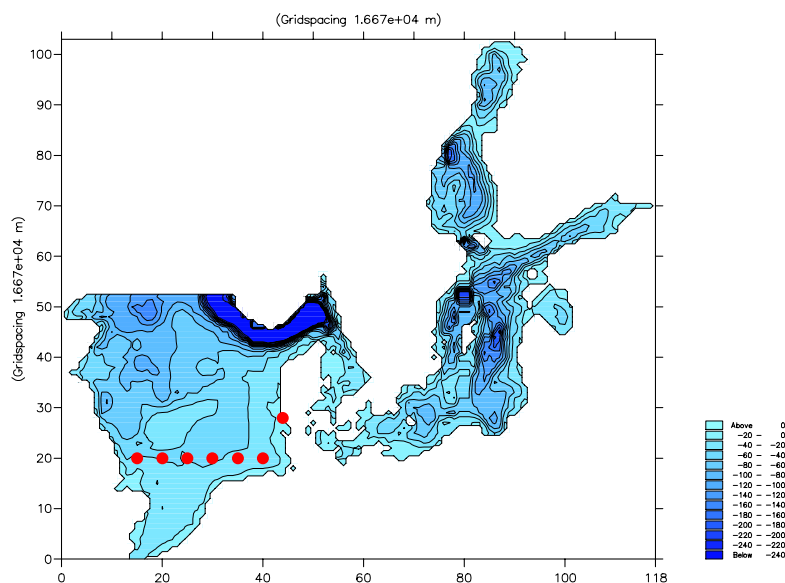


Figure 4.14: *Mike 21 set-up used for the friction tests. The location of the data points in Table 4.11 and Table 4.12 are indicated by the dots.*

4.6 Summary of Seasonal Variations in M_2

A summary of the findings of the investigations of the seasonal signal is that the accuracy of the T/P data enables off-shore observations of the deviations in the main constituent M_2 . This new knowledge about the spatial behaviour of the seasonal signal has been used as validation for a numerical model. The model results confirm that the seasonal signal is caused by non-linear

Low friction model run	Point 1	Point 2	Point 3	Point 4	Point 5	Point 6	Esbjerg
Amplitude [cm]	0.74	0.46	0.30	0.25	0.37	0.65	0.51
Rel. amplitude [%]	0.50	0.52	0.53	0.58	0.82	0.99	1.09
Phase lag [°]	198	196	190	177	172	176	178

High friction model run	Point 1	Point 2	Point 3	Point 4	Point 5	Point 6	Esbjerg
Amplitude [cm]	0.68	0.44	0.27	0.24	0.36	0.60	0.48
Rel. amplitude [%]	0.47	0.51	0.52	0.60	0.86	1.02	1.13
Phase lag [°]	198	196	193	179	175	177	181

Table 4.11: *The modulation wave for the two Mike 21 T model runs calculated for the six data points on the line across the North Sea - numbered from west to east - and for the Esbjerg grid point.*

Low friction model run	Point 1	Point 2	Point 3	Point 4	Point 5	Point 6	Esbjerg
Amplitude [cm]	0.93	0.60	0.40	0.46	1.01	1.77	1.37
Rel. amplitude [%]	0.63	0.68	0.73	1.08	2.28	2.77	2.69
Phase lag [°]	162	169	174	168	167	170	192

High friction model run	Point 1	Point 2	Point 3	Point 4	Point 5	Point 6	Esbjerg
Amplitude [cm]	0.90	0.58	0.38	0.45	0.97	1.69	1.34
Rel. amplitude [%]	0.63	0.69	0.74	1.12	2.38	2.94	2.94
Phase lag [°]	160	169	174	172	170	171	192

Table 4.12: *The modulation wave for the two Mike 21 T+S model runs calculated for the six data points on the line across the North Sea - numbered from west to east - and for the Esbjerg grid point.*

interaction, and by that is a shallow water phenomena, which was previously indicated from investigations based on coastal tide gauge data. The model tests reveal that the main part of the seasonal signal is a barotropic phenomena and caused by the non-linear interaction, with a strong dependency to the tide-surge interaction. The influence from the non-linear bed friction is shown to be significant. Furthermore the model simulations indicate that the seasonal signal in the North Sea area may have slightly different causes. The seasonal variations along the northern part of the British east coast seem to be more influenced by a locally generated signal than in the southern part of the North Sea, where the variations seem to be more influenced from a signal generated remote in the North Sea. This is partly validated by the tide gauge data, but the tide gauge observations show in general a more blurred pattern than obtained from the model results, indicating that the generation of the seasonal signal is more complicated than what is captured in the barotropic models alone. This could be due to small scale and near coastal shallow water effects not captured in the models, and also contributions to the signal from baroclinic processes. Baroclinic effects from small scales as fresh water plumes and up to large scales in both space and time as the steric effect might contribute to the seasonal signal.

Unfortunately it has not been possible within this study to test the influence from any baroclinic processes with model data.

M. Amin, POL, UK, has previously suggested that the observed seasonal signal in the tidal constituent M_2 might be caused by larger friction in the winter months (due to the higher wave amplitudes) that will extract more energy from the tidal wave, and opposite in the summer months, where less energy will be extracted from the tidal wave. The results shown here from the few tide gauges located in both hemispheres do support this theory with positive deviations in the M_2 amplitude in summer time and negative deviations in winter time in each hemisphere. Also the model results found with the high dependence on bed friction and the strong influence from the atmospheric fields tend to confirm this theory.

Inclusions in tidal predictions

Inclusions of the MA_2 and MB_2 constituents in a tidal prediction at a specific location will reveal an average seasonal variation in the M_2 constituent. The accuracy of this seasonal signal will depend on the variability of the tide-surge interaction in that area. To determine if the MA_2 and MB_2 constituents has to be included in a tidal prediction at a specific station, a counterbalance of the signal to noise ratio of the seasonal signal at that station has to be done. If large inter annual variabilities in the MA_2 and MB_2 constituents exist, the error introduced in the tidal predictions by including these constituents might be of the same order of magnitude as the error of not resolving for the seasonal signal. However, by not including significant MA_2 and MB_2 constituents in a prediction will for certain introduce an error in the tidal prediction.

Chapter 5

Atmospheric Effects on Sea Level

5.1 The Wind Effect

The atmospheric winds play an important role in transferring momentum into the ocean. The part of the ocean influenced by the wind energy input is named the oceanic top boundary layer, or the Ekman layer which has a vertical scale of the order 10-100 m depending on the wind and the stratification in the water column. The magnitude of the wind input on the ocean surface is estimated from the empirical drag formulation

$$\tau(W) = c_D(W) \rho_a W_{10}^2, \quad (5.1)$$

where the wind stress τ on the surface is a function of the wind speed at 10 m W_{10} , the density of the atmosphere ρ_a , and a drag coefficient c_D depending on the roughness of the surface and the wind speed W .

5.1.1 The Ekman Transport

In the open and deep ocean with the assumptions of a simple situation with a constant blowing wind, the vertical transport of the wind energy in the water column will be caused by a balance between the friction force and the Coriolis force. The resulting velocity profile will form the Ekman current spiral with decreasing and rotated velocity vectors with depth, named after V. W. Ekman, who in 1902 described this system. Integrated over the water column the volume transport will be to an angle of 90° to the right (left) on the northern (southern) hemisphere relative to the atmospheric wind above the atmospheric boundary layer. For an atmospheric low pressure system the Ekman volume transport will force the water to diverge away from the low pressure center, and cause a depression of the sea level at the center of the atmospheric low pressure system. For an atmospheric high pressure system the Ekman volume transport will force the water to converge, and cause a sea level rise below the high pressure system.

5.2 The Pressure Effect

In addition to the wind effect also the atmospheric pressure causes movements in the water. An atmospheric pressure anomaly will force the water mass to move and set up a new sea level to

balance the new pressure situation.

5.2.1 The Inverse Barometer Effect

Assuming hydrostatic pressure and that the sea has reached an equilibrium situation with the atmospheric pressure field (i.e. no water currents) a stationary pressure anomaly in the atmosphere will cause an inverse anomaly in the sea level given by

$$\Delta\eta = -\frac{\Delta P_a}{\rho g}, \quad (5.2)$$

where $\Delta\eta$ is the sea level deviation, ΔP_a the atmospheric pressure anomaly, ρ the water density, and g the gravity. An atmospheric pressure anomaly of 1 hPa will cause an inverse response in the sea level of approximately 1 cm. This is named the stationary inverse barometer (IB) effect. An estimate of the time for the sea to reach the full developed static inverse barometer effect in equilibrium with the atmospheric pressure anomaly can be obtained from the governing equations. For the simple situation of a suddenly applied atmospheric anomaly ΔP_a and assuming no initial motion in the water before the anomaly is applied the time dependency of the linear sea response from $\eta(t=0)=0$ to η_{max} can in 1 dimension be shown to be of the form

$$\Delta\eta = -\frac{\Delta P_a}{\rho g} [1 - e^{-k \cdot c_f \cdot t}], \quad (5.3)$$

where t is the time from $t = 0$ where the atmospheric anomaly was applied, $c_f = \sqrt{gh}$ the phase velocity of the ocean wave set up to adjust for the pressure anomaly, and k an appropriate wavenumber for the atmospheric pressure system. For the North Sea with a mean water depth of $h = 70$ m, and a typical length scale of a mesoscale atmospheric system of $k = 1/(100 \text{ km})$, the time scale for the sea level to adjust to a suddenly applied atmospheric anomaly from $\eta(t=0)=0$ to the static IB effect is estimated from Eqn. 5.3 to be of the order of half an hour.

An extension of the stationary inverse barometer situation was proposed by *Proudman* (1953) by allowing the atmospheric pressure anomaly to move with the constant velocity c_a . The response in the sea level can then be found from the equations of motion to be of the form

$$\Delta\eta = -\frac{\Delta P_a}{\rho g (1 - \frac{c_a^2}{c_f^2})} \quad (5.4)$$

This is named the dynamical inverse barometer effect, and the sea response is seen to depend on the relative velocities between the atmospheric system and the generated oceanic wave. A larger response in the sea level than for the stationary case in Equation 5.2 is seen for a situation with a small relative velocity difference. Friction will, of course, prevent the sea level response to grow to infinity.

5.2.2 Deviations from the Inverse Barometer Effect

Observations of relatively large deviations from the theoretical deduced stationary inverse barometer effect have been reported and studied in several papers. One obvious possible explanation

for an effect less than the theoretical predicted inverse barometer effect for an atmospheric system consisting of simple pressure anomaly cell with corresponding geostrophic winds may be caused by the two contrary contributions to the sea level change from the pressure and the wind as described in Section 5.1.1.

Hamon (1966) investigated tide gauge data from around Australia and found large deviations from the theoretical static inverse barometer effect. *Hamon* found values of the IB effect both above and less than the theoretical value of 1 cm/hPa, with a large dependency on the location of the tide gauges. Also a large frequency dependency of the values was observed. *Hamon* suggested that the atmospheric caused sea level response might consist of the static inverse pressure response and a dynamical response

$$\eta_{atm.} = \eta_{IB} + \eta_{dyn.} = \eta_{IB} + \eta_p + \eta_w \quad (5.5)$$

where the dynamical response is divided into both a pressure and a wind contribution. To explain the observed large IB deviations *Hamon* investigated the effect from wind set-up along the coast but concluded that this effect could explain only a small part of the observed deviations. *Hamon* therefore suggested, and made probable, that the observed IB deviations might be explained by the effects from a travelling shelf wave.

In addition to the non-isostatic pressure responses observed over shelf regions deviations from the static response have also been reported from more open sea areas, e.g. *Woodworth et al.* (1995), who analyzed islands tide gauges in the southern Atlantic. They found a pronounced deviations from the theoretical IB effect at a time scale of 5 days, and suggested a global atmospheric 5-day pressure wave to be the most likely forcing mechanism. Analyses of altimetry data do in general support these findings from the tide gauge observations with large deviations from the theoretical IB effect (*Fu and Pihos*, 1994; *Gaspar and Ponte*, 1997, 1998; *Woodworth et al.*, 1995). Numerical simulations have been performed to further investigate the IB effect, and the correlation between the pressure and wind effect (*Gaspar and Ponte*, 1997, 1998; *Ponte*, 1994). *Ponte* (1994) found from numerical simulations in the northern Atlantic that the static barometer effect dominates the sea level variability compared to the dynamical effect (Eqn. 5.5) for time scales larger than a few days, and that a significant anti correlation between the simulated pressure and wind induced sea level deviations causes a decrease in the IB effect of 10-20 % for the northern Atlantic. Furthermore relative good agreements between the IB effect determined from T/P altimetry observations and a global numerical model have been found by *Gaspar and Ponte* (1997, 1998). From model simulations forced with atmospheric pressure only and with both atmospheric pressure and winds they were able to estimate that deviations from the theoretical IB effect might be due to the dynamical response in the sea level caused by both the pressure-driven and the wind-driven dynamical effects.

The variability of the atmospheric pressure shows a significant latitude dependency with larger variability at higher latitudes than at lower latitudes. For periods larger than a few days the static atmospheric pressure contribution dominates the total atmospheric induced sea level variations (e.g. *Ponte* (1994)). The IB effect will therefore play a larger role than the dynamical effects at high latitudes, which is consistent with that the largest deviations from the theoretical IB effect are found at low latitudes (*Gaspar and Ponte*, 1997, 1998; *Ponte*, 1994).

5.2.3 Estimation of the IB Effect in the Eastern North Sea

The inverse barometer effect has been estimated for Esbjerg and Hanstholm along the Danish coast to represent the shallow and coastal area in the North Sea highly influenced by local wind effects. Eight years of 3 hourly residual sea levels (observations - tidal prediction) from the on-shore tide gauges in Esbjerg (1991-1997) and Hanstholm (1992-1998) are plotted in Figure 5.1 as function of atmospheric pressure observations from the synop stations at Blåvands Huk 23 km WNW of Esbjerg, and from Thisted Airport 20 km SSE of Hanstholm. The IB effect is estimated by a linear regression to be -2.0 cm/hPa and -1.4 cm/hPa for Esbjerg and Hanstholm, respectively. These IB deviations from the theoretical value show that the theoretical IB value is highly interrupted in this area and that the dynamical response dominates over the static IB response along the Danish coast. These IB values are comparable with the values found by *Hamon* (1966) from tide gauges on the western and southern coast of Australia. As described above Hamon concluded that a shelf wave was more likely to explain the IB deviations than a local wind set-up. No further investigations of the cause to the IB deviations along the Danish coast have been performed, but a tendency is seen in Figure 5.1 for the Esbjerg data for larger deviations from the theoretical IB value for the extreme pressure anomalies - both for the high and low pressure values. This may indicate that the wind effect and wind set-up/set-down from the strong winds associated with the strong pressure anomalies may play an important factor in explaining the large deviation in this area from the theoretical IB value of -1 cm/hPa. When the extreme sea level residuals for ± 100 cm are excluded for the Esbjerg data the IB effect is estimated to be -1.6 cm/hPa. For the off-shore station at Horns rev the IB effect is estimated to be -0.6 cm/hPa and -1.3 cm/hPa, for the two data periods, respectively (see Appendix A). This supports that the wind set-up along the coast may explain part of the large deviation from the theoretical value for the IB values estimated at Esbjerg.

5.3 Atmospheric Tide

The tidal forces do also effect the air masses in the atmosphere and cause atmospheric tides. In altimetry observations corrections for the atmospheric load (IB effect) are often required, as for instance for ocean tidal analyses, and the atmospheric tides may interact with the loading corrections. *Ray* (1994) emphasized that effort should be taken to avoid atmospheric tidal signal when corrections for the atmospheric loading are made, by using the static IB effect, as mismodelling of the atmospheric tide will directly go into the sea level estimate and especially the ocean tide.

The atmospheric tides is here estimated for 8 years (1991-1997) of atmospheric pressure observations from the synop station in Blåvands Huk located 23 km WNW of Esbjerg. The spectrum from a Fourier transformation of the 8 years of data is shown in Figure 5.2. The spectrum is seen to be highly dominated by long periodic signals, and less than 3% of the energy is located at frequencies larger than $f=0.00001$ Hz ($T < 28$ days). Peaks at the diurnal and semi-diurnal tidal frequencies ($f=1.2 \cdot 10^{-5}$ Hz and $f=2.3 \cdot 10^{-5}$ Hz respectively) are seen, and the largest tidal signals are found from a harmonic tidal analysis to be 0.22 hPa and 0.17 hPa for the S_2 and S_1 tidal constituents, respectively. This estimates the effect of the atmospheric tides on the sea

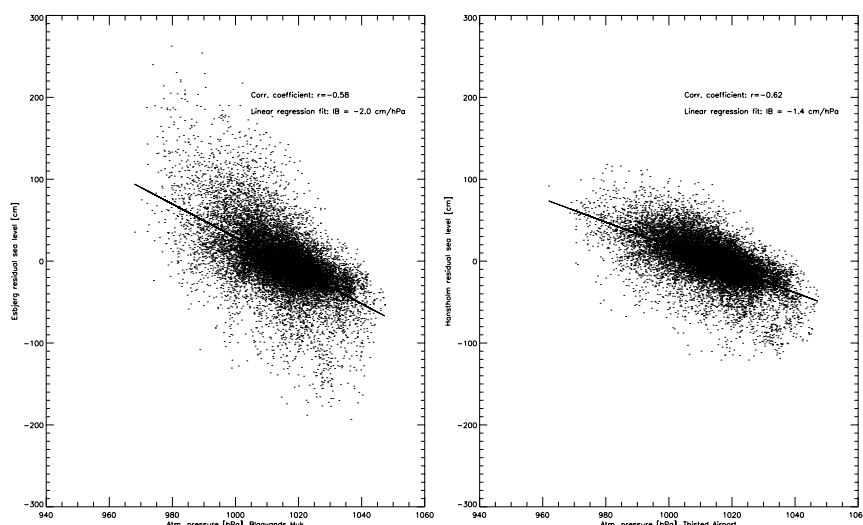


Figure 5.1: Scatter plot of residual sea level as function of atmospheric pressure observations at Esbjerg (left) and Hanstholm (right).

level in this area to be of the order of less than half a centimeter.

5.4 “The Summer Wave 1998”

The most severe sea level changes caused by the weather are in the North Sea due to winter storm surges with time scales of hours to days and on a large spatial scale. To illustrate severe effects on a significantly smaller time and spatial scale possible caused by the atmospheric system, the situation of the 21/7 1998 will be described.

In the morning of the 21. of July 1998 abrupt and severe sea level changes - for the Danish area - were observed along the Danish North Sea coast. The maximum sea level residuals and the corresponding arrival times are shown in Table 5.1 at four tide gauges. Time series for the observed sea level at three of the stations Hvide Sande, Torsminde and Thyborøn are available and are shown in Figure 5.3. The sea level increased at a rate of up to 18 cm/min and occurred with local maxima at about 9.30-10.00 UTC on increasing tide with the tidal maximum at about 13 UTC. The total disturbance of the sea level had a time scale of about 1 hour.

Station	Latitude	Time [UTC]	Residual [m]
Hvide Sande	56° 00' N	9.34	0.4
Torsminde	56° 22' N	9.42	0.5
Ferring	56° 32' N	9.45	0.6
Thyborøn	56° 42' N	9.56	0.6

Table 5.1: Observed sea level residual in the morning at 21/7 1998.

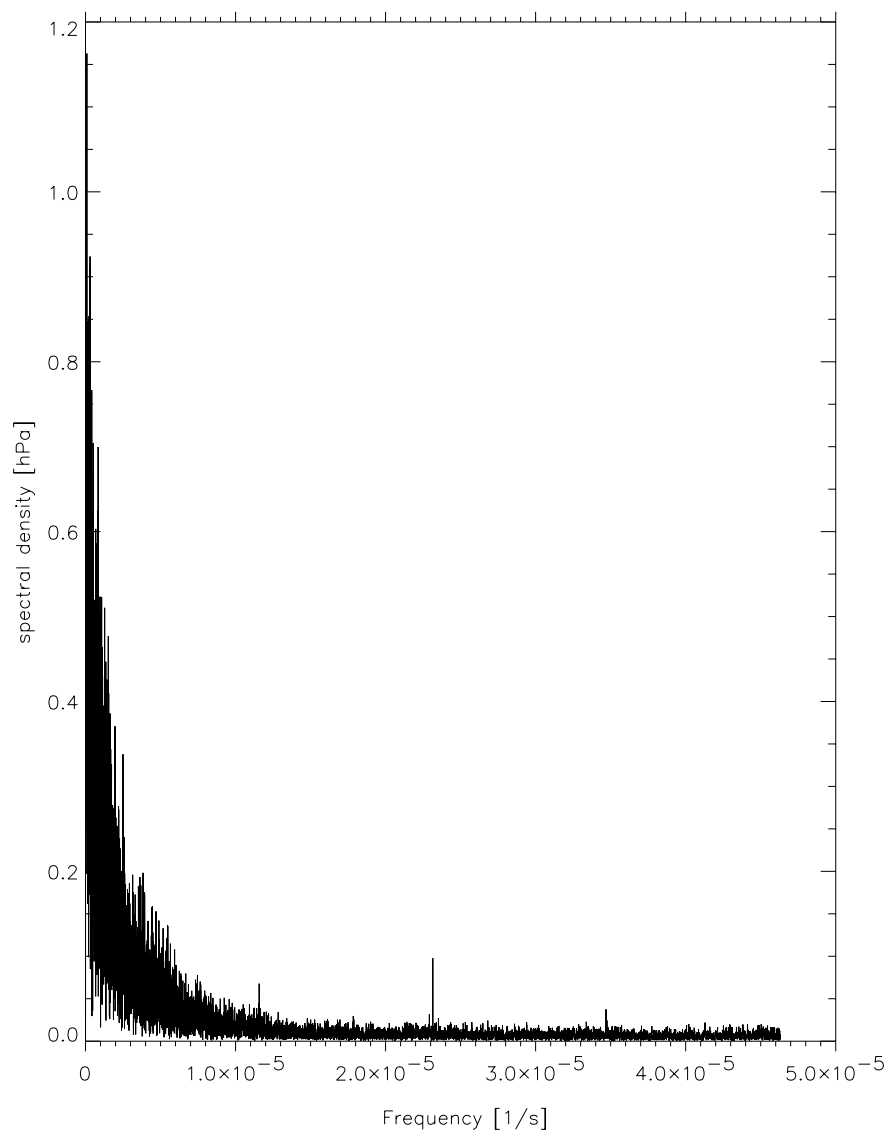


Figure 5.2: *FFT analysis of atmospheric pressure observations from Blåvands Huk, Denmark.*

Long ocean waves that enter the North Sea propagate around in the North Sea as Kelvin waves with reflection at the southern coast. The arrival time of the abrupt sea level at the stations in Table 5.1 excludes such a long wave propagation along the Danish coast from south to north, as this would require an unrealistic high wave speed in this area of more than 200 km/h. Due to the shallow water depth in this area the barotropic wave speed $c_f = \sqrt{gh}$ is less than 70 km/h. The ocean wave, therefore, has to be generated locally inside the North Sea, and an explanation has been looked for in the atmospheric system.

In the morning of the 21. July a low pressure system was developed north east of Scotland, and a severe thunderstorm was observed east of the low pressure system over the central part of the North Sea. The thunderstorm was observed by a satellite image and by the lightning observation system. A propagation of the system towards NNE was detected with a speed of 10-12 m/s. The meteorological situation at the 21. of July is described in more detail in *Aakjær et al. (1998)*. This meteorological situation has similarities with the meteorological situation that occurred over Copenhagen the 30. of June 1997, where a severe thunderstorm was followed by an abrupt change in the atmospheric pressure of about 7 hPa on a time scale of less than one hour. For the situation at the 21/7 1998 atmospheric pressure and wind observations were only available from an oil platform in the Gorm oil field, about 100 km west of the thunderstorm track. The observations provided by Mærsk Olie og Gas A/S and DHI showed an atmospheric low pressure system with a duration of approximately 1 day from the evening of 20/7. The pressure observations during this 1 day low system are very fluctuating with an abrupt increase in the pressure in the morning of 21/7 of about 4 hPa over a time scale of one hour. This indicate that a larger pressure anomaly may have occurred at the center of the thunderstorm. Assuming an atmospheric pressure anomaly of about 5-7 hPa, as was observed for the situation in June 1997 over Copenhagen, the dynamical inverse barometer effect (Eqn. 5.4) estimates that an ocean wave with an amplitude of 8-11 cm may have been generated.

By assuming conservation of momentum in the water column and using the relation between the phase speed and particle velocity for a long wave, the following simple estimate of the shoaling effect for a long wave is found

$$\frac{\eta_0}{\eta_1} = \sqrt{\frac{h_1}{h_0}}, \quad (5.6)$$

where the subscripts denote two vertical sections, η is the wave height and h the water depth. For the case with an ocean wave amplitude of about 10 cm at a water depth of 40 m at the location of the thunderstorm, the wave amplitude will increase to nearly 40 cm at a water depth of 3 m, where the tide gauges measured the wave. Due to the lack of pressure observations from the thunderstorm area it can not be proved that the thunderstorm generated the ocean wave. However, the time scale and the velocity of the thunderstorm, together with the estimated size of the pressure anomaly, make the thunderstorm to a very probable explanation.

At Christmas night 1983 a somehow similar situation with an abrupt atmospheric pressure anomaly of 6 hPa was observed. This atmospheric pressure anomaly moved from the northern part of the North Sea over Denmark, and abrupt sea level changes were observed along the

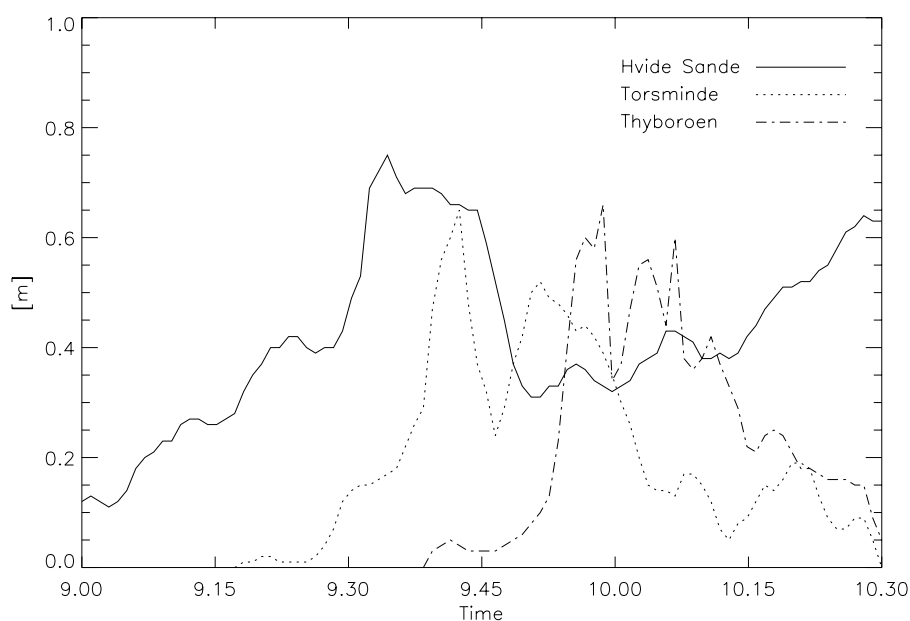


Figure 5.3: Observed sea level at 21/7 1998 from three pressure gauges provided by the Danish Coastal Authority. Data are four minutes averages of 0.5 sec sampled observations.

Danish North Sea coast with residuals of up to 1 m. The ocean wave was calculated to enter the coast from the same direction as the propagation of the atmospheric pressure system (*Højerslev, 1984; Nielsen and Klausen, 1984*). Those two situations from 1983 and 1998 demonstrate that very abrupt sea level changes on time scales of less than one hour may be caused by abrupt changes in the atmospheric system. The generation of such short periodic and relative strong sea level disturbances may be a relatively rare phenomenon, as it requires both abrupt and strong atmospheric perturbations, and a velocity of the atmospheric system to be comparable with an ocean wave propagation. However, the occurrence of abrupt sea level changes may on the other hand happen more frequently, than what would be the impression from inspection of tide gauge records, as the standard 15-minutes sampling interval may fail to observe these disturbances. This was actually the case with the situation at 21. of July 1998, where only one of the 15-minutes sampling tide gauges (Ferring) along the Danish North Sea coast caught the wave. Also the post-processing quality check of the tide gauge observations may exclude such short periodic phenomena and regard such abrupt sea level changes as instruments failures.

Chapter 6

Tidal Modelling

Model simulations have been performed with the Mike 21 model in order to identify possible improvements of the operational storm surge warning system for the North Sea by including tidal information obtained from altimetry. Tidal information is introduced in the model at the open model boundaries, and the effect from the inclusion of tidal information obtained from altimetry at the model boundary has been validated and is described in Section 6.1. The model simulations have furthermore been used to estimate the effect of the atmospheric influence on the ocean tides. This has been performed by validation of the model derived tidal constituents from model simulations with high and low resolution atmospheric forcings and without atmospheric forcing. These results are described in Section 6.3.1.

The Mike 21 model has been run with different boundary and atmospheric forcing fields as shown in Table 6.1 for a one year period. The period 1/8 1997 - 1/8 1998 was chosen in order to cover the data period from the deployed off-shore instrument at Horns Rev. The model is run with a time step of 300 s giving a CFL criterion (or Courant number) which should ensure a stable wave solution. The CFL criterion defined as

$$c_f \cdot \frac{\Delta t}{\Delta s / \sqrt{2}},$$

for a 2D model where $c_f = \sqrt{gh}$ is the barotropic phase velocity, Δt the time step, and Δs the grid space, estimates the number of grid points the wave information travel during one time step. For the main part of the model domain the Courant number is less than 1. A maximum Courant number is found in the Norwegian trench of less than 5, which should still ensure a stable wave solution. In the coarse model domain of 9 n.m. ocean waves with a minimum wavelength of 33 km are resolved, and all the shallow water tides with wave lengths on scales of several hundreds of km are therefore resolved by the model.

6.1 Tidal Forcing

Mike 21 has two open boundaries, a southern boundary in the British Channel, and a northern boundary between the northern part of Scotland and Stavanger, Norway. The tidal forcing

Run	Tidal forcing	Atm. forcing
M21-T	German maps	none
M21-TAltimetry	Altimetry	none
M21-TEC	German maps	ECMWF
M21-THIR	German maps	HIRLAM

Table 6.1: *Tidal and atmospheric forcing used in the Mike 21 model simulations.*

consists of the tidal waves introduced into the model at the two open boundaries. This is, as mentioned in Chapter 3, common practice for hydrodynamical modelling in the North Sea, as the uncertainty in determining the tidal constituents at the open boundaries may be larger than the contribution generated internally in the North Sea from the tidal potential. In the current model set up used for the storm surge warning system at DMI the southern boundary tidal wave is generated from tidal constituents obtained from the Admiralty Tables at the stations Dungeness, U.K., and Wissant, France (*Admiralty*, 1996). The tidal wave at the southern boundary is generated from the main constituents O_1 , K_1 , S_2 and M_2 plus corrections for the higher order shallow water constituents. At the northern open boundary the tides are caused by a tidal wave propagating into the North Sea from the Atlantic Ocean west of the British Isles, and a tidal wave propagation southwards from the Norwegian Sea. Information about the tidal constituents at this open model boundary is currently obtained from readings of old German calculated tidal maps covering the North Sea (*Marineobservatorium*, 1942). The tidal wave is generated from the following ten tidal constituents: O_1 , P_1 , K_1 , N_2 , μ_2 , M_2 , S_2 , K_2 , M_4 and MS_4 .

With the objective to estimate if the model simulated tides in the North Sea can be improved by inclusion of altimetry observations, a new tidal forcing field at the northern model boundary has been constructed. The new tidal information at the northern boundary is obtained from the global tide model Andersen-Grenoble (AG95.1) by Ole B. Andersen, KMS. The tide model AG95.1 is an extension of the hydrodynamical model FES94.1 (*Provost et al.*, 1994) by inclusion of two years of T/P altimetry data (see *Shum et al.* (1997) for details about the AG95.1 model). This new tidal boundary forcing field is generated from the seven constituents: O_1 , P_1 , K_1 , N_2 , M_2 , S_2 and K_2 .

A validation of the simulated tides from two model runs forced with the northern tidal boundary generated from the former German maps readings and the altimetry based observations is shown in Table 6.2. The validation is made for eight tidal constituents as a vector RSS (described in Appendix C) with respect to a data set consisting of nine in-situ instruments located around the North Sea coast: eight tide gauges (Wick, Leith, North Shields, Lowestoft, Sheerness, Esbjerg,

	O_1	K_1	N_2	M_2	S_2	M_4	MS_4	M_6
M21-Taltimetry	1.2 cm	2.5 cm	6.0 cm	11.6 cm	8.0 cm	4.9 cm	3.3 cm	1.4 cm
M21-T	2.0 cm	1.8 cm	5.2 cm	12.3 cm	6.9 cm	5.6 cm	3.5 cm	1.5 cm

Table 6.2: *RSS for validation of the Mike 21 tidal forcing fields to nine tide gauges.*

Hanstholm, and Hirtshals) and the off-shore instrument at Horns Rev. Small improvements in the model simulated tides are seen for the altimetry based tidal forcing compared to the former readings from the German tidal maps for the constituents O_1 , M_2 and M_4 with improvements of 0.7 cm - 0.8 cm, whereas a less accurate validation to the in-situ observations are seen for the constituents K_1 , N_2 and S_2 , with a larger RSS error of up to 1.1 cm for the S_2 constituent. A total RSS error summed over the 8 constituents shows no difference in the accuracy between the altimetry based and the German maps based tidal forcing fields.

Figure 6.1 shows the model derived phase lag for the largest tidal constituent, M_2 , for the two different tidal forcing fields at the northern model boundary. The most important difference between the M_2 phase lag maps shown is the location of the northern amphidromical point. The Mike 21 run with the northern tidal boundary based on the altimetry locates the amphidromical point south west of Norway, whereas the Mike 21 run with the northern tidal boundary based on the readings from the German maps places the co-tidal lines as the amphidromical point would be located in-land in Norway. The tide gauge records available from Tregde and Stavanger in Norway give no indication of the position of the amphidromical point, but most of the available maps of the M_2 constituent do agree on the “in-land” location (e.g. *Pugh (1987)*; *Marineobservatorium (1942)*). The German map based tidal forcing at the northern boundary is, therefore, chosen for the rest of the Mike 21 simulations described here. To explain part of the difference in the location of the amphidromical point it is worth to notice that the current model set up has been extensively calibrated with the northern tidal boundary based on the tidal constituents from the German maps. Specifically the bed friction parameterization in this complicated area with a steep topography at the Norwegian Trench has been tuned. This has influenced the tidal pattern in the area, and a re-calibration with the altimetry based tidal boundary may result in a re-positioning of the M_2 amphidromical point.

6.2 Tidal Validation and Model Inter comparison

To estimate the accuracy of the Mike 21 derived tidal constituents a further validation including off-shore tidal observations mainly from oil platforms, and an inter comparison with a global tide model have been performed together with Ole B. Andersen, KMS. The coarse Mike 21 model grid with the 9 n.m. (16.7 km) resolution has been validated with 22 in-situ observations for an off-shore area in the central part of the North Sea, and the finer model domain with a spatial resolution of 3 n.m. (5.6 km) has for the eastern North Sea been validated at 8 stations (both off-shore and coastal). The station locations are shown in Figure 6.2 for the central and the eastern North Sea area to the left and right in the figure, respectively. Data from the global tide model AG95.1 by Ole B. Andersen, KMS, was chosen for the model inter comparison. This global model has a spatial resolution of $0.5^\circ \times 0.5^\circ$.

A validation of the tidal constituents derived by the two model simulations has been performed for the four constituents: O_1 , K_1 , M_2 and S_2 . The calculated RSS values of the two in-situ validation data sets are shown in Tables 6.3 and 6.4 for both the Mike 21 and the AG95.1 models. For the validation with the 22 stations in the central part of the North Sea a better accuracy in the determination of the tidal constituents is obtained from the Mike 21 model than

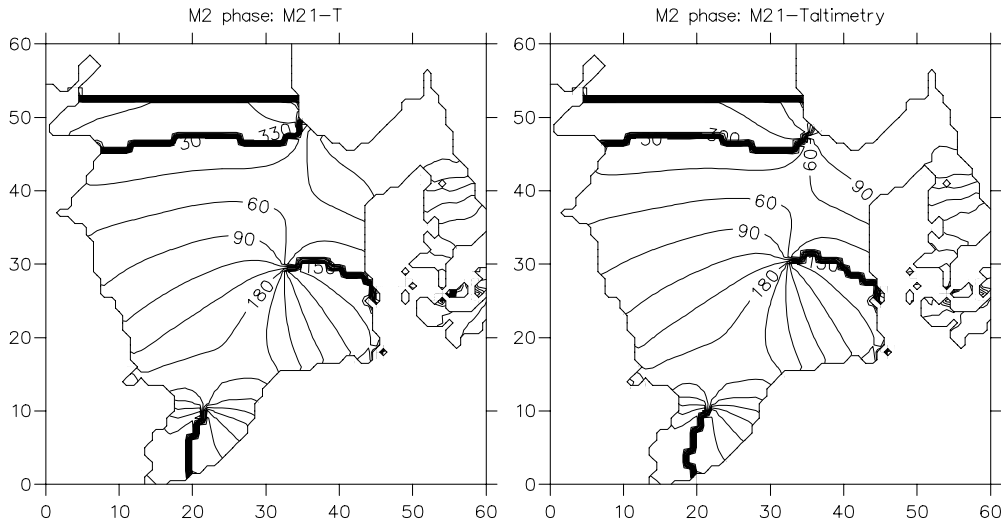


Figure 6.1: *Mike 21* derived M_2 phase lag for the model run forced with northern tidal boundary field based on the German tidal constituent maps (left), and based on altimetry (right).

from the AG95.1 model. This would be expected due to the much higher spatial resolution in the *Mike 21* model with twice the resolution in the longitudes and triple the resolution in the latitudes than the AG95.1 model. For the validation with the 8 stations located in the eastern part of the North Sea both models show a significantly decrease in the accuracy of estimating the M_2 and S_2 constituents. This reveals that both models have problems in reproducing the shoaling effect in the coastal area. For the two diurnal constituents only a small decrease in the accuracy is observed for both models, compared to the validation set in the central North Sea.

	O_1	K_1	M_2	S_2
Mike 21 9 n.m. grid (M21-T)	1.1 cm	1.3 cm	3.7 cm	1.8 cm
AG95.1	1.3 cm	1.3 cm	7.5 cm	3.4 cm

Table 6.3: *RSS* values for validation of *Mike 21* (9 n.m. grid) and AG95.1 to 22 in-situ observations located in the central part of the North Sea.

	O_1	K_1	M_2	S_2
Mike 21 3 n.m. grid (M21-T)	1.8 cm	1.7 cm	11.8 cm	10.7 cm
AG95.1	1.8 cm	1.4 cm	25.8 cm	8.8 cm

Table 6.4: *RSS* values for validation of *Mike 21* (3 n.m. grid) and AG95.1 to 8 stations (both on- and off-shore) in the eastern part of the North Sea.

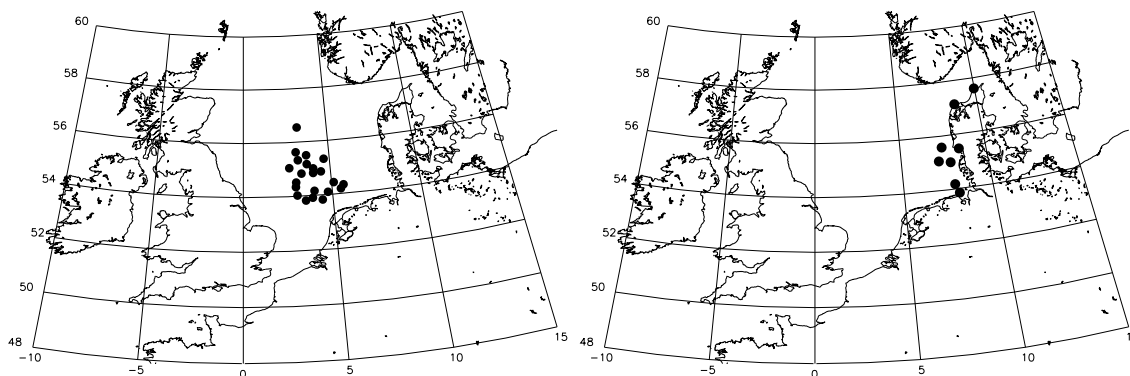


Figure 6.2: *Validation points for the model derived tidal constituents.*

6.3 Atmospheric Forcing

With the objective to estimate the effect of the atmosphere on the ocean tidal constituents Mike 21 simulations have been performed with and without atmospheric forcing, and with both a low and high resolution in the atmospheric forcing. The atmospheric forcing has been obtained from the ECMWF model with 1.5° spatial resolution and 6 hourly temporal resolution, and from the DMI-HIRLAM-E model with a 0.15° (rotated grid) spatial resolution and 3 hours time resolution. The atmospheric data are interpolated to the Mike 21 coarse model domain (16.7 km) by a bi-linear interpolation.

The atmospheric pressure at mean sea level, and the wind at 10 m above the sea surface, is transferred into the hydrodynamical model via the momentum equation. The atmospheric wind is transformed into surface stress by the empirical drag formulation (Eqn. 5.1), with the following expression for the drag coefficient C_D (Vested *et al.*, 1992):

$$C_D = \begin{cases} 0.0016 + 0.001 \frac{W}{W_t} & \text{for } W < W_t \\ 0.0026 & \text{for } W \geq W_t \end{cases}$$

with a threshold value for the wind $W_t = 24$ m/s.

6.3.1 The Atmospheric Influence on the Tidal Constituents

An estimate of the effect on the tidal constituent of the atmospheric fields in the North Sea has been carried out from the model runs forced with the two atmospheric forcing fields. A validation of the model derived tidal constituents is shown in Table 6.5 with respect to the data set consisting of nine in-situ observations (Wick, Leith, North Shields, Lowestoft, Sheerness, Horns Rev, Esbjerg, Hanstholm and Hirtshals).

The RSS measures in Table 6.5 are very similar for the two model simulations, and no significant influence on the model estimated tidal constituents of the two different atmospheric forcing fields

	O_1	K_1	N_2	M_2	S_2	M_4	MS_4	M_6
M21-THIR	2.0 cm	1.9 cm	5.1 cm	12.0 cm	6.9 cm	5.4 cm	3.4 cm	1.4 cm
M21-TEC	1.9 cm	1.8 cm	5.1 cm	12.1 cm	6.9 cm	5.5 cm	3.4 cm	1.5 cm

Table 6.5: *RSS for validation of the Mike 21 estimated tidal constituents to nine tide gauges.*

is found. In comparing the RSS values for the validation of the model run without atmospheric forcing (M21-T) in Table 6.2 small improvements for the validation with the nine in-situ points are found for the constituents O_1 , N_2 , M_2 , M_4 , MS_4 and M_6 . The largest relative improvement of 7% is found for M_6 . A slightly less accurate estimation of the K_1 constituent is found with an increase in the RSS error of 4% for the HIRLAM forcing included. The largest absolute improvement of 0.2 cm (2%) is found for the M_2 constituent for the HIRLAM forcing included. No improvement is found for the S_2 constituent. The most crucial difference between the two atmospheric forcing fields may be the time resolution, as the 6 hourly values from the ECMWF atmospheric model implies the critical frequency, f_c , to be at the frequency of the second largest constituent S_2 . But from the RSS values in Table 6.5 it may be concluded that the ECMWF fields seem to resolve the S_2 atmospheric tidal contribution to the same degree as the HIRLAM fields - at these nine on-shore validation points.

The spatial distribution of the magnitude of the atmospheric influence on the S_2 constituent is shown in Figure 6.3. The Figure shows the difference in the model derived S_2 amplitude between the model run with the atmospheric forcing included, and the pure tidal run. A slightly different spatial pattern is obtained for the two atmospheric forcing fields applied. A larger influence is in general seen from the ECMWF forcing field. Along the British east coast a decrease is seen in the S_2 amplitude of 0.5 cm and 0.7 cm for the HIRLAM and ECMWF fields, respectively. In the north-eastern part of the North Sea the ECMWF forcing field is seen to cause an increase in the S_2 amplitude of 0.2 cm., whereas the HIRLAM field introduces nearly no influence in this area. These differences introduced on the ocean S_2 amplitude might be due to different interactions at the S_2 frequency caused by the different time resolution of the two atmospheric fields. No significant influence on the phase lag of the S_2 constituent was found in the North Sea area. In the Skagerrak a delay in the phase lag of up to 5° (corresponding to 10 min.) was found for the model run with the atmospheric forcing included compared to the tidal run.

In Figure 6.4 is shown the atmospheric influence on the model derived M_2 constituent. The influence on the M_2 constituent show very much the same pattern for the two different atmospheric forcing fields applied. An increase in the influence on the M_2 amplitude is seen for the coastal areas. Along the British east coast the M_2 amplitude is seen to be decreased by the inclusion of the atmospheric forcing. The largest influence is found for the Skagerrak area with a decrease of up to 1.5 cm and 2.0 cm for the ECMWF and HIRLAM fields, respectively. The atmospheric influence is therefore in this area of about 10% of the M_2 tidal range. The larger influence on the M_2 amplitude from the HIRLAM than the ECMWF forcing field might be caused by the higher resolution in both space and time.

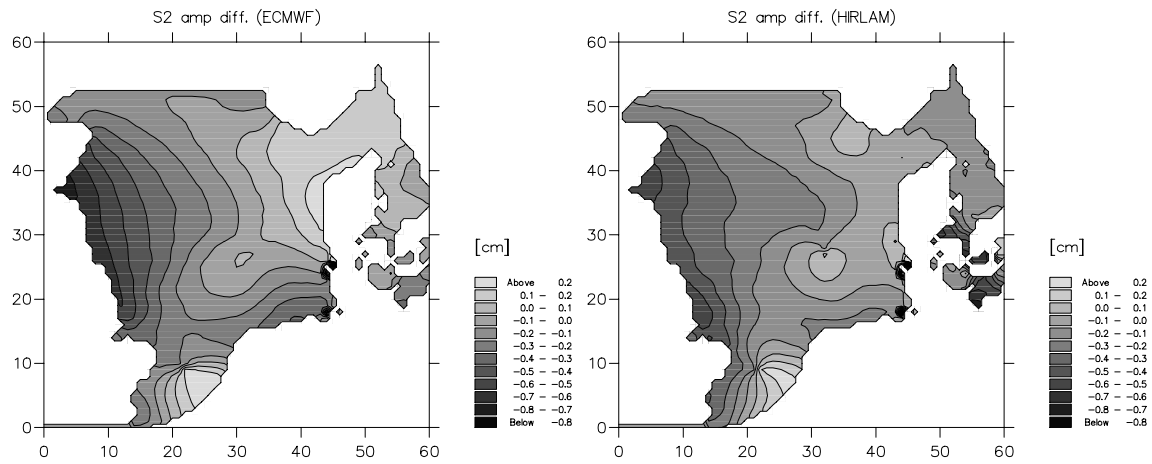


Figure 6.3: *The atmospheric influence on the model derived S_2 amplitude. For model runs: (M21-TEC)-(M21-T) to the left, and (M21-THIR)-(M21-T) to the right. Contour interval is 0.1 cm.*

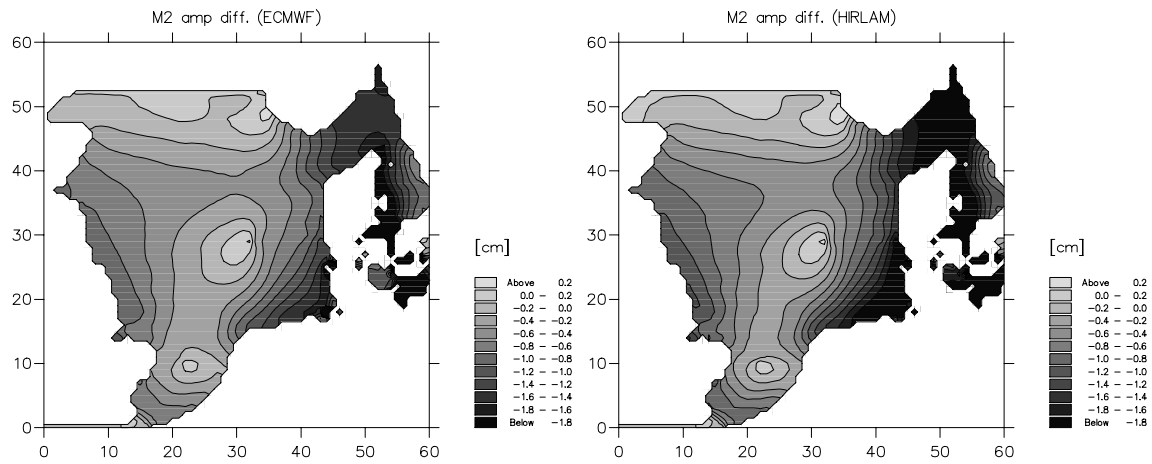


Figure 6.4: *The atmospheric influence on the model derived M_2 amplitude for model runs: (M21-TEC)-(M21-T) to the left, and (M21-THIR)-(M21-T) to the right. Contour interval is 0.2 cm.*

Chapter 7

Observed and Modelled Sea Level Variability in the North Sea

7.1 Study in the Eastern Part of the North Sea

Sea level data from the off-shore bottom pressure gauge at Horns Rev located 50 km off the Danish west coast have been used to investigate and identify local effects on the existing Danish coastal tide gauges, and to validate T/P data in this near-coastal and shallow water area.

The eastern part of the North Sea is an important area with respect to the Danish storm surge warning system, as the largest storm surges occur in this area. The sea level variability decreases significantly north of the Wadden Sea area, due to a lower tidal range, as seen in Table 7.1, where the variability in the sea level and sea level residual are shown together with a measure of how much of the observed sea level variance that can be explained by the tidal signal, calculated as the explained variance:

$$\left(1 - \frac{\text{var}(\text{residual})}{\text{var}(\text{observations})}\right) \times 100 \%$$

Tide gauge	Obs. st.dev	Res. st.dev	Explained var.
Horns Rev (autumn)	0.38 m	0.24 m	61%
Horns Rev (winter)	0.43 m	0.33 m	40%
Esbjerg	0.68 m	0.39 m	67%
Hvide Sande	0.45 m	0.35 m	40%
Torsminde	0.43 m	0.37 m	26%
Hanstholm	0.30 m	0.27 m	19%
Hirtshals	0.26 m	0.23 m	22%

Table 7.1: *Sea level variability and tidal wave dominance in the eastern part of the North Sea coast. For the on-shore stations the values are estimated from 5 years of data.*

7.1.1 On-shore Tidal Amplification

To identify local effects on the tidal wave the on-shore amplification - the shoaling effect - of the tidal constituents have been investigated. In Table 7.2 are listed the tidal amplitudes at the Horns Rev station for all constituents of diurnal and higher frequencies with amplitudes larger than 1 cm. Also the two friction generated constituents M_6 and $2MS_6$ are listed. To show the tidal amplification the tidal amplitudes at the on-shore stations in Esbjerg and Hvide Sande are listed together with the amplification factor for the tidal amplitudes from Horns Rev towards Esbjerg and Hvide Sande, respectively. A significant different pattern is observed for the on-shore tidal amplification towards Esbjerg located in an area with islands between the station and the open sea, and towards Hvide Sande located on the coast directly to the open sea. At Esbjerg the long diurnal tidal waves are amplified significantly less than the shorter tidal waves. This may be caused by resonance effects in the area around Esbjerg or that the islands act as obstacles for the tidal wave propagation. The tidal pattern from Esbjerg is, therefore, seen not to represent the tidal pattern at nearby open water locations. The amplification of the tidal wave from off-shore towards Hvide Sande north of the Wadden Sea shows significant amplifications of the tidal constituents generated by the non-linear friction (M_6 and $2MS_6$). No significant amplification of the linear tidal constituents are observed. The area just north of the Wadden Sea is, therefore, seen to be highly dominated by friction that extracts momentum out of the tidal wave for propagation northwards of Horns Rev.

Constituent	Horns Rev [cm]	Esbjerg [cm]	Amplification factor	Hvide Sande [cm]	Amplification factor
Q_1	1.8	2.7	1.5	1.7	0.9
O_1	6.6	8.1	1.2	6.7	1.0
P_1	1.6	2.8	1.8	2.1	1.3
K_1	4.8	6.1	1.3	4.1	0.9
μ_2	2.5	6.9	2.7	2.5	1.0
N_2	5.8	10.2	1.8	6.0	1.0
ν_2	1.1	5.6	5.1	2.5	2.2
M_2	32.8	69.4	2.1	34.3	1.0
L_2	2.9	7.0	2.4	2.9	1.0
S_2	8.4	17.6	2.1	8.1	1.0
K_2	2.3	5.3	2.3	2.2	1.0
MN_4	1.1	2.2	2.0	1.8	1.7
M_4	3.1	6.1	2.0	3.7	1.2
MS_4	1.5	3.1	2.0	1.5	1.0
M_6	0.6	2.0	3.2	2.7	4.5
$2MS_6$	0.8	1.9	2.3	2.5	3.1

Table 7.2: Amplitudes of tidal constituents at Horns Rev (period 2), Esbjerg and Hvide Sande and the amplification of the tidal amplitudes from Horns Rev towards Esbjerg (column 4) and towards Hvide Sande (column 6).

7.1.2 On-shore Sea Level Amplification

The sea level variability obtained from T/P data in the eastern part of the North Sea have been studied, with the objective to estimate the degree of information that can be obtained from altimetry, and to validate how well the altimeter performs in this near coastal area. Two T/P ground tracks continues towards the Danish North Sea coast as shown in Figure 7.1. The northern satellite track is a descending track and the southern an ascending track, and both tracks are, therefore, directed from the sea towards the land. The two satellite tracks reach the coast very close to two tide gauges located at Torsminde and Hvide Sande¹, for the northern and southern satellite track, respectively. The sea level variability obtained from five years of T/P data (cycles 1-194) are shown in Figures 7.2 and 7.3 for the ascending and descending track, respectively. The sea level variability is calculated for all the along track data points from the two cross-over points seen in Figure 7.1 and towards the coast. The depth contour lines are shown in Figure 7.1. For the ascending satellite (the southern) track data from Horns Rev and Hvide Sande are available for validation of the T/P values. The standard deviation from the two data periods from Horns Rev (0.38 m for the 3 months autumn period, and 0.43 m for the 5 months winter/spring data period, respectively) are shown in Figure 7.2 together with the coastal sea level variability calculated from five years of data from Hvide Sande located 12 km NNE of the last T/P data point towards the coast. With the reservations that the statistic measures are calculated for different periods for all the three data sources (T/P data, Horns Rev and Hvide Sande observations), a good validation of the T/P data is seen for the Horns Rev data (located 5 km N of the nearest T/P data point), with approximately 70% and 90% of the sea level variance (85% and 95% of the standard deviation) obtained by the T/P data compared to the variance obtained in the Horns Rev in situ data for the winter and autumn period, respectively. The shoaling effect across the bank at Horns Rev is seen to be well captured by the T/P data. The T/P data clearly reflect that the satellite ground track after passing the bank is directed along the depth contour lines. For the last data points toward the coast the shoaling effect is seen as an increase in the sea level variability. The satellite at the descending (the northern) track is approaching the coast in a direction approximately normal to the depth contours, which is observed in the data as a slow increase in the sea level variability towards the coast. The only available in-situ data for validation along this track are obtained from the tide gauge station at Torsminde located 10 km SSE of the last T/P data point, and a relatively good validation of the T/P obtained variability is seen. The last satellite data point towards the coast is seen to fail. This is obviously caused by the ocean-land border, as the footprint of the radar signal will observe both the sea and the land.

As the T/P satellite has a 10 days repeat period the obtained sea level variability is based on 10-days sampled observations. The influence of the sampling interval on the in-situ observations from Horns Rev has therefore been tested. The standard deviations calculated from the Horns Rev instrument for an hourly and a 10-days sampling (arbitrarily chosen, and not at the T/P sampling), respectively, are shown in Table 7.3. Only a small increase is seen in the variability caused by the coarse time sampling. This reflects that the sea level variability is nearly uncorrelated at a time lag of 10 days in agreement with the results from the autocorrelation shown

¹both gauges operated by the Danish Coastal Authority.

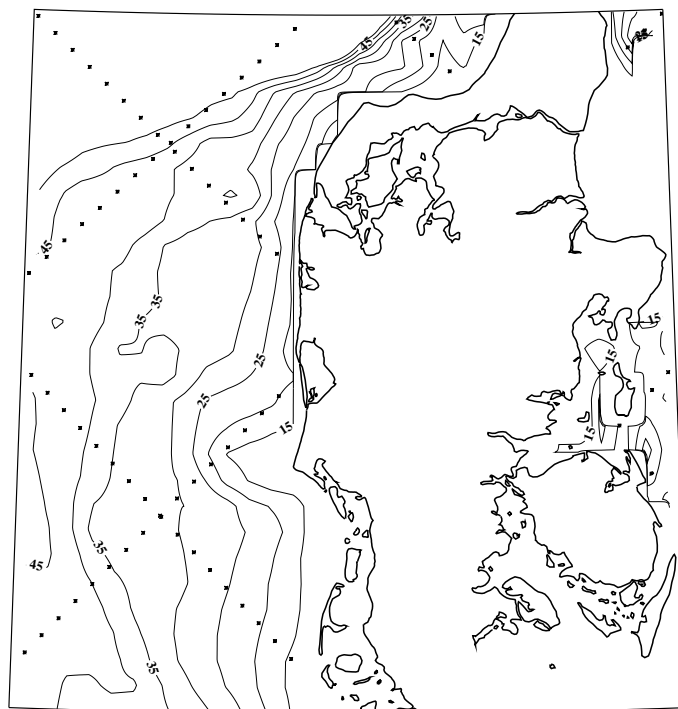


Figure 7.1: *T/P ground tracks (small crosses) towards the Danish North Sea coast. The contour lines show the water depth.*

in Figure 2.3 for the sea level observations from Esbjerg. It may therefore be concluded that the coarse sampling interval for the T/P observations does not disturb the obtained sea level variability information, and the altimeter is able to observe approximately 80% of the sea level variance observed by the in-situ instrument at Horns Rev.

The sea level variability from T/P shown in Figures 7.2 and 7.3 was calculated from a large data set of 174 data samplings. To estimate the quality of the sea level data obtained by the altimeter for a shorter period the standard deviation at the along track data point closest to Horns Rev has been calculated for the period late August 1997 - April 1998 (24 data samples) to be 0.52 m. This is a much higher value than the standard deviation found from the data set obtained from the 4 years of T/P data with a value of 0.36 m. Based on this single validation point it seems like a long data record is crucial for obtaining good results for the sea level variability.

	In-situ 1 hour	In-situ 10 days
St. dev.	0.41 m	0.43 m

Table 7.3: *Standard deviation calculated for hourly and 10-days samplings from the Horns Rev observations.*

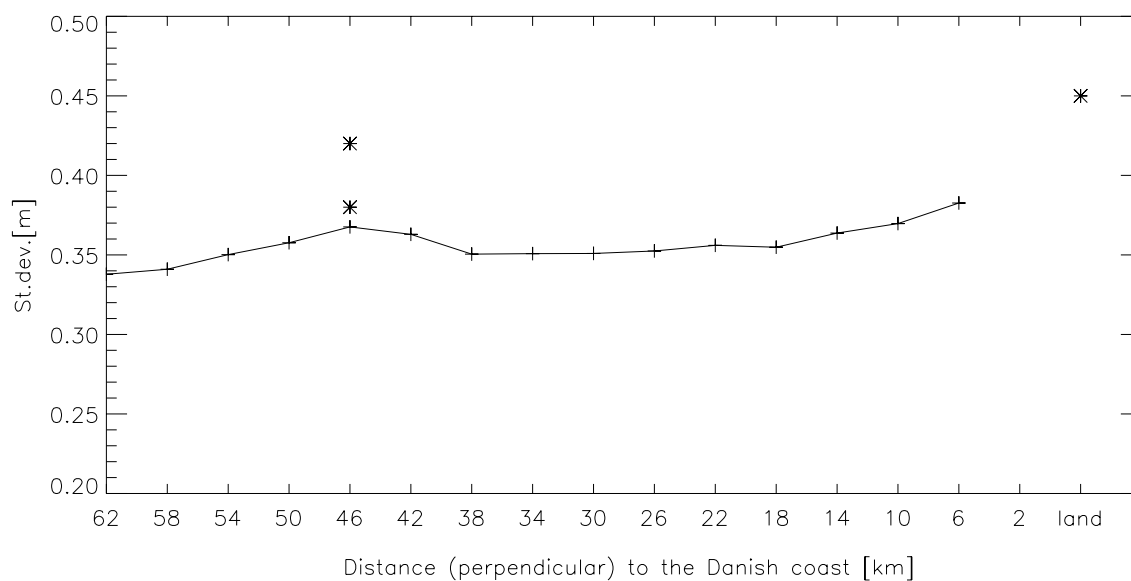


Figure 7.2: Sea level standard deviation obtained from T/P along track data at the ascending ground track towards the Danish North Sea coast. The in-situ values from the Horns Rev and Hvide Sande are also shown (*).

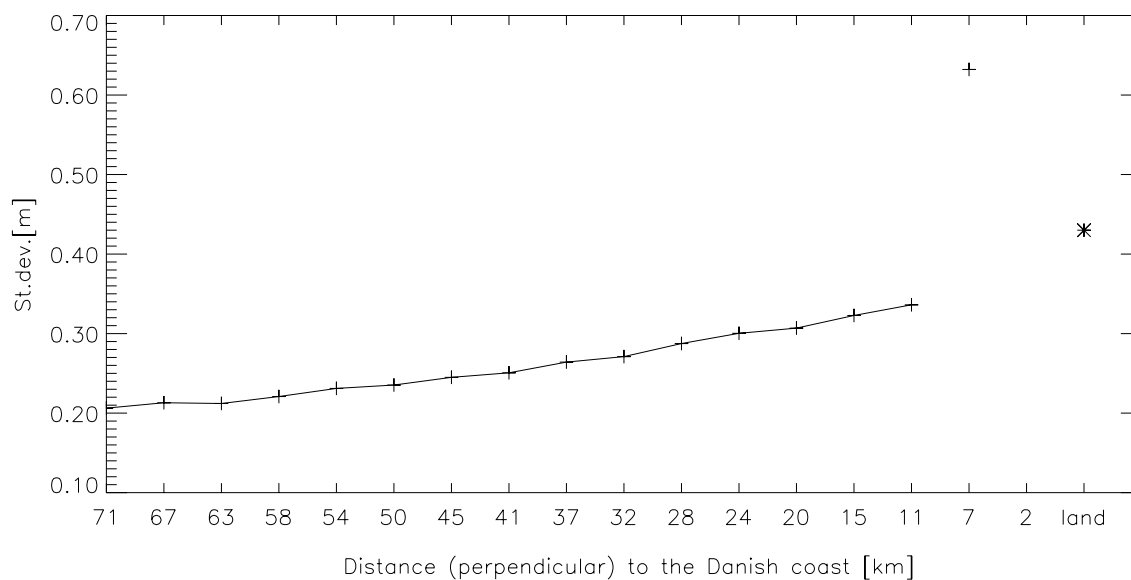


Figure 7.3: Sea level standard deviation obtained from T/P along track data at the descending ground track towards the Danish North Sea coast. The in-situ value from Torsminde is also shown (*).

7.2 Validation of Model and Altimetry data

7.2.1 Validation with the Horns Rev off shore observations

The ability of the hydrodynamical model to capture the sea level variability in the off-shore area has been tested. A validation has been performed with model derived sea level information at Horns Rev where the in-situ observations were available for the period 26/8 1997 - 29/4 1998. The standard deviation for the sea level time series at the Horns Rev data point obtained from the model simulations, and the standard deviation for the time series of the difference $\eta_{model} - \eta_{obs.}$ are shown in Table 7.4. For comparison the standard deviation for the Horns Rev in-situ observations is as listed above 0.41 m for the whole data period. Results are shown in Table 7.4 from the model runs M21-T, M21-THIR, and M21-TEC (see Table 6.1 for the model runs description), and for model data extracted from both the coarse and fine resolution grid. A significant increase in the sea level variability is seen - as expected - for the model runs with atmospheric forcing included. Furthermore a slightly better performance is seen for the high resolution forcing (HIRLAM) compared to the low resolution (ECMWF), with 72% and 70% of the observed sea level variance at Horns Rev (observed variance = 0.165 m²) explained by the model, respectively. For all the model simulations no influence of the grid resolution on the sea level variability is seen for this one off-shore validation point.

Model	Grid resolution	St. dev. ($\eta_{m21\ run}$)	St. dev. ($\eta_{m21\ run} - \eta_{obs.}$)
M21-T	3 n.m.	0.27 m	0.32 m
M21-T	9 n.m.	0.27 m	0.32 m
M21-THIR	3 n.m.	0.41 m	0.22 m
M21-THIR	9 n.m.	0.41 m	0.22 m
M21-TEC	3 n.m.	0.40 m	0.23 m
M21-TEC	9 n.m.	0.40 m	0.22 m

Table 7.4: Standard deviations and validation for the model simulated sea level time series at Horns Rev.

7.2.2 Altimetry and model inter-validation

To estimate the agreement between the model simulated sea levels and the T/P observations an inter-validation for the whole North Sea area has been performed together with Ole B. Andersen, KMS. The inter-validation included 948 T/P data points in the North Sea. The Mike 21 simulated sea levels (in the 9 n.m. resolution) were interpolated in both space and time to these altimeter points.

The three months period 1/12 1997 - 1/3 1998 was chosen for this inter-validation. In this period a maximum of 8 T/P repeat cycles were available. In practice the data set was reduced to 5 repeat cycles at a spatial coverage of 426 points for the T/P observations to be available at all the spatial points. To eliminate the influence from false signals in the altimetry signal all values above 1.0 m in both the T/P observations and the model simulations were removed.

The standard deviation of the T/P observed sea level heights for the five repeat periods are shown in Figure 7.4 (top). The shallow water effect is seen to be captured by the altimeter with large variabilities in the sea level height in the southern and near-coastal part of the North Sea. In Figure 7.4 (bottom) is shown the standard deviation for the sea level anomalies, calculated as the difference between the T/P observed and model simulated (M21-THIR) sea level heights. A large reduction in the standard deviation is seen for the sea level anomalies compared to the sea level heights.

The spatial mean taken over the 426 data points of the standard deviations are listed in Table 7.5 for sea level heights from the T/P observations and the model simulations (for both a simulation with only tidal forcing and a simulation with full forcing). Also listed are the standard deviations for the sea level anomalies obtained from the differences between the observed and simulated sea level heights. The tidal model simulation is seen to capture about 68% of the observed sea level variabilities and the model simulation with the full forcing is seen to capture about 54% of the variability at these data points.

	Mean st.dev	Mean variance
Sea level heights: T/P	30 cm	900 cm ²
Sea level heights: M21-T	23 cm	529cm ²
Sea level heights: M21-THIR	26 cm	676 cm ²
Sea level anomalies: T/P - (M21-T)	17 cm	289 cm ²
Sea level anomalies: T/P - (M21-THIR)	20 cm	420 cm ²

Table 7.5: *The spatial mean standard deviation and variances for the 426 data points*

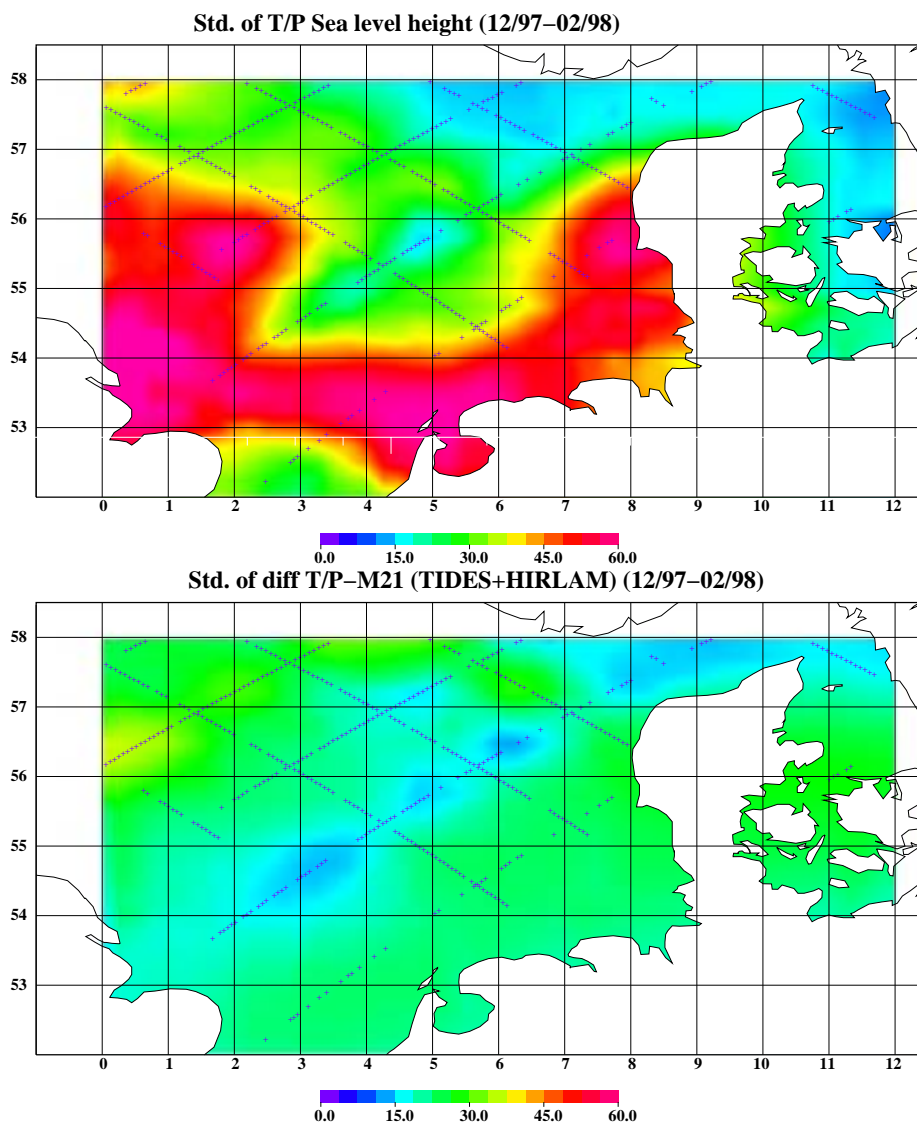


Figure 7.4: The standard deviation for the T/P observed sea level heights (top), and the sea level anomalies from the difference between the T/P observations and the model (M21-THIR) simulations (bottom). Both plots are calculated on basis of the 426 points in space and 5 points in the time domain. Ole B. Andersen, personal communication.

Chapter 8

Conclusion

Information about sea level variations obtained from different in-situ measurements, numerical models and altimetry observations has been combined and validated in the North Sea area with the objectives to obtain new knowledge about the sea level variations.

One of the main results is the new knowledge in understanding the processes causing the seasonal variations in the main tidal constituent M_2 . This phenomenon has previously been observed in coastal tide gauge data, but the T/P altimetry observations have an accuracy that enables an estimation of these modulations in the M_2 constituent. The T/P data have, therefore, provided valuable new knowledge for the off-shore area with information about the spatial behaviour of these variations. This off-shore information has in combination with the coastal tide gauges been used to validate results from numerical models. The numerical model has identified the phenomenon as caused by non-linear interaction, and by that as a shallow water phenomenon, which was indicated previously from the coastal tide gauges. The model results furthermore estimate a large part of the seasonal signal in the M_2 constituent as a barotropic phenomenon caused by non-linear interaction between the tidal waves and the surges.

The off-shore instrument deployed by the GEOSONAR project at Horns Rev 50 km west of the Danish North Sea coast has provided useful measurements. These observed sea level data have been used to validate both T/P altimetry observations and model simulations in this near-coastal and shallow water area. A validation of T/P observations at Horns Rev shows that for a sufficient large data set in the time domain the altimeter is able to catch 80% of the sea level variance observed at Horns Rev. A validation of the Mike 21 model simulated sea level showed that 72% of the observed sea level variance was caught by the model. The validation at this particular off-shore point therefore indicates that improvements of the model can be expected by including statistical information of sea level obtained from altimetry.

The direct inter-validation between the T/P observations and the model simulated sea level heights performed on 948 data points in the North Sea gave rather encouraging results. More than half of the variability observed in the altimetry data was captured by the model in these preliminary test, where only data from a 3 months period was included in the analysis. Inclusion of a longer data set in the analysis may reveal an even better comparison between the altimetry data and the model simulations.

One of the objectives for this study was to identify if any possible improvements of the existing storm surge warning system can be achieved by including altimetry information. The initial studies performed showed promising results for the use of T/P data in order to improve the model, both with respect to tidal information as input to the model, and with respect to statistical information of the sea level variability. The high quality estimates of the sea level variability that can be obtained from T/P observations - when using time series longer than a year - may be used for validation of the model simulated sea level for the large off-shore area, where nearly no validation previously has been feasible.

The high quality tidal information that is available from altimetry offers the potential to enlarge the model area. The present northern boundary of the model area excludes external surges entering the North Sea to be included in the storm surge calculations. External surges are known to have caused storm surges in cases where the operational warning system failed (e.g. *Huess* (1995)), and an enlargement of the model area will therefore improve the warning system for cases where external surges occur.

Furthermore, the improved knowledge obtained from the analyses of the seasonal variations in the M_2 tidal constituent may also turn out to be useful for model calibration. The non-linear interaction between the tides and surges was found to be highly controlled by the bottom friction in the model, and a validation of the seasonal variations may serve as a tool for calibration of the bottom friction parameterization in the model.

Acknowledgment

This PhD project has been carried out as part of the GEOSONAR project supported by the Danish Earth Observation Programme, and I would like to thank for the financial support. Karsten B. Kristensen is acknowledged for initiating this PhD study. My supervisors Niels K. Højerslev at the Geophysical Department, University of Copenhagen, and Erik Buch at DMI are acknowledged for their support during the study. A special thank to Erik for taking over the formal responsibility of the project at DMI after Karsten had left DMI and the project.

Within the GEOSONAR group Ole B. Andersen and Olwijn Leeuwenburgh, KMS, are acknowledged for the co-operation on the seasonal tidal modulation work, and Ole is acknowledged for helping with the model validation for the off-shore area with respect to both in-situ and altimetry observations, and for the model intercomparison between the Mike 21 and AG95.1 models.

Philip L. Woodworth, Proudman Oceanographic Laboratory (POL), U.K., is greatly acknowledged for making a half year visit at POL possible. It was a very inspiring stay. I would like to thank Philip L. Woodworth and Roger A. Flather for valuable ideas and input to the investigations of the seasonal tidal modulation. Also Jane A. Smith and Jason Holt at POL are acknowledged for kindly providing model data.

Bjarne Amstrup, DMI, is acknowledged for providing the ECMWF model fields and for proof-reading the thesis. I would also like to thank my colleagues in the ocean group at DMI for their help during the study.

References

- Aakjær, P., N. W. Nielsen, and V. Huess, *Flodbølgen ved Vesterhavet d. 21. juli 1998*, Vejret, 76. Danish Meteorological Society, Lyngbyvej 100, Copenhagen, Denmark. (In Danish), 1998.
- Aas, E., *Metoder i Fysisk Oseanografi*, Institut for geophysics, Oslo University, Norway. (In Norwegian), 1986.
- Admiralty, *Tide Tables, Volume 1, 1997*, Published by the Hydrographer of the Navy, United Kingdom, 1996.
- Amin, M., The fine resolution of tidal harmonics, *Geophysical Journal of the Royal Astronomical Society.*, *44*, 293–310, 1976.
- Amin, M., On analysis and prediction of tides on the west coast of Great Britain, *Geophysical Journal of the Royal Astronomical Society.*, *68*, 57–78, 1982.
- Andersen, O. B., Ocean tides in the northern North Atlantic and adjacent seas from ERS 1 altimetry, *Journal of Geophysical Research*, *99*, (C11), 22 557–22 573, 1994.
- Andersen, O. B., Global ocean tides from ERS 1 and TOPEX/POSEIDON altimetry, *Journal of Geophysical Research*, *100*, (C12), 25 249–25 259, 1995.
- Andersen, O. B., Shallow water tides in the northwest European shelf region from TOPEX/POSEIDON altimetry, *Journal of Geophysical Research*, *104*, (C4), 7729–7741, 1999.
- Andersen, O. B., P. L. Woodworth, and R. A. Flather, Intercomparison of recent ocean tide models, *Journal of Geophysical Research*, *100*, (C12), 25 261–25 282, 1995.
- Baker, T. F., and G. A. Alcock, Time variations of ocean tides, in *Proc. 9th Int. Symp. Earth Tides. New York, 1981*, edited by J. T. Kuo, pp. 341–348, Schweizerbart, Stuttgart, 1983.
- Bell, C., J. M. Vassie, and P. L. Woodworth, *POL/PSMSL Tidal Analysis Software Kit 2000 (TASK-2000)*, Permanent Service for Mean Sea Level, CCMS Proudman Oceanographic Laboratory, Bidston Observatory, Birkenhead, Merseyside CH43 7RA, U.K., 1999.
- Cartwright, D. E., A unified analysis of tides and surges round north and east Britain, *Phil. Trans. R. Soc., London, A*, *263*, 1–55, 1968.
- Cartwright, D. E., and A. C. Edden, Corrected tables of tidal harmonics, *Geophysical Journal of the Royal Astronomical Society.*, *33*, 253–264, 1973.

- Cartwright, D. E., and R. J. Taylor, New computations of the tide-generating potential, *Geophysical Journal of the Royal Astronomical Society*, *23*, 45–74, 1971.
- Cazenave, A., K. Dominh, G. C. Gennero, and B. Ferret, Global mean sea level changes observed by TOPEX-POSEIDON and ERS-1, *Phys. Chem. Earth*, *23*, 1069–1075, 1998.
- Cazenave, A., K. Dominh, F. Ponchaut, L. Soudarin, J. F. Cretaux, and C. L. Provost, Sea level changes from Topex-Poseidon altimetry and tide gauges, and vertical crustal motions from DORIS, *Geophysical Research Letters*, *26*, 14, 2077–2080, 1999.
- Corkan, R. H., An annual perturbation in the range of tide, *Proc. R. Soc. London A*, *144*, 537–559, 1934.
- DHI, *MIKE 21. User Guide and Reference Manual, Release 2.7*, Danish Hydraulic Institute, Hørsholm, Denmark, 1998.
- Doodson, A. T., Harmonic development of the tide-generating potential, *Proceedings of the Royal Society of London, A* *100*, 305–329, 1921.
- Flather, R. A., A tidal model of the north-west European continental shelf, *Mémoires Société Royale des Sciences de Liège, 6^e série, tome X*, 141–164, 1976.
- Foreman, M. G. G., *Manual for Tidal Heights Analysis and Prediction*, Institute of Ocean Sciences, Victoria B.C, Canada, 1977.
- Foreman, M. G. G., W. R. Crawford, and R. F. Marsden, De-tiding: Theory and practice, in *Quantitative Skill Assessment for Coastal Ocean Models. Coastal and Estuarine Studies Volume 47*, edited by D. R. Lynch and A. M. Davies, pp. 203–239, The American Geophysical Union, 1995.
- Fu, L.-L., and G. Pihos, Determining the response of sea level to atmospheric pressure forcing using TOPEX/POSEIDON data, *Journal of Geophysical Research*, *99*, (C12), 24 633–24 642, 1994.
- Fu, L.-L., E. J. Christensen, C. A. Y. Jr., M. Lefebvre, Y. Menard, M. Dorrer, and P. Escudier, TOPEX/POSEIDON mission overview, *Journal of Geophysical Research*, *99*, (C12), 24 369–24 381, 1994.
- Gaspar, P., and R. M. Ponte, Relation between sea level and barometric pressure determined from altimeter data and model simulations, *Journal of Geophysical Research*, *102*, (C1), 961–971, 1997.
- Gaspar, P., and R. M. Ponte, Correction to Relation between sea level and barometric pressure determined from altimeter data and model simulations, *Journal of Geophysical Research*, *103*, (C9), 18 809, 1998.
- Godin, G., *The Analysis of Tides*, Liverpool University Press, 1972.
- Groves, G. W., and R. W. Reynolds, An orthogonalized method of tide prediction, *Journal of Geophysical Research*, *80*, 4131–4138, 1975.
- Hamon, B. V., Continental shelf waves and the effects of atmospheric pressure and wind stress

- on sea level, *Journal of Geophysical Research*, 71, 2883–2893, 1966.
- Højerslev, N. K., *Julebølgen ved Vestkysten, 1983*, Vejret, 21. Danish Meteorological Society, Lyngbyvej 100, Copenhagen, Denmark. (In Danish), 1984.
- Højerslev, N. K., and I. Andersen, *Klimavariationer på mesoskala beskrevet ved vandspejlsændringer og hydrografiske forhold*, Technical Report 90-7 (In Danish). Danish Meteorological Institute, Copenhagen, Denmark, 1990.
- Huess, V., *Eksternt genererede stormflodsbølger i Nordsøen*, Master Thesis, Niels Bohr Institute for Astronomy, Physics and Geophysics, University of Copenhagen, Copenhagen, Denmark. (In Danish), 1995.
- Hvidberg-Knudsen, M., K. Bolding, J. Nielsen, and O. Brink-Kjær, *Analyse af tidevand i Esbjerg*, Danish Hydraulic Institute, Hørsholm, Denmark. (In Danish), 1994.
- Keers, J. F., An empirical investigation of interaction between storm surge and astronomical tide on the east coast of Great Britain, *Deutsche Hydrographische Zeitschrift*, 21, 118–125, 1968.
- Leeuwenburgh, O., O. B. Andersen, and V. Huess, Seasonal tide variations from tide gauges and altimetry, *Phys. Chem. Earth (A)*, 24, No. 4, 403–406, 1999.
- Marineobservatorium, *Karten der Harmonischen Gezeitenkonstanten für das Gebiet der Nordsee*, Oberkommando der Kriegsmarine, Marineobservatorium Wilhelmshaven, Germany, 1942.
- Mitchum, G. T., Comparison of TOPEX sea surface heights and tide gauge sea levels, *Journal of Geophysical Research*, 99, 24541–24553, 1994.
- Munk, W. H., and D. E. Cartwright, Tidal spectroscopy and prediction, *Phil. Trans. R. Soc., A* 259, 533–581, 1966.
- Nielsen, N. W., and T. Klausen, *Vejret julenat 1983*, Vejret, 18. Danish Meteorological Society, Lyngbyvej 100, Copenhagen, Denmark. (In Danish), 1984.
- Nielsen, P. B., and J. W. Nielsen, *Analyse og prediktion af tidevand i Esbjerg.*, Internal note. The Royal Danish Administration of Navigation and Hydrography and the Danish Meteorological Institute, Copenhagen, Denmark. (In Danish), 1998.
- Ponte, R. M., Understanding the relation between wind- and pressure-driven sea level variability, *Journal of Geophysical Research*, 99, 8033–8039, 1994.
- Prandle, D., and J. Wolf, The interaction of surge and tide in the North Sea and River Thames, *Geophysical Journal of the Royal Astronomical Society.*, 55, 203–216, 1978.
- Proctor, R., and I. D. James, A fine resolution 3D model of the southern North Sea, *J. Mar. Sys.*, 8, 285–295, 1996.
- Proudman, J., *Dynamical Oceanography*, Methuen, London, and Wiley, New York, 1953.
- Provost, C. L., M. L. Genco, F. Lyard, P. Vincent, and P. Canceil, Tidal spectroscopy of the world ocean tides from a finite element hydrodynamical model, *Journal of Geophysical Research*, 99 (C12), 24 777–24 798, 1994.

- Pugh, D. T., *Tides, surges and mean sea-level. A Handbook for Engineers and Scientists*, John Wiley & Sons Ltd., 1987.
- Pugh, D. T., and J. M. Vassie, Tide and surge propagation off-shore in the Dowsing Region of the North Sea, *Deutsche Hydrographische Zeitschrift*, 29, 5, 163–213, 1976.
- Pugh, D. T., and J. M. Vassie, Seasonal modulations of the principal semidiurnal lunar tide, in *Mixing and Transport in the Environment*, edited by K. J. Beven, P. C. Chatwin, and J. H. Milbank, pp. 247–267, John Wiley & Sons Ltd., 1994.
- Ray, R. D., Atmospheric tides and the TOPEX/Poseidon meteorological corrections, *TOPEX/POSEIDON Research News*, October 1994, 12–14, 1994.
- Ray, R. D., and G. T. Mitchum, Surface manifestation of internal tides generated near Hawaii, *Geophysical Research Letters*, 23, 2101–2104, 1996.
- Reistad, M., and K. Iden, Updating, correction and evaluation of a hindcast data base of air pressure, wind and waves for the North Sea, the Norwegian Sea and the Barents Sea, in *Research Report No. 9*, Norwegian Meteorological Institute, 1998.
- Shum, C. K., P. L. Woodworth, O. B. Andersen, G. D. Egbert, O. Francis, C. King, S. M. Klosko, C. L. Provost, X. Li, J.-M. Molines, M. E. Parke, R. D. Ray, M. G. Schlax, D. Stammer, C. C. Tierney, P. Vincent, and C. I. Wunsch, Accuracy assessment of recent ocean tide models, *Journal of Geophysical Research*, 102 (C11), 25 173–25 194, 1997.
- Smithson, M. J., *Pelagic Tidal Constants 3*, The International Association for the Physical Sciences of the Ocean (IAPSO). Publication Scientifique No. 35, 1992.
- Sparre, A., *The Climate of Denmark. Summaries of Observations from light vessels III. Sea temperature. Climatological papers no. 10*, Danish Meteorological Institute, Copenhagen, Denmark, 1984a.
- Sparre, A., *The Climate of Denmark. Summaries of Observations from light vessels IV. Salinity A. Means, Extremes and frequency. Climatological papers no. 11*, Danish Meteorological Institute, Copenhagen, Denmark, 1984b.
- Thomsen, H., Iagttagelser af de harmoniske tidevandskonstanter variation ved nogle danske vandstandsstationer, in *Det Danske Meteorologiske Institut, Faglige Meddelelser*, vol. 8, Danish Meteorological Institute, Copenhagen, Denmark. (In Danish), 1973.
- UNESCO, *Tenth report of the joint panel on oceanographic tables and standards*, UNESCO Technical Papers in Marine Sci. No. 36. UNESCO, Paris, 1981.
- Verboom, G. K., J. G. De Ronde, and R. P. van Dijk, A fine grid tidal flow and storm surge model of the North Sea, *Continental Shelf Research*, 12, 213–233, 1992.
- Vested, H. J., H. R. Jensen, H. M. Petersen, A.-M. Jørgensen, and B. Machenhauer, An operational hydrographic warning system for the north sea and the danish belts., *Continental Shelf Research*, 12, No. 1, 65–81, 1992.
- Woodworth, P. L., and J. P. Thomas, Determination of the Major Semidiurnal Tides of the Northwest European Continental Shelf From Geosat Altimetry, *Journal of Geophysical Re-*

search, 95, (C3), 3061–3068, 1990.

Woodworth, P. L., S. M. Shaw, and D. L. Blackman, Secular trends in the mean tidal range around the British Isles and along the adjacent European coastline, *Geophys. J. Int.*, 104, 593–609, 1991.

Woodworth, P. L., S. A. Windle, and J. M. Vassie, Departures from the local inverse barometer model at periods of 5 days in the central South Atlantic, *Journal of Geophysical Research*, 100, 18281–18290, 1995.

Wunsch, C., and D. Stammer, Satellite altimetry, the marine geoid, and the oceanic general circulation, *Annu. Rev. Earth Planet. Sci.*, 26, 219–253, 1998.

